

SANDIA REPORT

SAND2017-13820

Unlimited Release

Printed December 2017

Novel Method to Characterize and Model the Multiaxial Constitutive and Damage Response of Energetic Materials

Md Fazle Rabbi, Robert Mach, Carlos A. Catzin, Calvin M. Stewart, Michael J. Kaneshige

Prepared by
Sandia National Laboratories
Albuquerque, New Mexico 87185 and Livermore, California 94550

Sandia National Laboratories is a multimission laboratory managed and operated by National Technology and Engineering Solutions of Sandia, LLC, a wholly owned subsidiary of Honeywell International, Inc., for the U.S. Department of Energy's National Nuclear Security Administration under contract DE-NA0003525.



Sandia National Laboratories

Issued by Sandia National Laboratories, operated for the United States Department of Energy by National Technology and Engineering Solutions of Sandia, LLC.

NOTICE: This report was prepared as an account of work sponsored by an agency of the United States Government. Neither the United States Government, nor any agency thereof, nor any of their employees, nor any of their contractors, subcontractors, or their employees, make any warranty, express or implied, or assume any legal liability or responsibility for the accuracy, completeness, or usefulness of any information, apparatus, product, or process disclosed, or represent that its use would not infringe privately owned rights. Reference herein to any specific commercial product, process, or service by trade name, trademark, manufacturer, or otherwise, does not necessarily constitute or imply its endorsement, recommendation, or favoring by the United States Government, any agency thereof, or any of their contractors or subcontractors. The views and opinions expressed herein do not necessarily state or reflect those of the United States Government, any agency thereof, or any of their contractors.

Printed in the United States of America. This report has been reproduced directly from the best available copy.

Available to DOE and DOE contractors from
U.S. Department of Energy
Office of Scientific and Technical Information
P.O. Box 62
Oak Ridge, TN 37831

Telephone: (865) 576-8401
Facsimile: (865) 576-5728
E-Mail: reports@osti.gov
Online ordering: <http://www.osti.gov/scitech>

Available to the public from
U.S. Department of Commerce
National Technical Information Service
5301 Shawnee Rd
Alexandria, VA 22312

Telephone: (800) 553-6847
Facsimile: (703) 605-6900
E-Mail: orders@ntis.gov
Online order: <http://www.ntis.gov/search>



Novel Method to Characterize and Model the Multiaxial Constitutive and Damage Response of Energetic Materials

Md Fazle Rabbi, Robert Mach, Carlos A. Catzin, Calvin M. Stewart
Department of Mechanical Engineering
The University of Texas at El Paso
500 W. University
Suite A126
El Paso, TX 79968-0521

Michael J. Kaneshige
Weapon Product Support
Sandia National Laboratories
P. O. Box 5800
Albuquerque, New Mexico 87185-MS1454

Abstract

Simulant polymer bonded explosives are widely used to simulate the mechanical response of real energetic materials. In this paper, the fracture resistance of a simulant polymer bonded explosive (PBX) is experimentally investigated. The simulant is composed of 80 wt.% soda lime glass beads (SLGB) and 20 wt.% high impact Polystyrene 825 (HIPS). Brazilian disk tests are performed to characterize the tensile and compressive properties. Fracture toughness and energy tests are performed in the semi-circular bending (SCB) configuration on 80, 81, 82, and 83 wt% SLGB compositions. Digital image correlation is performed to record the surface displacements and calculate surface strains during testing. The micromechanical behavior of ductile and brittle fracture are evaluated using digital microscopy and scanning electron microscopy of the fracture surface. It is determined that (i) the manufacturing process produces a credible simulant of PBX properties, and (ii) the SCB test measures fracture resistance with a reasonable coefficient of variation.

ACKNOWLEDGMENTS

This project is supported by Sandia National Laboratories. We are truly thankful to Michael J. Kaneshige for his unconditional support during this time period. We would also like to express our gratitude to him for providing insight, knowledge, and expertise that assisted the research greatly. His comments on our newly developed novel method of manufacturing mock energetic materials, mechanical testing methods, and digital image correlation technique helped us to understand the sources of uncertainty in our experiments. We are also thankful to Jaime Moya and Vieta M. Crain from Sandia National Laboratories for their cooperation.

This research work would not have been possible without our advisor Dr. Calvin M. Stewart's countless support, guidance, and feedback. He mentored us throughout the process, providing encouragement to solve in-situ problems and constantly inspire us with his broad vision. We appreciate his time and effort to make this research successful.

We greatly acknowledge the chair of the Mechanical Engineering department Professor Ahsan R. Chowdhury for providing the facility and proper environment to conduct research and arranging useful training on time to time basis. We are also grateful to Dr. David Roberson for helping us in the early days of developing a manufacturing process for our mock energetics. We deeply appreciate our research team who gave suggestion at various stages of this research.

TABLE OF CONTENTS

1.	INTRODUCTION	13
2.	MATERIAL AND TEST METHODS	16
2.1.	Material and Manufacturing	16
2.2.	Semi-Circular Bending Test (SCB)	18
2.3.	3D Digital Image Correlation	20
3.	RESULTS AND DISCUSSION	20
3.1.	Tensile and Compressive Properties	20
3.2.	Fracture Resistance	21
3.3.	Digital Image Correlation	25
3.4.	Fractography	27
3.5.	Discussion	33
4.	CONCLUSIONS.....	34
	REFERENCES	35
	APPENDIX: INTERIM REPORT ON MANUFACTURING AND DIC OF PBX	39
1.	INTRODUCTION	39
1.1.	Technical Approach	40
1.2.	Relationship to Prior and Other On-going Work	41
1.3.	Goals, Objectives, and Project Milestones	42
1.4.	Year 1 Outcomes.....	42
2.	MATERIALS.....	43
2.1.	Material Justification	44
2.1.1.	High Impact Polystyrene (HIPS)	46
2.1.2.	Soda Lime Glass Beads.....	47
2.2.	Particulate Composite	48
2.3.	Microstructural Characterization	49
3.	SPECIMEN MANUFACTURING PROCESS OF MOCK PBX/HPC	49
3.1.	Overview and Background Information	49
3.1.1.	Personal Protective Equipment and Safety	50
3.1.2.	Manufacturing and Equipment.....	50
3.1.3.	Manufacturing Procedure of Heterogeneous Particulate Composite (HPC)	51
3.1.4.	Manufacturing Issues	56
3.2.	SPECIMEN MACHINING	61
3.2.1.	Machining Equipment.....	61
3.2.2.	Machining Process	61
3.2.3.	Bridgman Notch Procedure for Mock Polymer-Bonded Explosive	62
3.3.	MECHANICAL TESTS	62
3.3.1.	Overview	64
3.3.2.	Uniaxial Compression Test.....	65
3.3.3.	Indirect Tensile (Brazilian) Test	69
3.3.4.	Semi-Circular Bending (Half Brazilian) Test	71
3.3.5.	Bridgman Notch Test	73

4.	DIGITAL IMAGE CORRELATION (DIC)	76
4.1.	Digital Image Correlation Overview	76
4.1.1.	Introduction	77
4.1.2.	3-D Digital Image Correlation	80
4.1.3.	DIC Parameters	80
5.	RESULTS & DISCUSSION.....	82
5.1.	Uniaxial Compression.....	82
5.2.	Indirect Tensile (Brazilian) Test	85
5.3.	Semi-Circular Bending (Half Brazilian) Test	88
5.4.	Bridgman Notch Test.....	89
	REFERENCES	90

FIGURES

Figure 1.	Comparative plot of different PBXs with (a) fracture toughness range and binder weight percentage, (b) fracture energy and binder weight percentage.....	14
Figure 2.	Specimen preparation (a) manufacturing setup (b) product (c) incised view	16
Figure 3.	Temperature, Pressure, and Time Process of Manufacture	17
Figure 4.	Semi-circular bending test (a) setup (b) strain energy measurement	17
Figure 5.	Digital image correlation (a) 3D setup and (b) speckled specimen with exaggerated notch	19
Figure 6.	Stress-Strain Response of PBX simulant (80-10 wt.%) in (a) indirect tension and (b) compression.....	20
Figure 7.	Load-displacement curve for PBX with a brittle and ductile failure.....	21
Figure 8.	Load-displacement curve for PBX simulant at (a) 80-20, (b) 81-19, (c) 82-18, and (d) 83-17 wt% compositions	22
Figure 9.	Fracture resistance and corresponding COV of PBX simulant with respect to binder wt%: (a) Fracture Toughness and (b) Fracture Energy	24
Figure 10.	(a) Load-displacement curve corresponding to von Mises strain (b) crack propagation with time and (c) von Mises strain contours for an 80-20% composition	25
Figure 11.	Micrograph of SCB specimen (a) notch tip, (b) mid-section, (c) top section, and (d) complete crack path.....	27
Figure 12.	(a) PBX Simulant after testing, (b) Brittle fracture of face I and II at 1000x 1000 pixel, (c) Ductile fracture of face I and II at 1000 x 1000 pixel, (d) Measurement of SLGB of fracture surface	28
Figure 13.	Notch disconformity of 80-20 wt.% PBX simulant	29
Figure 14.	SEM micrographs of ductile specimen at various locations of fracture surface, (a) Top left, (b)Top center (c) Top right, (d) Mid left, (e) Mid center, (f) Mid right, (g) Notch left, (h) Notch center and (k) Notch right.....	30
Figure 15.	SEM micrographs of brittle specimen at various locations of fracture surface, (a) Top left, (b)Top center (c) Top right, (d) Mid left, (e) Mid center, (f) Mid right, (g) Notch left, (h) Notch center and (k) Notch right.....	31

Figure 16. SEM image of a specimen (a) machined surface before fracture, (b) ductile surface and (c) brittle surface after fracture	32
Figure 17. 3D surfacing image of (a) ductile, and (b) brittle specimen.....	32
Figure 18. Depiction of crack path (a) in ductile and (b) brittle materials	33
Figure 19. PBX used as a Solid Rocket Propellant.....	39
Figure 20. High Impact Polystyrene Pellets	46
Figure 21. SEM of an ultra-thin section of HIPS.....	46
Figure 22. Molecular Structure of HIPS	47
Figure 23. Stress-Strain curve of HIPS at different test temperatures: determined on injection-molded test specimens.....	47
Figure 24. Stress-Strain curve of general purpose polystyrene and HIPS in a tensile test in accordance with ISO 527	47
Figure 25. Micron size Soda Lime Glass Beads	47
Figure 26. Composition 1 and its internal structure.....	48
Figure 27. Composition 3 and its internal structure.....	48
Figure 28. Comparison of the different Compositions	48
Figure 29. Optical Microscopy of HPC optimal composition (50-50).	49
Figure 30. Station Preparation with Tools for Manufacturing Process.	51
Figure 31. HIPS (Left) and SLGB (Right).....	51
Figure 32. Weighing of Constituent Material.	51
Figure 33. Resulting Desired “Clumpy” Texture of Soda Lime Glass Beads with H ₂ O.....	52
Figure 34. Applying Silicone Release Spray to PBX Mold.....	52
Figure 35. Placing and locking with cylindrical mold in pneumatic press.	53
Figure 36. Electrical Heater applied to the cylindrical mold.	53
Figure 37. RAM control and die moved fully up.....	53
Figure 38. Moving die adjusted up to eliminate the space with the mold.	54
Figure 39. Pouring in of mixture into metallic tube (A). Locking, external die being place on top of cylindrical mixture to compress the mixture (B). Locking die turned to ‘locked’ position to ensure safe compression of materials (C).....	54
Figure 40. Heat Sinks applied over the metallic mold.....	55
Figure 41. Mock PBX sample within the metallic mold (A). The mock PBX sample after removal from the mold (B), and the locking die as well (C).....	55
Figure 42. Interior Voids within Defective PBX Samples Made with 2 grams of H ₂ O.	57
Figure 43. Several Defective PBX Samples Made with no amount of water.....	57
Figure 44. Inner Face (Left) and Top Face (Right) of a PBX Samples Made with 2 grams of H ₂ O (A) and the Inside of Another PBX Sample Made with 2 grams of H ₂ O (B).	58
Figure 45. Outer Face (Left) and Inner Face (Right) of PBX Samples Made with .5 grams of H ₂ O.....	59
Figure 46. (A) Inner face (left) and top and bottom face (B) of a PBX Specimen manufactured with the finalized manufacturing process.....	59
Figure 47. Voids Within Defective PBX Samples Made with Optimized Process.	60
Figure 48. Flawed PBX Due to Pressure Failure.....	61
Figure 49. Bridgman Notch Specimen.....	62
Figure 50. CAD Model of Bridgman Notch Specimen.	62
Figure 51. Uniaxial compression test configuration	66

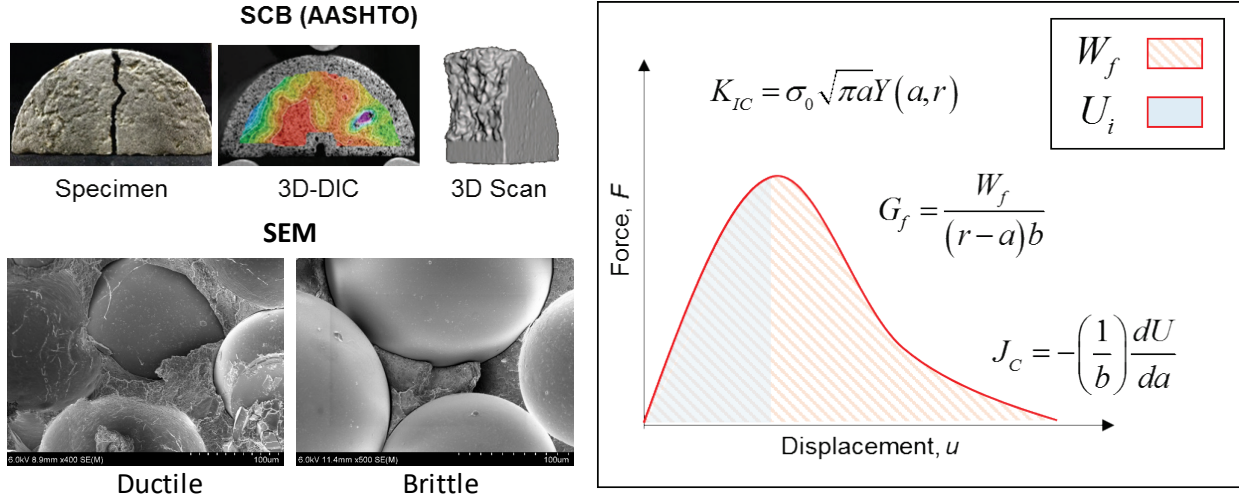
Figure 52. Typical Stress-Strain curve.....	66
Figure 53. Quasi Static Uniaxial compression Testing Specimen.....	68
Figure 54. Indirect tension test configuration.....	69
Figure 55. Indirect Tensile (Brazilian) Specimen before Speckle pattern.....	71
Figure 56. Semi-circular bending test configuration.....	71
Figure 57. Expected Load versus displacement curve.....	72
Figure 58. Semi-circular (Half-Brazilian) testing Specimen.....	73
Figure 59. Bridgman notched testing configuration.....	74
Figure 60. Characterizations of 3D stress state.....	74
Figure 61. Bridgman Notch Testing Specimen.....	76
Figure 62. Digital Image Correlation Contour Examples.....	77
Figure 63. Actual VIC-3D Setup Used During Mechanical Tests. Uniaxial compression test shown.	78
Figure 64. Examples of High-Quality Speckle Patterns.	79
Figure 65. Speckle pattern on Testing Specimens.....	80
Figure 66. Calibration Pad and post processing images report examples.....	81
Figure 68. Initial Effective Poisson's Ratio.....	82
Figure 67. Stress vs Strain curve of glass-HIPS specimen.....	82
Figure 69. Effective Poisson's Ratio at different applied strain.....	83
Figure 70. Displacement Vector Prior to total fracture.....	83
Figure 71. Strain components contour distribution of (a) extensive strain (b) compressive strain and (c) shear strain prior to total failure.....	84
Figure 72. Fractured Specimen.....	84
Figure 74. Stress vs Strain Curve of Brazilian Test.....	85
Figure 73. Virtual gauges and extensometer applied to Brazilian Specimen.....	85
Figure 75. Effective Poisson's ratio of Brazilian Specimen.....	86
Figure 76. Strain components contour distribution of (a) extensive strain (b) compressive strain	86
Figure 77. Equivalent Strain Contour.....	87
Figure 78. Fracture morphology.....	87
Figure 79. Stress vs Strain curve of SCB specimen.....	88
Figure 80. Equivalent Strain of SCB specimen.....	88
Figure 81. Vector Field of displacement for a post-failure SCB specimen.....	88
Figure 82. Stress vs Time plot of Bridgman notch specimen.....	89

TABLES

Table 1. Survey of Fracture Parameters of PBX and PBX simulants [7-10].....	14
Table 2. Specimen dimensions.....	18
Table 3. Fracture resistance of the 80-20 wt% specimens.....	23
Table 4. Fracture resistance of the 81-19 wt% specimens.....	23
Table 5. Fracture resistance of the 82-18 wt% specimens.....	23
Table 6. Fracture resistance of the 83-17 wt% specimens.....	24
Table 7. Different Polymer Binder Materials used in the manufacturing process of PBX.	45
Table 8. Energetic materials and their simulant counterpart.	45
Table 9. Different manufactured compositions of the glass-HIPS mock PBX.....	49

Table 10. MERG Testing Equipment	63
Table 11. Expected Failure modes table for HPC.....	82

EXECUTIVE SUMMARY



This study aims to create a scientific breakthrough in the ability to predict the mechanical behavior of energetic materials through the design of a new multiaxial testing method using three dimensional (3D) digital image correlation (DIC). This breakthrough has the possibility of leading to the development of new continuum damage mechanics (CDM) based constitutive models for the volumetric and deviatoric response of energetic materials.

A new method is developed and optimized to manufacture a polymer bonded explosive (PBX) simulant. After reviewing literature, soda lime glass beads (SLGB) were selected as a mock energetic particulate as it provides a high modulus contrast between the energetic particles and binder material with a particle density similar to real energetics. Other physical properties of real energetic crystals are ignored for the simplification of the manufacturing process. High impact polystyrene (HIPS) is used as binder due to its viscoelastic properties. The optimization of our simulant manufacturing process is illustrated within this Report and the early development of this process comprehensively explained in the Appendix. Brazilian disk tests were performed on PBX simulants with a 80-20 wt.% SLGB-HIPS composition to establish the credibility of PBX simulant. The semi-circular bending tests (SCB) were performed on 80, 81, 82, and 83 wt% SLGB compositions. The fracture energy and fracture toughness of the four PBX simulant compositions are calculated and compared to each other. The displacement and strain field on the surface of the specimen is computed using 3-D digital image correlation (3D-DIC) systems. Using the 3D-DIC software, the Von Mises strain is calculated and applied to evaluate the fracture mechanics under quasi-static loading condition. The notch tip and fracture surface of specimens are examined using a Hitachi TM 1000 Tabletop Scanning Electron Microscope and a Hitachi S 4800 Scanning Electron Microscope.

It is observed that stress is concentrated at the machined notch tip. During the fracture process, crack initiation, interfacial debonding, and slip drive crack propagation through the particle-binder interface. During crack propagation, SLGB particles are observed to fall out of the fracture surface indicating weak adhesion of the particulate-binder interface. Upon loading, the strain at notch tip increases until the peak load is reached and a single tortuous crack is observed. Brittle fracture is observed in specimens with short notch depths while ductile fracture is

observed in specimens with long notch depths. The problem of brittle and ductile fracture persists in all four compositions. The machined notch, crack path, and fracture surface are examined using SEM micrographs. The machined notch depth and width exhibited a high coefficient of variation due to SLGB pull out and polymer flow when cutting the notch. This nonconformity generates a large variation in fracture toughness and fracture energy from batch to batch. It is found that the notch tip condition is one of the major parameters that dominate the uncertainty of brittle and ductile failure. Due to the high uncertainty of experiments, a focus was placed on exploring this uncertainty with a large test matrix of experiments (70+).

In future work, experiments will be prepared to explore the strain rate (0.001 to 1 s^{-1}) and temperature (ambient to 75°C) effects. There is a need to develop a microstructure-level DIC system to obtain a more accurate and clearer picture of the micromechanics within these materials. An outcome of this novel characterization method will be the development of a CDM-based constitutive model for the prediction of the “batch-to-batch” mechanical behavior of energetic materials. This model will be used to simulate the service conditions of mock polymer bonded explosive (PBX) material including uniaxial and multiaxial states of static and dynamic loading.

NOMENCLATURE

Abbreviation	Definition
PBX	Polymer Bonded Explosive
K_{Ic}	Fracture toughness
SCB	Semi-Circular Bend
LEFM	Linear Elastic Fracture Mechanics
EPFM	Elastic-Plastic Fracture Mechanics
G_f	Fracture resistance
DIC	Digital Image Correlation
SEM	Scanning Electron Microscope
SLGB	Soda Lime Glass Beads
HIPS	High Impact Polystyrene
CNC	Computer Numerical Controlled
J_c	Critical strain energy release rate
W_f	Work of fracture
W	Area under the experimental load-displacement curve
W_{tail}	Area under an extrapolated continuation/tail of the curve to zero
P_i	Applied load
u_i	Load-line displacement
u_c	Load line displacement value at which the test is stopped
$Y_{I(0.8)}$	Dimensionless geometric factor
σ_0	Applied stress
CCD	Charge-Coupled Device
UTS	Ultimate Tensile Strength
IDT	Indirect Tensile Strength
COV	Coefficient of Variation

1. INTRODUCTION

Polymer bonded explosives (PBXs) are a complex class of particulate composite material that is formed by two constituent materials: energetic crystals in a polymer binder [1]. These PBXs may also consist of a small percent of additives like plasticizers, oxidizers, and antioxidants that are added to the ratio composition to improve the explosive output and decrease the effects of aging [2]. The energetic crystals typically comprise about 60 to 98% of the total mass of the composite, depending on the desired explosive output [3]. PBXs are relatively insensitive to shock. This is due to the viscoelastic-plastic polymer binder that absorbs mechanical energy to prevent friction between the energetic crystals that would result in detonation. Fracture resistance is a key metric to evaluate the sensitivity of solid explosives. To improve the insensitivity characteristics of PBXs, credible simulants that replicate the mechanical behavior and fracture resistance of real PBX have been developed. The fracture resistance of the simulants could then be safely optimized to determine the ideal composition for future PBXs.

Many quantitative studies on the fracture resistance of PBXs have been performed. Chen et al performed SCB fracture tests on a generic PBX simulant to calculate plain strain fracture toughness, K_{Ic} and determined that the dominant fracture mode is decohesion of the particle-binder interface [4]. The researchers then performed a comparative study of the fracture toughness of three-point bending, semi-circular bending (SCB), and flattened Brazilian disc tests and determined that the fracture toughness of PBX is consistent irrespective to specimen geometry [7]. The team went on to applied high-speed DIC to characterize the K_{Ic} as a function of strain rate using a split Hopkinson pressure bar and found that the fracture resistance increases with the strain rate [8]. Liu et al went on to measure the variation of fracture toughness as a function of crack growth [9]. A craze zone is observed where sizable aligned polymer molecules form bridges at the crack tip. Fracture characterization and prediction using the fracture toughness is not sufficient, since the craze zone redistributes stress creating a large process zone such that the local stress-intensity factor may not even exist [9].

Polymer bonded explosives exhibit a viscoelastic-plastic response, where cracks tend to grow through the polymer binder, along the binder-particle interfaces. This tortuous cracking process creates a large plastic zone that exceeds the small-scale plasticity limitation of linear elastic fracture mechanics (LEFM). Fracture toughness has continued to be applied to analyze the fracture resistance of PBXs despite the deficits of LEFM [4-9]. As an alternative, elastic-plastic fracture mechanics (EPFM) can be introduced to measure the fracture resistance. In EPFM, fracture resistance is measured using the fracture energy, G_f better known as the critical strain energy release rate, J_c . Efforts to explore the utility of as a fracture resistance metric for PBXs are underway [10,11].

Table 1. Survey of Fracture Parameters of PBX and PBX simulants [6-11]

Name	Type	K_{Ic} ($MPa\sqrt{m}$)	G_f ($KJ \cdot m^{-2}$)	Reference
RM-03-AG	Mock 89.5/10.5	0.602±0.030 0.659±0.026	0.016 0.042	[11]
LX-17	PBX 92.5/7.5	0.317±0.024 0.366±0.019	0.012 0.030	
PMMA	Plexiglas	1.749±0.325	1.157	
PBS 9501	Mock 95/5	N/A	0.111	[10]
EDC1032	Mock 85/15	N/A	0.657	
EDC1037	Mock 91/9	N/A	0.0153	
Mock 900-21	Mock 94/6	0.200±0.010	N/A	[9]
N/A	Mock-95/15	0.523±0.038 0.498±0.023 0.530±0.010	N/A	[8]
JOB-9003	PBX	0.240±0.010	N/A	[6]
JO-9159	PBX	0.170±0.010		
JB-9014	PBX	0.370±0.010		

Note: N/A means not available

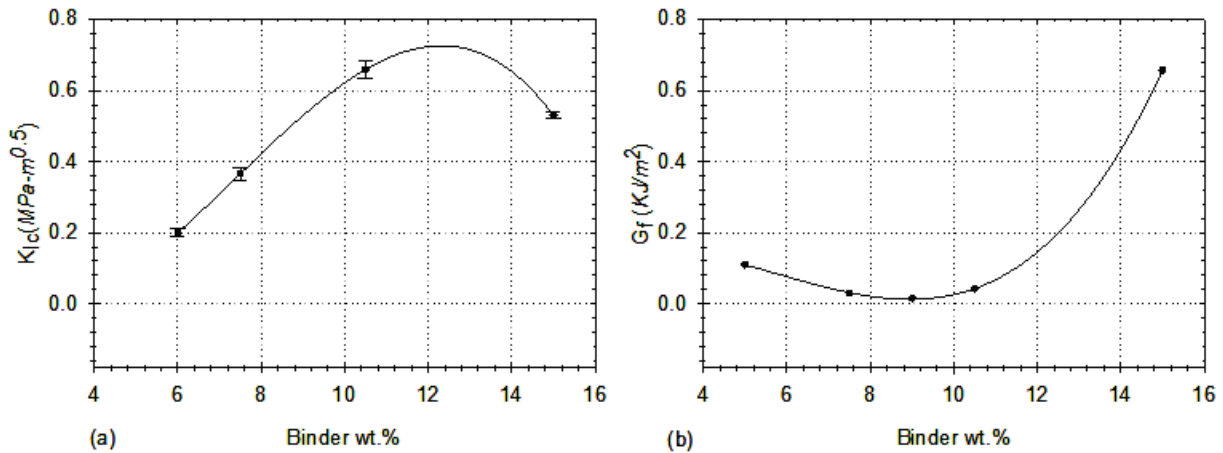


Figure 1. Comparative plot of different PBXs with (a) fracture toughness range and binder weight percentage, (b) fracture energy and binder weight percentage

Fracture toughness and energy with different binder weight percentages, composed from several dissimilar mock PBXs, are stated in Table 1. Most of the mechanical property data available in literature for PBX is of simulants. The PBX simulants are different both chemically and by weight percentage and produce unique fracture resistance. When this fracture toughness and energy are plotted with respect to weight percentage, an interesting trend is observed as shown in Figure 1. There exists a binder wt.% where the fracture toughness is maximized and the fracture energy is minimized. This trend may not be true due to the different materials used in the PBXs.

The motivation of this study is to determine if a similar trend can be observed in a PBX composed of the same materials at different binder wt.%.

Strain field distribution on PBX simulants, in particular near notch tip for different compositions has been analyzed to evaluate deformation pattern by Digital image correlation (DIC) method. It is a non-contact displacement measurement technique [4]. Quantitative and qualitative studies on the fracture behavior of PBX have been performed using DIC. The DIC method is applied as a real-time tool to locate the site of crack initiation and track propagation to rupture [9]. It has been applied to calculate the thermal expansion and Poisson's ratio [12]. It can be quantitatively applied to record strain using virtual strain gauges depicted as contours, isolines, and/or vectors [12,13]. Micro and SEM-based DIC have been employed to study the dynamic micro-cracking process at the binder-particle interfaces [14]. Three-dimensional DIC has been employed to measure the out of plane displacement in cylindrical PBX specimen [16]. The DIC method has been applied to study the shock sensitivity of PBX at high strain rates [17,18]. Studies using DIC have shown that the ASTM standard E1820 for fracture toughness of metallic materials is suitable for obtaining a homogenized description of fracture in PBXs [9]; however, further investigation into the fracture energy, G_f metric for PBXs need to be performed.

In this study, the fracture behavior and resistance of a polymer bonded explosive will be reported. An 80 wt.% soda lime glass and 20 wt.% high impact polystyrene PBX simulant is manufactured and subjected to indirect tensile and compression tests to establish the credibility of the simulant. The semi-circular bending (SCB) test is applied to measure the fracture toughness and energy. This process is repeated for three different compositions of PBX simulant that includes different notch dimension and manufacturing temperature. Statistical analysis of the two fracture resistance metrics is performed. Three-dimensional digital image correlation (3D-DIC) is performed to analyze the fracture behavior of the PBX simulant. Micrographs from a scanning electron microscope (SEM) are investigated to evaluate the bonding of the particle polymer interface, as well as the ductile and brittle nature of fracture and dissemination of crack path.

2. MATERIAL AND TEST METHODS

2.1. Material and Manufacturing

The PBX simulant in this study is composed of spherical soda lime glass beads (SLGB) and Polystyrene 825 [30]. The soda lime glass beads (SLGB) offers a high modulus contrast between the particle and binder plasticizer. The SLGB were manufactured by Jaygo Corp with an average diameter of $200\ \mu\text{m} \pm 50\ \mu\text{m}$, density of $1.02\ \text{g}\cdot\text{cm}^{-3}$, elastic modulus of 63 GPa, and Poisson's ratio of 0.20. The average diameter is within the range of the real energetic Pentaerythritol tetranitrate (PETN) at 44-850 μm .

High impact Polystyrene (HIPS) 825 is selected as the binder material because it is a classic and common binder employed in real PBX compositions [1]. The HIPS pellets were manufactured by Total Petrochemicals & Refining USA Inc. The Vicat softening and auto-ignition temperature of the HIPS is 205 and 440°C respectively with a melt flow at 200°F-5 kg of 8.0 g per 10 min. The product at room temperature has a density of $1.04\ \text{g}\cdot\text{cm}^{-3}$, elastic modulus of 2.275 GPa, tensile strength of 24.821 MPa, and Poisson's ratio of 0.35.

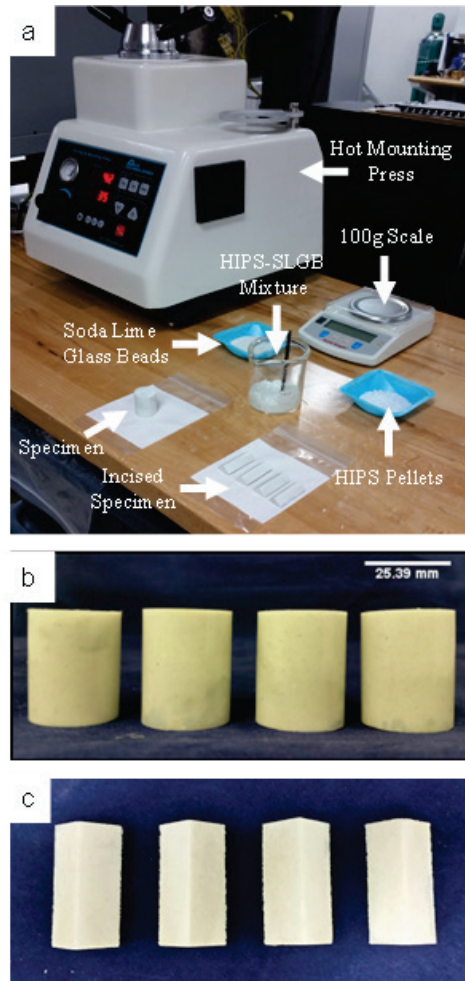


Figure 2. Specimen preparation (a) manufacturing setup (b) product (c) incised view

The PBX simulants are composed of varying weight percentages ranging from 80 wt% SLGB and 20 wt% HIPS to 83 wt% SLGB and 17 wt% HIPS. The manufacturing setup is depicted in Figure 2(a). The PBX simulant is prepared according to a newly established method [20]. A mixing beaker and stirring rod are used to prepare initial mixture of PBX simulant constituents. The SLGB is poured into the beaker and 0.5 mL of distilled water is added and mixed until the SLGB beads are well coated. The HIPS is added to the beaker and the mixture is stirred for 2 minutes. Water helps to induce a strong particle agglomeration effect where the SLGB binds to the HIPS pellets.

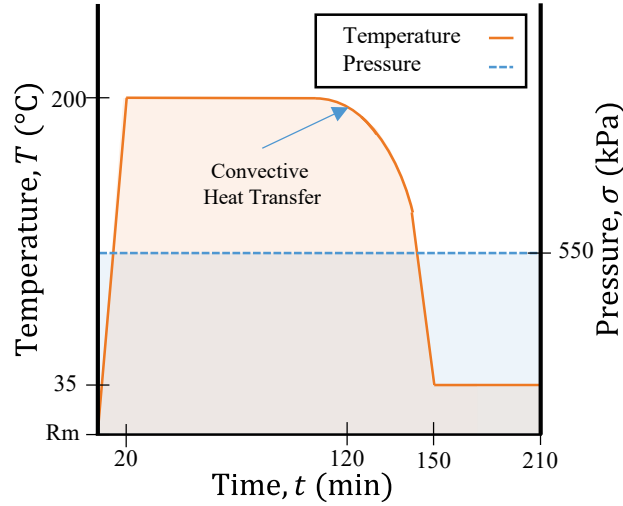


Figure 3. Temperature, Pressure, and Time Process of Manufacture

The PBX simulant is pressured together using hot pneumatic mounting press with a 25.4 mm mount. A temperature, pressure, and time manufacturing process plot is provided in Figure 3. Pressure is held at 550 kPa throughout compaction. The temperature is raised from room temperature to 200°C in 20 min and then held at 200°C for 100 minutes. The specimen is cooled using a water circulation tank for 30 minutes or until a temperature of 35°C is achieved. The pressure is held for an additional 60 min at 35°C before the manufacturing process is completed. The product is a 25.4 mm diameter and 34.3 mm length cylinder as shown in Figure 2(b). A symmetrically bisected specimen demonstrates the internal structure is visually defects free as shown in Figure 2(c).

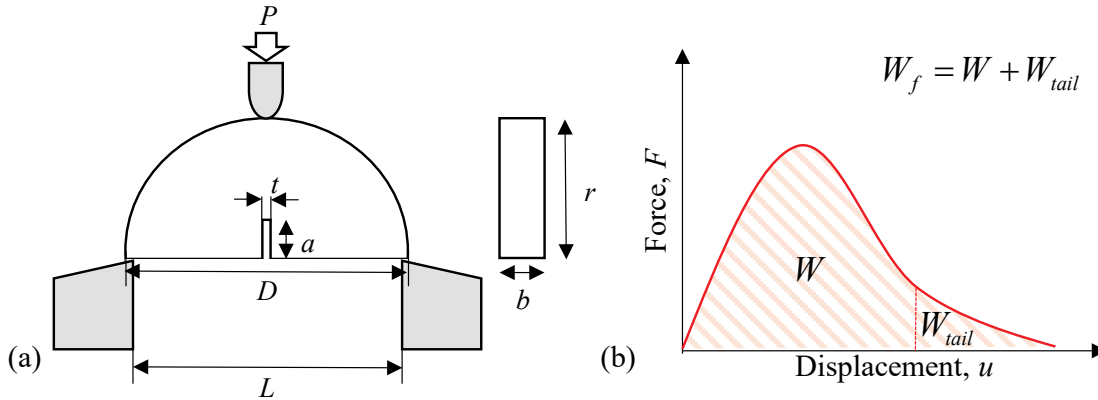


Figure 4. Semi-circular bending test (a) setup (b) strain energy measurement

Table 2. Specimen dimensions

Diameter, D	Thickness, b	Notch Depth, a	Notch Thickness, t	Notch Depth to Radius, a/r
(mm)	(mm)	(mm)	(mm)	
25.4	12.7	1.0	0.2	0.079

2.2. Semi-Circular Bending Test (SCB)

The SCB specimens are machined using a computer numerical control (CNC) machine. The dimensions are provided in Table 2. The SCB tests are conducted using an ADMET expert 5603 Table-Top universal test system with an MTESTQuattro controller. This electromechanical frame is equipped with a ± 4.5 kN load cell. During the test, the specimen is mounted in a three-point bend fixture and subjected to compression as illustrated in Figure 4(a) according to the AASHTO TP 105-13 standard [42]. Teflon tape and lubricate is applied to the compression platens to minimize friction. The distance between the support anvils, L is 23.4 mm. The diameter of the load and support anvils is 5 mm. An initial seating load of 80 N is imposed on the specimen. The SCB tests are executed under displacement control at a rate of 0.5 mm/min.

Fracture energy, G_f is calculated using the single-specimen geometry-specific solution of the critical strain energy release rate, J_c or a three-point bending specimen proposed by Rice [24]. The fracture energy is obtained by dividing the work of fracture, W_f the total area under the load vs. load line displacement curve depicted in Figure 4(b) by the ligament area, A_{lig} as follows

$$G_f = \frac{W_f}{A_{lig}}, \quad A_{lig} = (r - a)b; \quad (1)$$

where, G_f is the fracture energy (kJ-m^{-2}), W_f is the work of fracture (J), A_{lig} is the ligament area (mm^2), r is the specimen's radius (mm), a is the notch depth (mm), and b is the specimen thickness (mm). It should be noted that a unit conversion is needed to calculate G_f using the given units.

The work of fracture, W_f can be partitioned as follows

$$W_f = W + W_{tail} \quad (2)$$

where, W is the strain energy obtained from the area under the experimental load-displacement curve and W_{tail} is the area under an extrapolated continuation/tail of the curve to zero. The experimental strain energy, W is calculated using the quadrangle rule [25]

$$W = AREA = \sum_{i=1}^n (u_{i+1} - u_i) \cdot (P_i) + \frac{1}{2} \cdot (u_{i+1} - u_i) \cdot (P_{i+1} - P_i) \quad (3)$$

where P_i is the applied load and u_i is the load line displacement at the i step, and P_{i+1} is the applied load and u_{i+1} is load line displacement at the $i+1$ step. The extrapolated strain energy, W_{tail} is calculated by fitting a power law to the load-displacement curve as follows

$$P = \frac{c}{u^2} \quad (4)$$

This function is only valid for the portion of the post peak load-displacement curve below 60% of the peak. The extrapolated strain energy W_{tail} is calculated as

$$W_{tail} = \int_{u_c}^{\infty} P du = \int_{u_c}^{\infty} \frac{c}{u^2} du = \frac{c}{u_c} \quad (5)$$

where, u_c is the load line displacement value at which the test is stopped.

Fracture toughness, K_{Ic} is defined as the stress intensity factor corresponding to the initiation of the crack. The stress intensity factor should be computed as follows

$$K_{Ic} = Y_{I(0.8)} \sigma_0 \sqrt{\pi a} \quad (6)$$

where, $Y_{I(0.8)}$ is the dimensionless geometric factor, σ_0 is the applied stress, and a is the notch depth [24, 26]. The applied stress is calculated as $\sigma_0 = P_{max}/2rt$ where P_{max} is the peak load, and r and t are the specimen radius and specimen thickness respectively. The dimensionless geometric factor, $Y_{I(0.8)}$ is calculated [26] as follows

$$Y_{I(0.8)} = 4.782 + 1.219 \left(\frac{a}{r} \right) + 0.063 \exp \left[7.045 \left(\frac{a}{r} \right) \right] \quad (7)$$

where, a is the notch depth (mm) and r is the specimen's radius (mm).

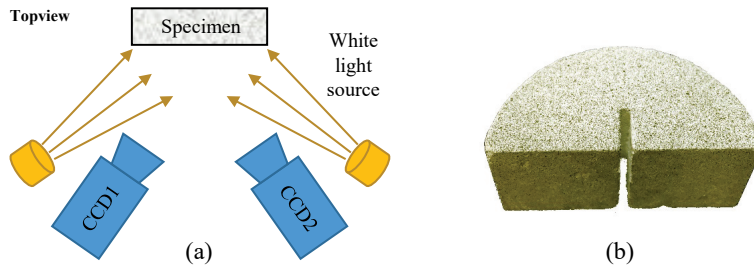


Figure 5. Digital image correlation (a) 3D setup and (b) speckled specimen with exaggerated notch

2.3. 3D Digital Image Correlation

In this study, the Correlated Solutions VIC-3D digital image correlation hardware and software package is employed. An illustration of the 3D-DIC setup is provided in Figure 5(a). Two charge-coupled device (CCD) cameras and 1500 Lumen LED white lights are focused on the specimen-testing zone. Photos of a calibration square are taken to provide a physical reference of pixel distances. Specimens are primed with a random speckle pattern as shown in Figure 5(b). The speckles act as physical reference points. The VIC-3D system and ADMET 5603 test machine are synchronized such that the ADMET load and VIC-3D displacement are at the same frequency. The 3D DIC software tracks the displacement of speckled reference points, compares the displacements to the calibrated physical reference, and calculates strain using the axioms of continuum mechanics. After testing, the images taken from 3D DIC are used to investigate the crack path, its evaluation with time and nature. The crack length is measured using an image processing and analysis software, ImageJ.

3. RESULTS AND DISCUSSION

3.1. Tensile and Compressive Properties

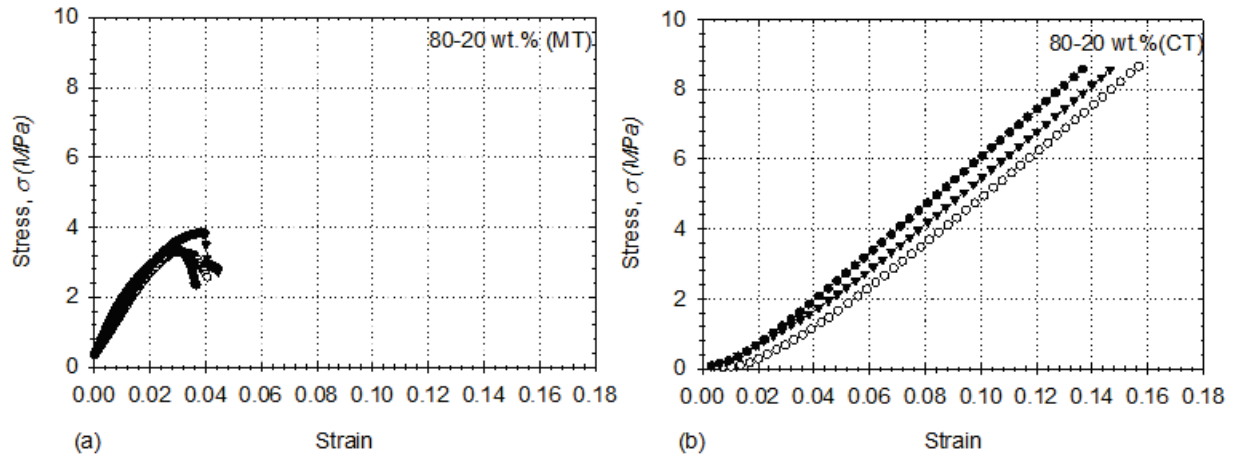


Figure 6. Stress-Strain Response of PBX simulant (80-10 wt.%) in (a) indirect tension and (b) compression

The tensile properties of the 80-20 wt.% PBX simulant are collected using indirect tensile (IDT) and compression tests based on ASTM D6931 and D695 respectively [21,22]. The average ultimate tensile strength (UTS) of the PBX simulant is measured 3.387 ± 0.5 MPa. Young's modulus of indirect tensile test is calculated as 128.6 MPa. Despite wide range of variability in mechanical properties of explosive materials, this 80-20 wt.% PBX simulant's ultimate tensile strength is aligned with PBX 9404 [41]. While specimens are undergoing the tensile tests, the specimens break apart comparatively quicker than compressive test as shown in Figure 6. It is observed that the specimens undergo extensive plastic deformation for compressive test and failure is ductile in nature. The IDT response of the PBX simulant is uniform in the elastic regime but varies once the material transitions into the plastic regime. The MT1, MT2, and MT3 tests are observed to harden non-linearly followed by a load drop that is arrested by a perfectly plastic response. This drop is likely due to a local weak-zone (perhaps a pileup of weakly bonded

SLGBs) where the particle-matrix interface breaks. The stiffness of the material is recovered via stress redistribution. In the IDT specimens, the crack initiates along the center of the specimens and propagates vertically toward the outer radius. In the cases involving a load drop, the primary crack bifurcates and secondary cracking initiates along the crack path.

3.2. Fracture Resistance

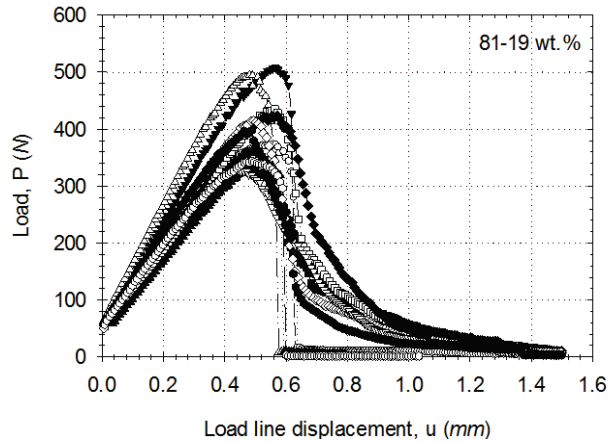


Figure 7. Load-displacement curve for PBX with a brittle and ductile failure

At all compositions both brittle and ductile fracture was observed. The reason for this random behavior is due to how the HIPS binder and SLGB particulate adhere during manufacturing. Example of this phenomena are depicted in Figure 7. Both the brittle and ductile fracturing specimens exhibit linear elastic regions; however, the brittle specimens have a higher slope at the load and displacement curve that indicate higher modulus of elasticity but less plasticity. The brittle specimens reached an average peak load of 417.12 N and fractured because they are unable to continue to carry load while the ductile specimen reach an average peak load of 385.99 N and gradually soften carrying load for a considerable amount of displacement. Among twelve 81-19 wt.% of PBX simulant semi-circular bending test, 28 percent are found brittle in nature and rest of 72 percent tests are found as ductile in nature. Ductile behaviors are prevailed because of the quantity and nature of polymer binder exists at 81-19 wt.% of PBX simulant. This brittle/ductile fracture issue is further described in section 3.4.

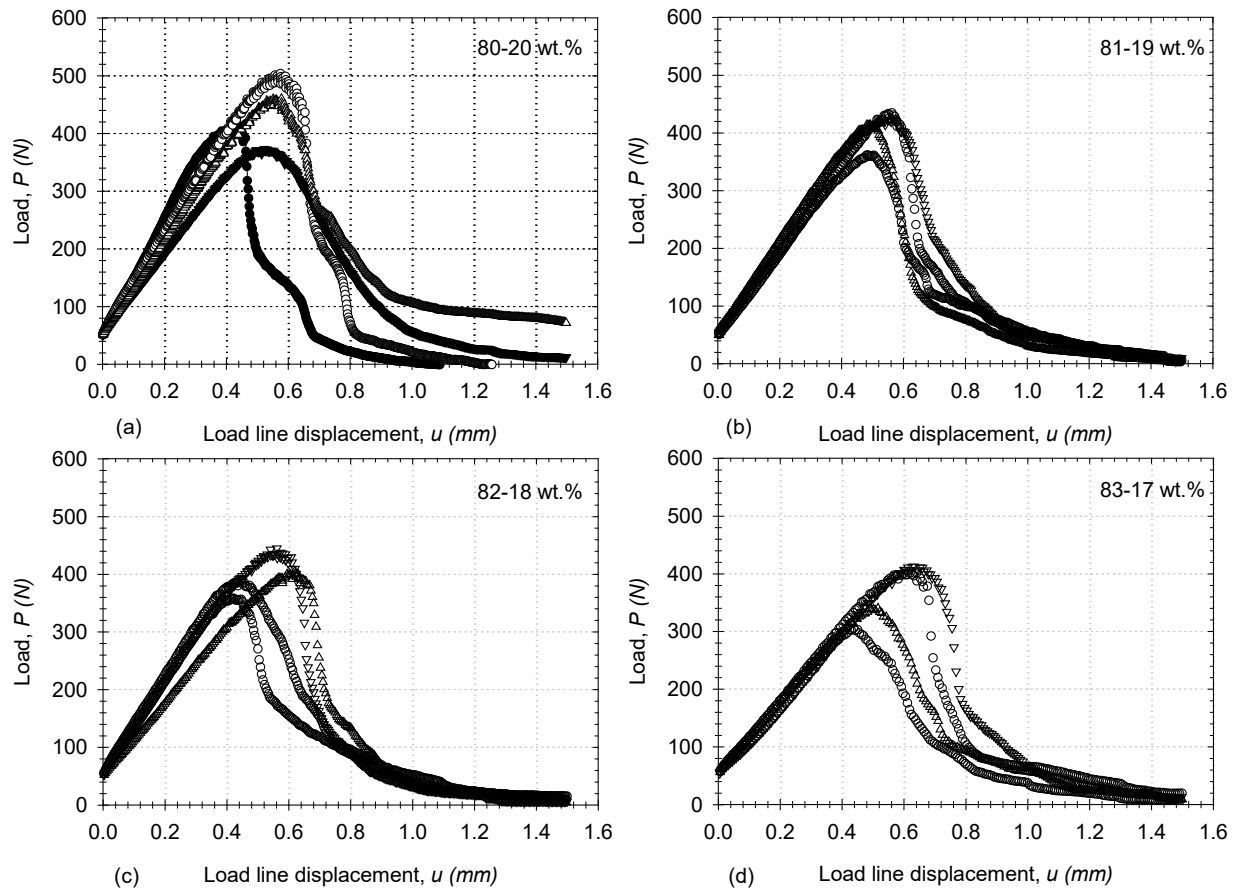


Figure 8. Load-displacement curve for PBX simulant at (a) 80-20, (b) 81-19, (c) 82-18, and (d) 83-17 wt% compositions

To analyze the fracture energy with respect to composition, the ductile behavior fracture test results were compared. SCB tests were ran for each weight percentage that was manufactured.

The load and displacement curves are shown in Figure 8. An average maximum load of 326, 401, 411, and 408 N are measured for the 83-17, 82-18, 81-19, and 80-20 wt% specimens respectively. The fracture energies are calculated for them to be 1.373, 1.504, 1.482, and 1.954 kJ/m² respectively. The coefficient of variation (COV) for fracture energy is also calculated for each weight percentage. For 83-17, 82-18, 81-19, and 80-20 wt% composition, the coefficient of variation of fracture energy are 30, 10, 8, and 26% respectively. This data is more elaborately stated in

Table 4 to Table 7.

Table 3. Fracture resistance of the 80-20 wt% specimens

Specimen Name	Notch Depth, a (mm)	Peak Load, P_{max} (N)	Work of Fracture, W_f (J)	Fracture Energy, G_f (kJ/m ²)	Fracture Toughness, K_{Ic} (MPa-m ^{0.5})
SN 1	0.770	464.33	0.304	2.139	0.374
SN 2	0.750	480.06	0.225	1.604	0.388
SN 3	0.630	499.71	0.190	1.271	0.348
SN 4	0.820	504.32	0.251	1.642	0.389
Average	0.743	487.11	0.243	1.664	0.375
St. Dev.	0.081	18.47	0.048	0.358	0.019
COV %	11%	4%	20%	22%	5%

Table 4. Fracture resistance of the 81-19 wt% specimens

Specimen Name	Notch Depth, a (mm)	Peak Load, P_{max} (N)	Work of Fracture, W_f (J)	Fracture Energy, G_f (kJ/m ²)	Fracture Toughness, K_{Ic} (MPa-m ^{0.5})
SN 1	0.919	362.61	0.200	1.413	0.318
SN 2	0.896	440.54	0.222	1.465	0.357
SN 3	0.802	424.75	0.243	1.657	0.337
SN 4	0.803	416.69	0.201	1.392	0.336
Average	0.855	411.148	0.216	1.482	0.337
St. Dev.	0.061	33.844	0.020	0.121	0.016
COV %	7%	8%	9%	8%	5%

Table 5. Fracture resistance of the 82-18 wt% specimens

Specimen Name	Notch Depth, a (mm)	Peak Load, P_{max} (N)	Work of Fracture, W_f (J)	Fracture Energy, G_f (kJ/m ²)	Fracture Toughness, K_{Ic} (MPa-m ^{0.5})
SN 1	0.613	359.01	0.185	1.282	0.256
SN 2	0.433	393.04	0.216	1.550	0.246
SN 3	0.660	446.37	0.227	1.608	0.337
SN 4	0.558	406.79	0.221	1.574	0.285
Average	0.566	401.304	0.212	1.504	0.281
St. Dev.	0.098	36.140	0.019	0.150	0.041
COV %	17%	9%	9%	10%	14%

Table 6. Fracture resistance of the 83-17 wt% specimens

Specimen Name	Notch Depth, a (mm)	Peak Load, P_{max} (N)	Work of Fracture, W_f (J)	Fracture Energy, G_f (kJ/m ²)	Fracture Toughness, K_{Ic} (MPa·m ^{0.5})
SN 1	0.720	407.07	0.235	1.642	0.316
SN 2	0.789	305.74	0.166	1.272	0.271
SN 3	0.798	420.89	0.246	1.697	0.338
SN 4	1.143	340.99	0.194	1.414	0.339
Average	0.863	368.672	0.210	1.506	0.316
St. Dev.	0.190	54.550	0.037	0.199	0.032
COV %	22%	15%	18%	13%	10%

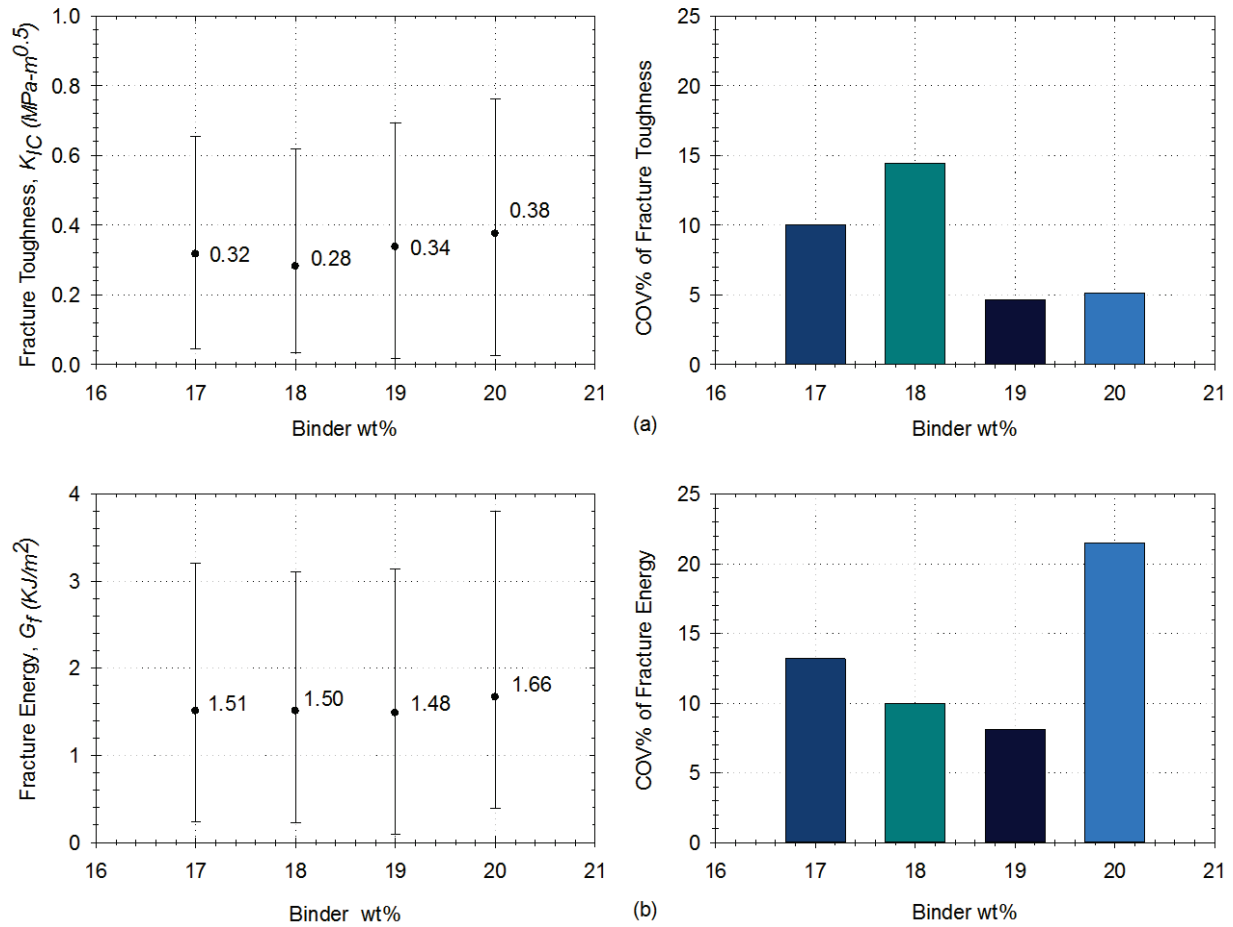


Figure 9. Fracture resistance and corresponding COV of PBX simulant with respect to binder wt%: (a) Fracture Toughness and (b) Fracture Energy

It is observed that even though the weight percentage of the SLGB decreases and the weight percentage of the Polystyrene pellets increases, the coefficient of variation for both fracture toughness and energy do not follow a monotonic pattern of decreasing or increasing as shown in Figure 9. However, it is assumed that the HIPS weight percentage is increased, the fracture toughness and strain energy release rate are increased. This is because the HIPS binder reduces the amount of voids that may occur at various matrices the SLGB have during manufacturing. This nature of alteration dominate PBX simulants ductile failure behavior.

3.3. Digital Image Correlation

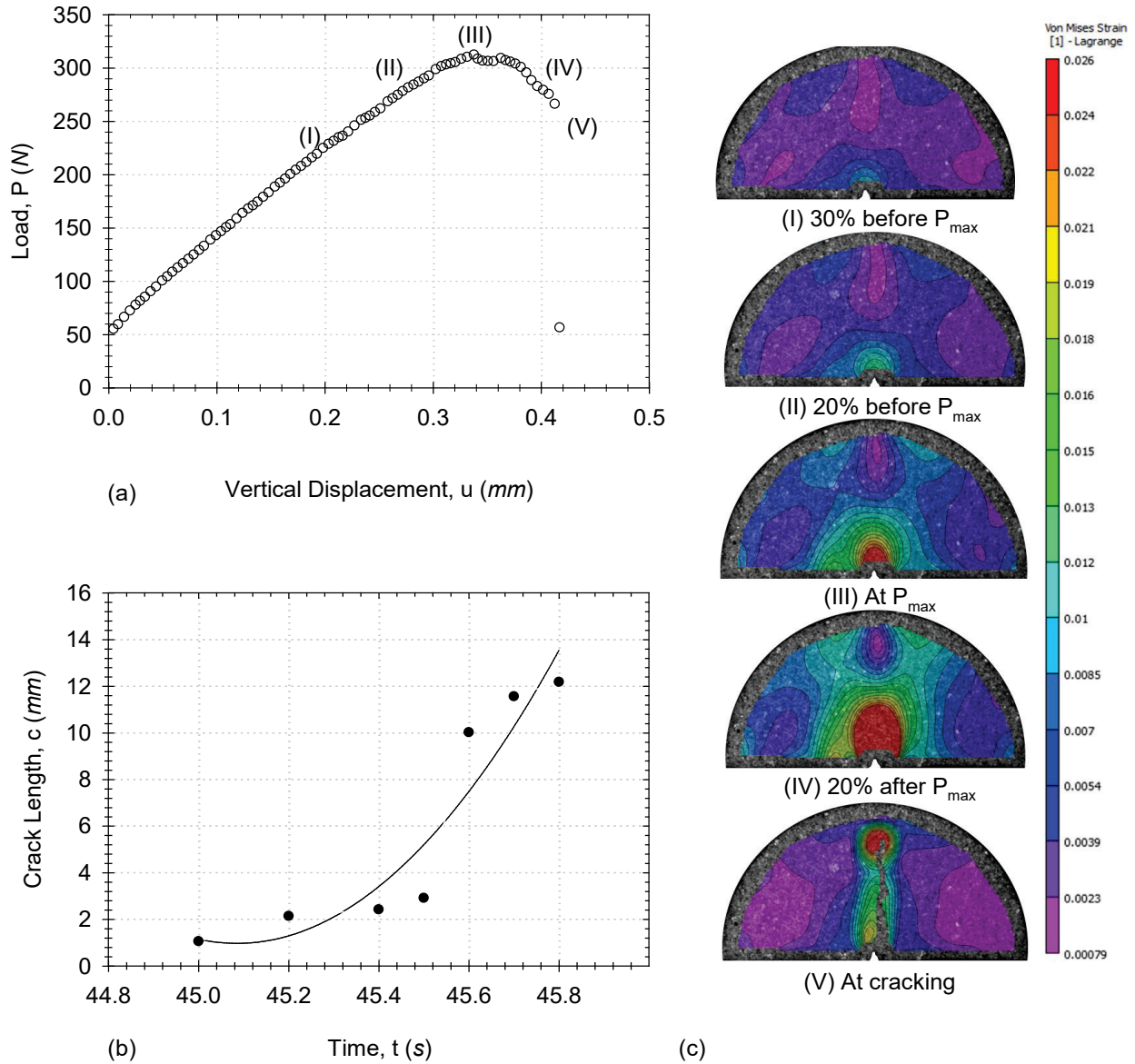


Figure 10. (a) Load-displacement curve corresponding to von Mises strain (b) crack propagation with time and (c) von Mises strain contours for an 80-20% composition

The 3D DIC system identified the primary crack initiation site, crack propagation path, and strain fields of the PBX simulant as shown in Figure 10.

Using the DIC system, contours of the von Mises strain are plotted over the specimen as shown in Figure 10(c). The von Mises strain, ε_{vm} is calculated as follows

$$\varepsilon_{vm} = \frac{1}{1+\nu'} \sqrt{\frac{1}{2} \left[(\varepsilon_1 - \varepsilon_2)^2 + (\varepsilon_2 - \varepsilon_3)^2 + (\varepsilon_3 - \varepsilon_1)^2 \right]} \quad (8)$$

$$\nu' = -\frac{\varepsilon_T}{\varepsilon_L}$$

where $\varepsilon_1, \varepsilon_2$ and ε_3 are the 1st, 2nd, and 3rd principal strains, ε_T and ε_L are the transverse and longitudinal strains, and ν' is the instantaneous Poisson's ratio. At 80% of peak load (I), a small strain concentration is observed at the notch. As the load increases, the strain concentration increases in size and intensity. At the peak load (III), ε_{vm} is maximized at 0.026. Low intensity strain concentrations appear on the outer radius of the specimen to the left and right of the load anvil. From the peak load (III) to post-peak load (IV), the size of the strain concentration increase suggesting the growth of the plastic zone. Between (IV) and (V), the critical strain energy release rate is exceeded and fracture occurs as indicated by the rapid extension of the crack.

Overall, the PBX simulant behaved like a heterogeneous material. Nevertheless, maximum peak load, fracture energy and fracture toughness showed high dependency on initial machined notch length. Upon fracture, the crack propagated from the notch tip and took a tortuous vertical path through the material. These findings help support the narrative that the manufacturing process in this study produces a credible PBX simulant.

3.4. Fractography

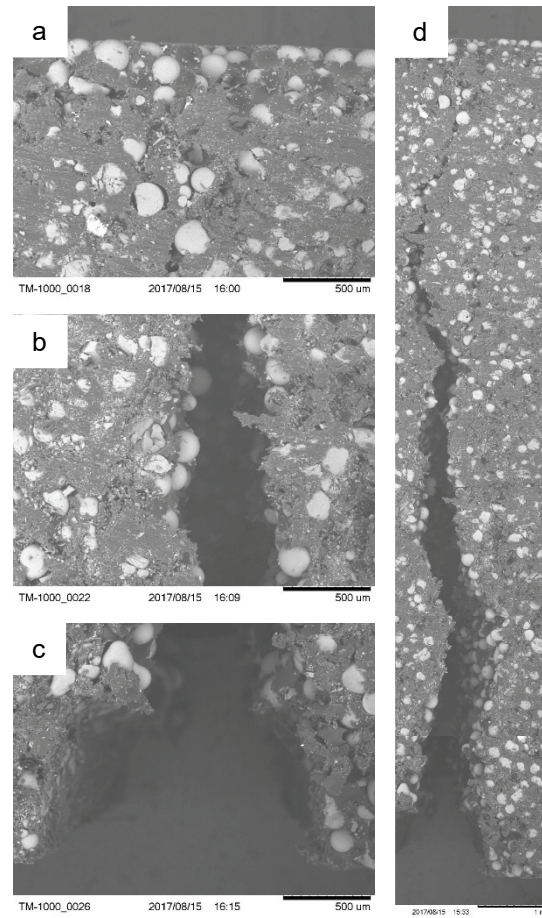


Figure 11. Micrograph of SCB specimen (a) notch tip, (b) mid-section, (c) top section, and (d) complete crack path

Scanning Electron Microscope was applied to analyze the crack propagation and the micromechanics of the failed specimens. An image of the notch tip was taken in order to observe the SLGB and HIPS matrix as shown in Figure 11(c). While there were usually a higher concentration of SLGB to HIPS, there was no major effect on crack initiation and crack propagation. SEM images of the crack path at midsection and notch tip are shown in Figure 11(b) and Figure 11(a) respectively. It is observed that cracking within the specimens occurred primarily in the HIPS binder due to the lack of fractured SLGB. Each specimen demonstrated cracking in a tortuous manner that was initiated by the prefabricated notch shown in Figure 11(d).

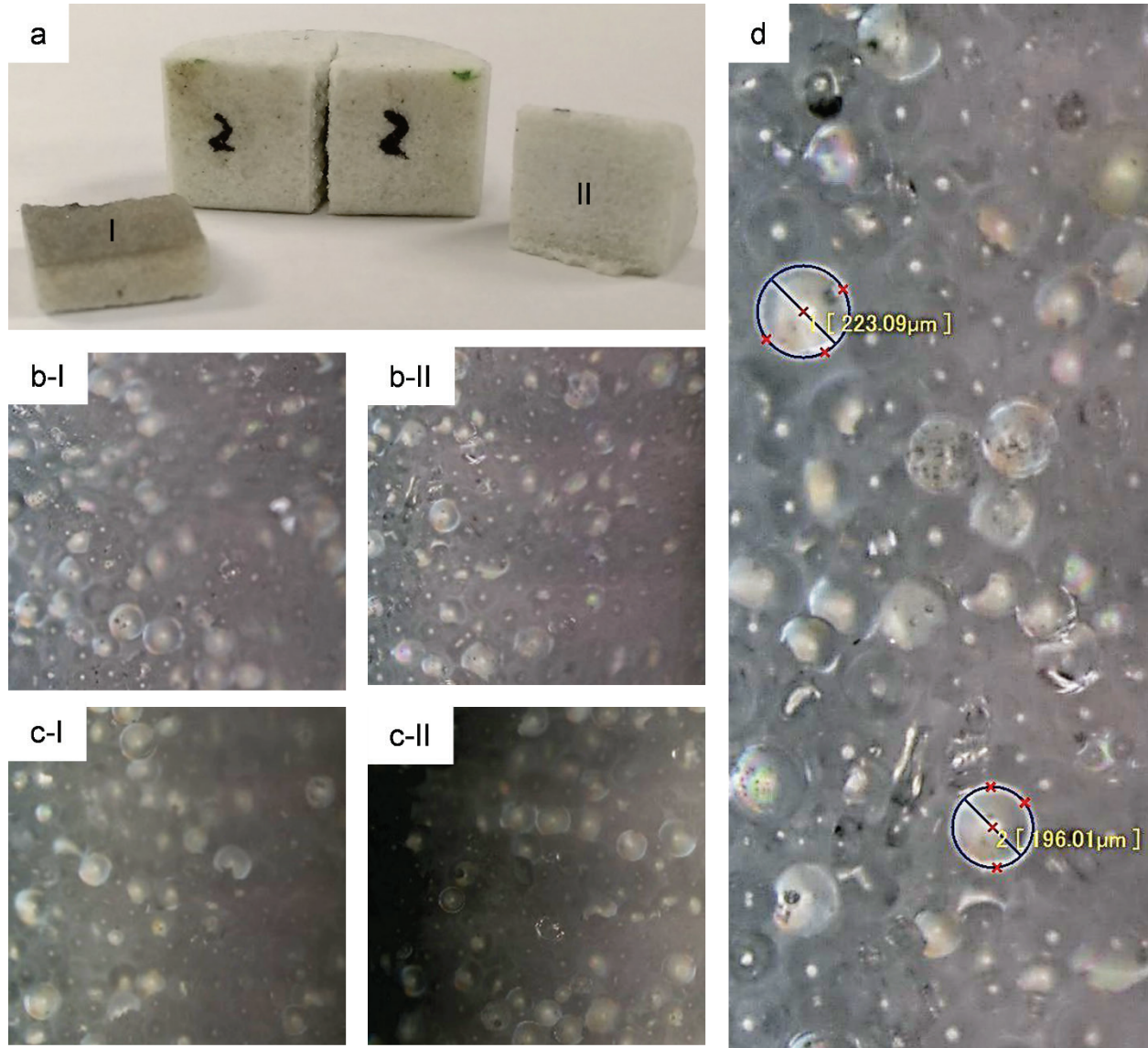


Figure 12. (a) PBX Simulant after testing, (b) Brittle fracture of face I and II at 1000x 1000 pixel, (c) Ductile fracture of face I and II at 1000 x 1000 pixel, (d) Measurement of SLGB of fracture surface

Micrograph of the fracture surface of ductile and brittle material taken by KEYENCE VHX 5000 digital microscope are shown in Figure 12. Higher density in SLGB particle is found in brittle materials. The diameter of SLGBs are calculated using built-in feature of that microscope. The average diameter is found $200 \pm 20 \mu m$. Total number of SLGB on the fracture surface of ductile and brittle material is counted for 1000 x 1000 pixel image to compare between them. SLGB particles are sparsely distributed over brittle fracture surface whereas spatial distribution of SLGB are found all over the fracture space.

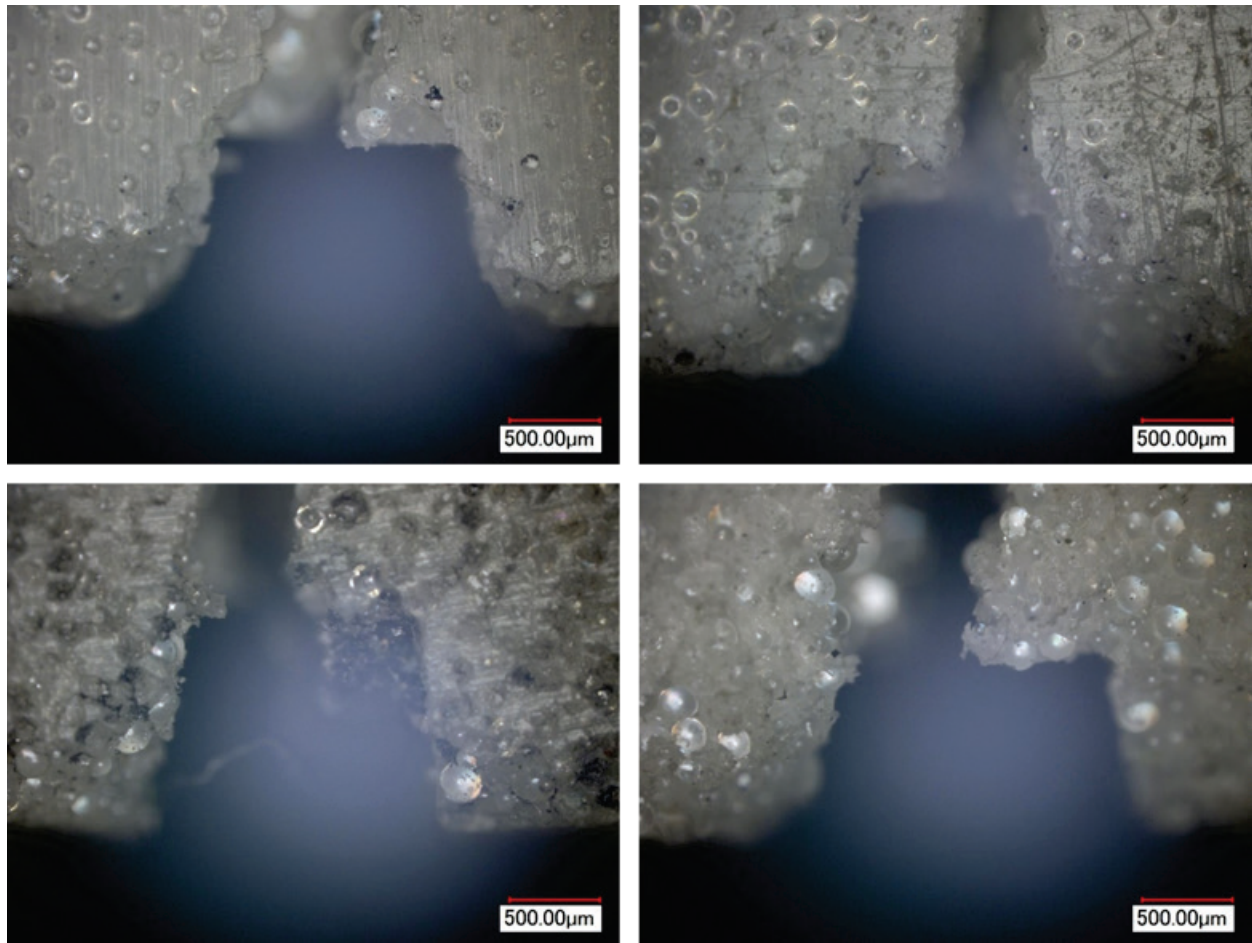


Figure 13. Notch disconformity of 80-20 wt.% PBX simulant

In all cases, there is no occurrence of bifurcation. It is observed that fracture occurs due to a pullout of the glass bead particles from the polymer binder as depicted in Figure 13. Various machine notch defects due to cutting polymer composite with high speed CNC machine are observed. Since HIPS has lower strength than SLGB, binder material near the notch edge encountered more deformation. SLGB are displaced and small concave cavities are noticed for pulling out the SLGB particles. Due to this disconformity at machine notch edge, crack initiation is originated from different part of notch section for different notch.

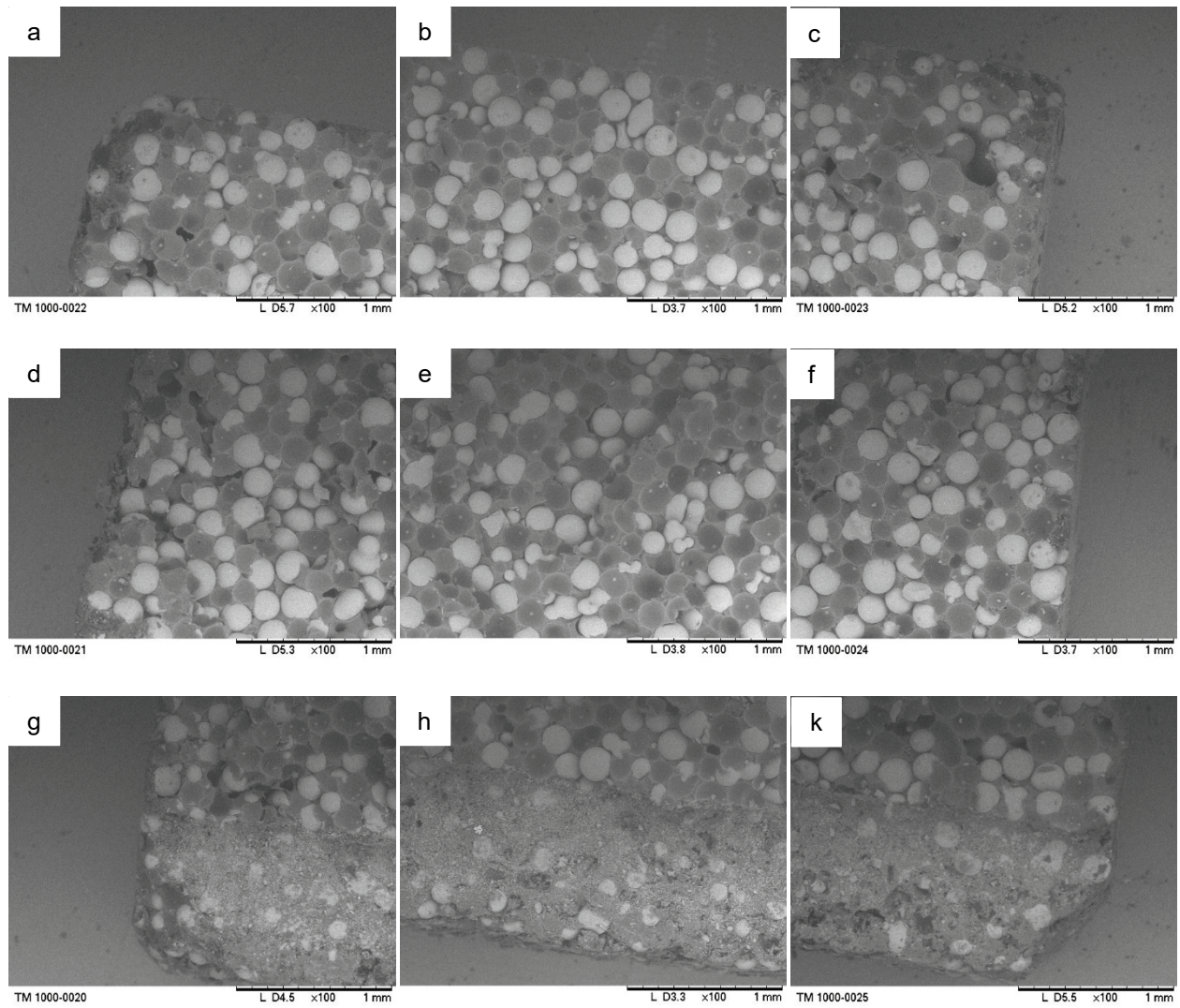


Figure 14. SEM micrographs of ductile specimen at various locations of fracture surface, (a) Top left, (b)Top center (c) Top right, (d) Mid left, (e) Mid center, (f) Mid right, (g) Notch left, (h) Notch center and (k) Notch right

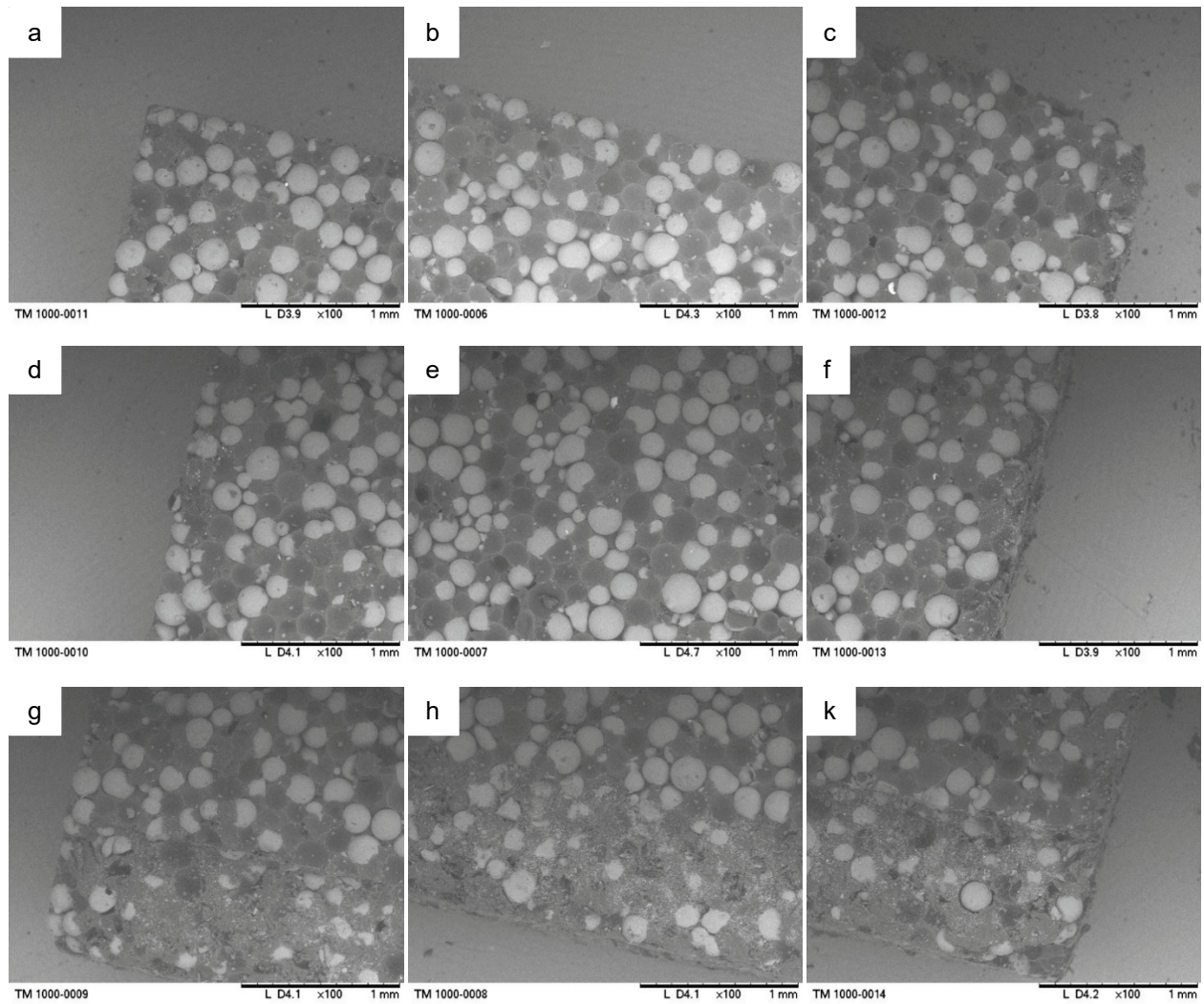


Figure 15. SEM micrographs of brittle specimen at various locations of fracture surface, (a) Top left, (b)Top center (c) Top right, (d) Mid left, (e) Mid center, (f) Mid right, (g) Notch left, (h) Notch center and (k) Notch right

Evidence of both ductile and brittle behaviors within various specimens are observed in Figure 14 and Figure 15. Throughout the different polymer to particle matrices, the ductile specimens appeared to have a deeper concavity from the pullout of the SLGB when compared to the brittle behavior. Another reason for the ductile and brittle behavior are the differences in the polymer to particulate matrices along the notches of each specimen. The ductile specimens have a higher concentration of polymer along the surface of the notch whereas the brittle specimens have a higher concentration of beads along the notch. The reason for this behavior is due to the how the specimens were manufactured. As there are higher concentrations of glass beads within an area, there are voids within the polymer-particle matrix which allow the crack to propagate.

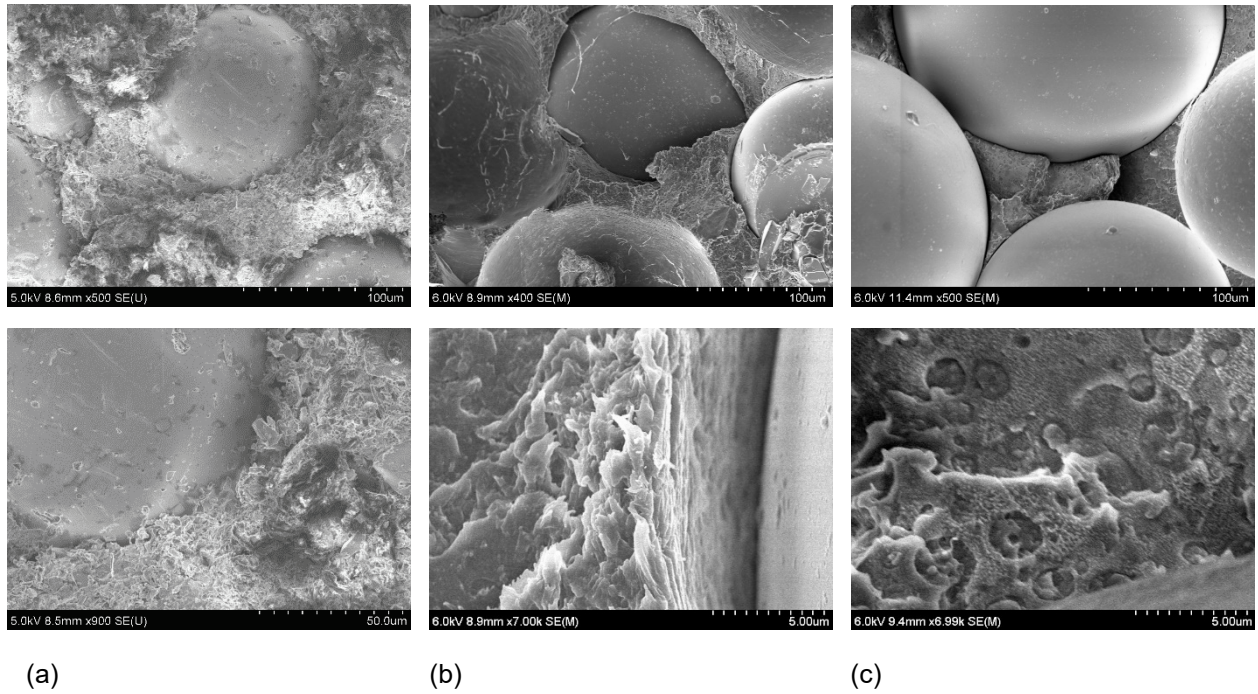


Figure 16. SEM image of a specimen (a) machined surface before fracture, (b) ductile surface and (c) brittle surface after fracture

Before conducting mechanical testing on the specimens, SEM images of the surface of the material were taken to observe any microstructural defects within the material as shown in Figure 16. It should be observed that the surface after machining is disproportional. There are also shattered glass particles within the polymer matrix and the glass beads. Lastly, it is noted that while most of the glass beads are coated within the polystyrene, there are many glass beads that are not fully bonded by the polystyrene. These microstructural defects affect whether the material exhibits ductile or brittle behavior while mechanical load is being applied.

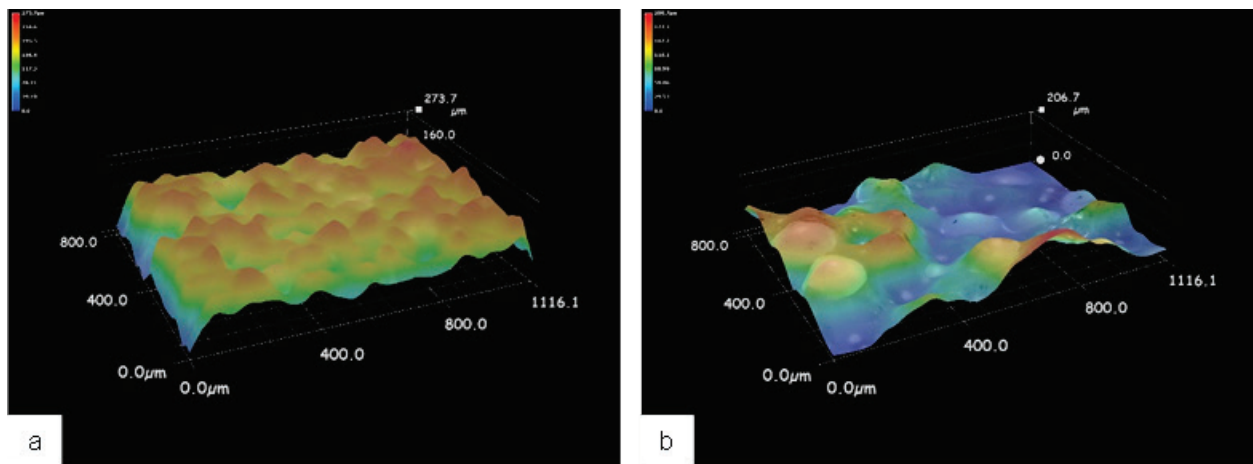


Figure 17. 3D surfacing image of (a) ductile, and (b) brittle specimen

The ductile and brittle failures of the PBX simulant specimens are further studied using stereo microscopy. Figure 17(a) depicts a 3-D surfacing image of the microstructure of a specimen which experienced ductile behavior and Figure 17 (b) illustrates a 3-D surfacing image of brittle behavior. In the ductile material, as load continued to be applied, there was a higher resistance to cracking due to the SLGB being better coated with the HIPS. As load was being applied to the brittle specimens, the crack had little resistance due to some of the glass beads not being fully coated in the polystyrene. This allowed for the crack path to pass around the glass beads and cause instantaneous failure.

3.5. Discussion

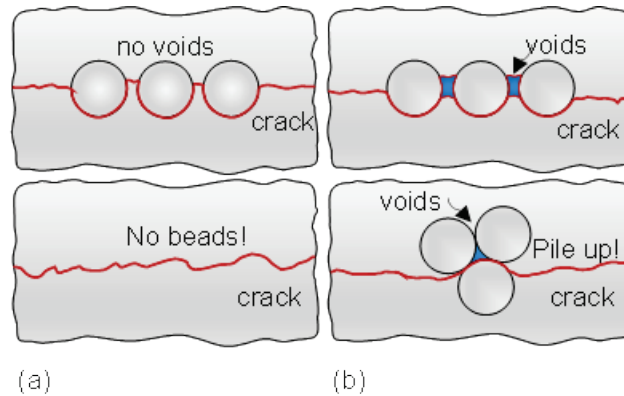


Figure 18. Depiction of crack path (a) in ductile and (b) brittle materials

During the tests that were run on the specimens with varying weight percentages, the materials either exhibited a ductile or brittle behavior. Upon further analysis, it was observed using a digital microscope and a SEM microscope that the specimens that contained a higher concentration of glass beads throughout the crack path experienced brittle mechanical failure and instantaneous cracking whereas specimens that had a higher concentration of polymer near the notch experienced the ductile behavior and a higher resistance to fracture. The brittle behavior is caused by the polymer not being able to flow through the glass beads during the manufacturing process which causes many voids within specimens shown in Figure 18. Once load is applied, these specimens obtain maximum stress before fracturing. The specimens that have a higher polymer concentration obtained a maximum stress before initial cracking. It should also be noted that even if the weight percentage of polymer to glass beads increases, the coefficient of variation may not change as a monotonic function.

4. CONCLUSIONS

This study was performed to evaluate the mechanical properties of a mock PBX specimen at different binder weight percentages. Additionally, the DIC technique was implemented to supplement the results obtained from the experimental data. The analysis performed using DIC technique satisfactorily showed the Von Mises strain in one of the testing configurations, the prediction of the initiation and propagation of the crack by using the strain fields from DIC post processing. The DIC technique has a high impact, as a tool, in the analysis of heterogeneous particulate composites. The mechanical properties at each testing configurations were extracted and analyzed. Digital microscopy was applied to analyze the surface of the specimens prior to testing and post testing. Analysis using digital microscopy showed that microstructural defects affected whether the specimens were ductile or brittle due to fracture. When comparing the results to different PBX and PBX simulant formulations, the properties vary in magnitude. The potential source of variability for the mock formulation can be categorized as the composition, material, and test related. To conclude, the following potential sources of variability were identified: PBXs are complex composite materials with high heterogeneity and anisotropy behavior. Alternative data analysis methods must be implemented to properly characterize the heterogeneous and anisotropic behavior of PBX.

REFERENCES

- [1] P.W. Cooper, S.R. Kurowski, Introduction to the technology of explosives, VCH, 1996.
- [2] C. Siviour, P. Laity, W. Proud, J. Field, D. Porter, P. Church, P. Gould, W. Huntingdon-Thresher, High strain rate properties of a polymer-bonded sugar: their dependence on applied and internal constraints, *Proc. R. Soc. A Math. Phys. Eng. Sci.* 464 (2008) 1229–1255. doi:10.1098/rspa.2007.0214.
- [3] C.M. Cady, C. Liu, P.J. Rae, M.L. Lovato, Thermal and loading dynamics of energetic materials, in: *Proc. SEM Annu. Conf.*, 2009: pp. 1–7.
- [4] P. Chen, Z. Zhou, F. Huang, Macro-Micro Mechanical Behavior of a Highly-Particle-Filled Composite Using Digital Image Correlation Method, *Advances in Composite Materials - Analysis of Natural and Man-Made Materials*, InTech, 2011.
- [5] Z. Zhou, P. Chen, F. Huang, S. Liu, Experimental study on the micromechanical behavior of a PBX simulant using SEM and digital image correlation method, *Opt. Lasers Eng.* 49 (2011) 366–370. doi:10.1016/j.optlaseng.2010.11.001.
- [6] Liang, Z., Huang, F., Duan, Z., Zhou, D., Yao, H. (2008). Experiment Study on Impact Damage of PBX Explosive and Simulation Material [J]. *Journal of projectiles, rockets, missiles and guidance*, 1, 038.
- [7] Z. Zhou, P. Chen, Z. Duan, F. Huang, Comparative study of the fracture toughness determination of a polymer-bonded explosive simulant, *Eng. Fract. Mech.* 78 (2011) 2991–2997. doi:10.1016/j.engfracmech.2011.08.017.
- [8] Z. Zhou, P. Chen, F. Huang, Study on dynamic fracture and mechanical properties of a PBX simulant by using dic and SHPB method, in: *AIP Conf. Proc.*, AIP Publishing, 2012: pp. 665–668. doi:10.1063/1.3686366.
- [9] C. Liu, C.M. Cady, P.J. Rae, M.L. Lovato, On the Quantitative Measurement of Fracture Toughness in High Explosive and Mock Materials, in: *14th Int. Detonation Symp.*, 2010: pp. 425–434.
- [10] D.M. Williamson, S.J.P. Palmer, W.G. Proud, Fracture studies of PBX simulant materials, *AIP Conf. Proc.* 845 II (2006) 829–832. doi:10.1063/1.2263450.
- [11] L. Ferranti Jr., F.J. Gagliardi, B.J. Cunningham, K.S. Vandersall, Measure Of Quasi-Static Toughness And Fracture Parameters For Mock Explosive And Insensitive High Explosive LX-17, in: *14th Int. Detonation Symp.*, Coeur d’Alene, ID, 2010.
- [12] Z.W. Liu, H.M. Xie, K.X. Li, P.W. Chen, F.L. Huang, Fracture behavior of PBX simulation subject to combined thermal and mechanical loads, *Polym. Test.* 28 (2009) 627–635. doi:10.1016/j.polymertesting.2009.05.011.

- [13] Z. Zhou, P. Chen, Z. Duan, F. Huang, Study on Fracture Behaviour of a Polymer-Bonded Explosive Simulant Subjected to Uniaxial Compression Using Digital Image Correlation Method, *Strain*. 48 (2012) 326–332. doi:10.1111/j.1475-1305.2011.00826.x.
- [14] M. Li, J. Zhang, C.Y. Xiong, J. Fang, J. M Li, Y. Hao, Damage and fracture prediction of plastic-bonded explosive by digital image correlation processing, *Opt. Lasers Eng.* 43 (2005) 856–868. doi:10.1016/j.optlaseng.2004.09.003.
- [15] P.J. Rae, S.J.P. Palmer, H.T. Goldrein, A.L. Lewis, J.E. Field, White-light digital image cross-correlation (DICC) analysis of the deformation of composite materials with random microstructure, *Opt. Lasers Eng.* 41 (2004) 635–648. doi:10.1016/S0143-8166(02)00179-3.
- [16] S.R. Heinz, J.S. Wiggins, Uniaxial compression analysis of glassy polymer networks using digital image correlation, *Polym. Test.* 29 (2010) 925–932. doi:10.1016/j.polymertesting.2010.08.001.
- [17] S.G. Grantham, C.R. Siviour, W.G. Proud, J.E. Field, High-strain rate Brazilian testing of an explosive simulant using speckle metrology, *Meas. Sci. Technol.* 15 (2004) 1867–1870. doi:10.1088/0957-0233/15/9/025.
- [18] M.A. Sutton, J.J. Ortu, H. Schreier, Image correlation for shape, motion and deformation measurements: Basic concepts, theory and applications, 2009. doi:10.1007/978-0-387-78747-3.
- [19] J. Akhavan, The chemistry of explosives, Royal Society of Chemistry, 2011.
- [20] Catzin, C.A., Reyes, J.G., Stewart, C.M., 2016, "Manufacturing Method for Mock Polymer Bonded Explosives", *MethodsX*.(Submitted)
- [21] ASTM, D6931-12 Standard Test Method for Indirect Tensile (IDT) Strength of Bituminous Mixtures, (2012). doi: 10.1520/D6931-12
- [22] ASTM, D695-15 Standard Test Method for Compressive Properties of Rigid Plastics, (2015). doi: 10.1520/D0695-15.
- [23] M. Jerabek, Z. Major, R.W. Lang, Uniaxial compression testing of polymeric materials, *Polym. Test.* 29 (2010) 302–309. doi:10.1016/j.polymertesting.2009.12.003.
- [24] J.R. Rice, P.C. Paris, J.G. Merkle, Some further results of J-integral analysis and estimates, in: *ASTM STP 536*, 1973: pp. 231–245. doi:10.1520/STP49643S.
- [25] ASTM, E1820-15a Standard Test Method for the Measurement of Fracture Toughness, (2015). doi: 10.1520/E1820-15A.
- [26] I.L. Lim, I.W. Johnston, S.K. Choi, Stress intensity factors for semi-circular specimens under three-point bending, *Eng. Fract. Mech.* 44 (1993) 363–382. doi:10.1016/0013-7944(93)90030-V.

- [27] J.A. Begley, J.D. Landes, The J integral as a fracture criterion, ASTM STP 514. (1972) 1–20. doi:10.1520/STP514-EB.
- [28] Chen, P. W., Huang, F. L., Ding, Y. S., 2007, “Microstructure, deformation and failure of polymer bonded explosives.” *J. Mater. Sci.*, **42**(13), pp. 5272-5280.
- [29] Chen, P. W., Xie, H. M., Huang, F. L. et al., 2006, “Deformation and failure of polymer bonded explosives under diametric compression test.” *Polymer Testing*, **3**(25), pp. 333-341.
- [30] Banerjee, B., Cady, C. M., and Adams, D. O., 2003, “Micromechanics simulations of glass-estane mock polymer bonded explosives,” *Modelling and Simulation in Materials Science and Engineering*, **11**(4), pp. 457–475.
- [31] D. M. HOFFMAN, BRUCE J. CUNNINGHAM & TRI D. TRAN (2003) “Mechanical Mocks for Insensitive High Explosives,” *Journal of energetic Materials*, 21:4, pp. 201-222.
- [32] Yong, Y., Zhang, J., and Zhang, J., 2009, "A modified Brazilian disk tension test." *International Journal of Rock Mechanics and Mining Sciences*, **46**(2), pp. 421-425.
- [33] Hondros, G., 1959, "The evaluation of Poisson's ratio and the modulus of materials of a low tensile resistance by the Brazilian (indirect tensile) test with particular reference to concrete." *Australian Journal of Applied Science*, **10**(3), pp. 243-268.
- [34] Huang, B., Shu, X., and Tang, Y., 2005, “Comparison of Semi-Circular Bending and Indirect Tensile Strength Tests for HMA Mixtures.” *Advances in Pavement Engineering*, pp. 1-12.doi: 10.1061/40776(155)14.
- [35] Mellor, M., and Hawkes, I., 1971, "Measurement of tensile strength by diametral compression of discs and annuli." *Engineering Geology*, **5**(3), pp. 173-225.
- [36] Kim, Y., Seo, Y., King, M., and Momen, M., 2004, "Dynamic modulus testing of asphalt concrete in indirect tension mode." *Transportation Research Record: Journal of the Transportation Research Board*, **1891**, pp. 163-173.
- [37] Fairhurst, C., 1964, "On the validity of the ‘Brazilian’ test for brittle materials, “*International Journal of Rock Mechanics and Mining Sciences*, **1**(4), pp. 535-546.
- [38] Liu, C., 2010, "Elastic constants determination and deformation observation using Brazilian disk geometry." *Experimental mechanics*, 50(7), pp. 1025-1039.
- [39] C. Liu & D.G. Thompson (2012) Deformation and failure of a heterogeneous high explosive, *Philosophical Magazine Letters*, 92:8, 352-361, DOI:10.1080/09500839.2012.673021

- [40] Cady, C. M. et al, 1998, "High and Low strain rate compression properties of several energetic material composites as a function of Strain Rate and temperature," C. Of, S. Energetic, M. Composites, vol. 836.
- [41] Baytos, J. F. (1980). *LASL explosive property data* (Vol. 4). Univ of California Press.
- [42] AASHTO TP 105-13. 2013. Standard Method for Determining the Fracture Energy of Asphalt Mixtures Using the Semi Circular Bend Geometry (SCB). American Association of State Highway and Transportation Officials, Washington, DC.

APPENDIX: INTERIM REPORT ON MANUFACTURING AND DIC OF PBX

1. INTRODUCTION

Polymer bonded explosives (PBXs) are complex particulate composites that are typically comprised of two fundamental materials: micron size energetic crystals and a polymeric binder material [43]. In some cases a small percent of additives like plasticizers, oxidizers, and antioxidants are added to the composition in order to improve the explosive output and decrease the effect of ageing respectively. The particular mechanical behavior of each respective constituent material will develop the mechanical properties of the new formed particulate composite or PBX. Therefore, it is important to consider the individual mechanical properties of each of the constituent materials, their differences, chemical composition, and distribution [44]. For instance, the elastic modulus of the energetic crystals or particles at room and at elevated temperatures, it is frequently much higher than that of the polymeric binder material. Furthermore, the ratio of the explosive component (energetic material) to the polymer binder is dependent on one material to the next depending on the explosive material specifications; but, typically, the energetic material comprises 80-95% of the total mass of the composite [43]. The geometry of the energetic crystals is not homogeneous. Rather, the energetic crystals geometry is a distribution of different sizes, maintained in a similar range, that make up a heterogeneous arrangement [45]. Also, the size of the energetic crystals has a big impact in the overall mechanical strength and ignition mechanism of the particulate composite or PBX. Compositions containing large size energetic crystals tend to be more explosive and provide a weaker structure than compositions containing both large and small size energetic crystals [44]. One of the main reasons that justifies the used of PBX in industry is their ability to be handle, machined, and lightly deformed while avoiding accidental stimuli. Therefore, the used of large size energetic particles in PBX reduces their mechanical strength and its ability to prevent accidental stimuli. A composition containing relative large and small energetic crystals will be the optimal choice to ensure safety during their application. PBXs are extensively used by engineers, specifically in



Figure 19. PBX used as a Solid Rocket Propellant

the aerospace industry for solid rocket propellant and in the military industry for explosive components and applications. Many innovative applications for PBX can be developed, but a lack of research inhibits the innovative applications. The high cost of gathering the constituent materials, expensive testing setups, and the arduous task of following safe handling procedures of explosives are some of the main issues that slow down the research process. Therefore, a precise and well developed method of manufacturing a standard mock PBX specimen that closely resembles the mechanical behavior of PBXs is required in order to safely study their mechanical behavior. Several methods of manufacturing Mock PBXs have been proposed in literature. However, many of the proposed methods lack the high volume fraction of the mock energetic material or details connecting the proper manufacturing process. Contrary to literature, in the current study, a

manufacturing process will be carefully described to facilitate the repeatable production of mock PBX. Once the mock PBX has been developed, it will be mechanically tested in order to characterize its mechanical properties and to measure the level or resemblance when compare to a typical PBX used in industry.

1.1. Technical Approach

Conventional contact strain measurement devices such as strain gages, extensometers, and linear variable differential transformers (LVDTs) can only measure local or average strain. The heterogeneous composition and consistency of PBXs contribute to slip, interfacial bond issues, and an overall inadequate measure of strain with these devices. Three-dimensional DIC allows for full-field and non-contact shape, displacement, and strain measurement of the surface of materials. This can help mitigate classical problems such as measuring the bulge (due to inadequate lubrication) of PBX subject to compression [46]. Several studies have been conducted by scientists at Los Alamos and Lawrence Livermore National Laboratories to characterize the properties of energetic materials using 2D DIC [47-49]. Most studies have focused on the tensile, compressive, thermal, fracture, and failure properties of these materials [50]. A particular novel use of 3D DIC is to study the multiaxial (volumetric and deviatoric) constitutive and damage behavior of PBX using a notched specimen under compression. In the past, the skeletal stress and elastic FE solution have been used in conjunction with rupture data of Bridgman notched specimens to elucidate the multiaxial damage and rupture behavior of metal subject to creep under tension [51-53]. The skeletal stress method is based on the observation that a symmetric specimen subject to simple loading conditions (tension, pressure, or bending) has a point at which stress remains unchanged (spatially and with time) and is insensitive to elastic, plastic, and creep phenomena [54,55]. Rupture data of uniaxial and Bridgman specimens is used to calibrate the Hayhurst triaxial stress that is dependent on the first principal, hydrostatic, and von Mises stresses [56]. Hayhurst stress is then implemented in the equivalent strain rate, damage evolution, and viscous potential function of a constitutive model. Although it has never been attempted, it is technically possible to use 3D DIC to elucidate the multiaxial damage/rupture using a Bridgman notched specimen of PBX under compression. The strain field in the vicinity of the notch can be extracted and used to identify the Hayhurst parameters or develop a PBX specific equation. It is hypothesized that by subjecting a novel Bridgman-type specimen to compression until fracture or buckling a reverse correlation between optical displacement and the analytical skeletal stress (or elastic FE solution) can be used to elucidate the multiaxial constitutive and damage behavior. These tests will be conducted at various strain rates (0.001 to 1 s^{-1}) and temperatures (ambient to 75°C). The primary technical challenge will be to identify the proper specimen geometry that accommodates size, finish, surface quality, heterogeneity, and other specimen design issues. The expected outcome is the development of a new test standard for the volumetric and deviatoric response of energetic materials. The objective of this topic will be achieved using the following general methodology. All mechanical testing will be performed at UTEP utilizing a mock PBX material. Conventional uniaxial specimens will be tested to collect the linear elastic properties of the material. Experiment design will begin with simple linear elastic simulations (in the limit of small

deformation) of various Bridgman notched geometries under compression towards mitigating challenges such as buckling, bulging, etc. Iterative manufacturing and testing will produce an ideal candidate. A test matrix of ideal candidate specimens will be manufactured into mock PBX specimens. Mechanical tests will be performed on both uniaxial and Bridgman specimens with 3D DIC measurements up to failure. A comparison between the finite element solution and DIC measurements of uniaxial and Bridgman specimens will be used to elucidate the multiaxial constitutive and damage response of the material. Once perfected, this technique will be transferred to Sandia for use on real PBX materials.

1.2. Relationship to Prior and Other On-going Work

Numerous constitutive models have been developed (or repurposed) to model the rate-dependence of energetic materials under various conditions (low strain rate, high strain rate, cook-off, etc.). A menagerie of phenomenological and mechanistic viscoelastic and viscoplastic models have been used including generalized Maxwell, standard linear solid, Prony series, Johnson-Cook, Campbell, Steinberg–Guinan–Lund, Zerilli–Armstrong, etc. [57]. Schapery and colleagues have made substantial contribution to developing constitutive theory for elastic media and particulate composites with coupled strain rate and damage laws [58, 59]. Extensions of this isotropic theory have been used to model the 3D constitutive response [60], introduce damage-induced anisotropy [61], introduce property degradation due to damage [62], etc. These features are analogous to those used in the CDM theory [63]. The advantage of the CDM theory is that it allows the seeding of an initial damage distribution. This distribution can be heterogeneously distributed throughout the mesh via pseudo-random variable generation. Recently, Stewart developed a pseudo-nonlocal CDM-based damage evolution equation [53]. The advantage of this equation is the ability to control the localization of CDM and produce delocalized damage distributions about flaws in addition to rupture predictions. The volume fraction and surface area of polymeric binder, crystalline energetic, and voids which constitute a PBX have considerable influence on the resulting mechanical properties, explosive performance, sensitivity, and chemical stability. Slight variations in the manufacturing process can contribute to stockpile consistency issues. Considerable testing is required to verify a batch of explosives meets specifications. The ability to rapidly predict the "batch-to-batch" mechanical behavior of PBX through an analysis of manufacturing parameters such as volume fraction and mean particle size would revolutionize the validation process. Xu and Sofronis have demonstrated that a rigorous homogenization theory based on volume fraction can be used to model the bulk constitutive response of a solid rocket propellant [64]. In this process, the mechanical properties associated with each constituent of the microstructure undergoes a homogenization process via volume fraction to produce composite mechanical properties that can be used within macro constitutive models. It is hypothesized that a CDM-based constitutive law using homogenization theory of composites [64], a pseudo-nonlocal damage evolution equation [53], a heterogeneous initial damage distribution [63], and a triaxial stress [56] can be used to predict the "batch-to-batch" mechanical behavior (compressive and creep) of mock PBX subject to low strain rate and varied temperature. The ability to predict the "batch-to-batch" mechanical behavior is a major breakthrough. The technical challenges are experimentally determining pre-existing defect quantity and intensity, measuring the volume fraction, and dealing with the varying heterogeneity of test specimens. UTEP and Sandia's proximity makes collaboration on this topic complementary. The establishment of a relationship between Sandia and UTEP will facilitate collaboration on future external funding opportunities.

1.3. Goals, Objectives, and Project Milestones

The overarching technical goals for this project are

- Conduct 3D DIC on mock PBX to measure the linear elastic and creep properties
- Conduct 3D DIC on Bridgman specimens to measure the multiaxial constitutive and damage behavior at various strain rates and temperatures
- Develop a constitutive model capable of predicting the “batch-to-batch” constitutive behavior including uniaxial and multiaxial states of loading

Concrete evidence of technical success will be shown through the publication of conference and journal articles in conjunction with the submission of yearly and the final SAND reports.

1.4. Year 1 Outcomes

The overarching technical goals proposed for year 1 of the project included:

- 3D digital image correlation of mock PBX(uniaxial specimen)
- A CDM-based constitutive model for mock PBX with heterogeneous damage distribution

The 3D DIC of mock PBX goal includes a submission to the 2015 SEM conference and a journal submission. However due to difficulties in gathering or obtaining mock PBX specimens, the technical goals for year 1 suffered a slight change to the following:

- Material Selection and Manufacturing of a Mock PBX(Particulate composite)
- Microstructural characterization of manufactured Mock PBX
- 3D DIC on Manufactured Mock PBX (Mechanical Testing).

In this report we present the outcomes of these goals. These goals include a submission to a conference and a journal paper. A technical presentation of the manufacturing process presented in this report will be presented in IMECE 2015. Several journal papers will be submitted in the near future.

2. MATERIALS

Several research studies have been performed in the manufacturing process of energetic materials to characterize their explosive sensitivity [65], hot spot generation [66], and deflagration or detonation initiation [67]. Only a few research studies have thoroughly covered the manufacturing process of a “simulant energetic material” or “mock” Specimen. In each of the recent research studies below an effort to replicate the constituent materials geometry, morphology, and properties was made in order to accurately simulate the mechanical properties of a PBX; however, some physical characteristics of PBXs are not taken into consideration for the simplification of the micromechanics towards a homogeneous assumption.

An example of the latter is found in Banerjee et al where instead of using energetic crystals, they used micron size soda lime glass beads that possess a similar mechanical behavior and physical properties compared to energetic crystals that are commonly used in the manufacturing process of PBXs [68]. The soda lime glass beads provide the high modulus contrast between the energetic particles and the binder material just like the energetic particles do in a typical PBX [68]. Such substitution is justified making glass-polymer mock PBX a reasonable substitute for mechanical testing. But important physical properties that contribute to the mechanical behavior are omitted, such as the high volume fraction of energetic particles to binder material and the particle morphology. Banerjee et al justifies the lack of such high volume fraction and particle morphology by stating that the effects caused by these physical properties are not needed to be considered in the calibration of their computational model of HPC [68]. It is important to remark that in Banerjee et al the diverse sizes of the energetic particles are considered in the development of their mock material. Summarizing, Banerjee et al describes the material selection process for a mock PBX, describes a brief manufacturing process of a glass-polymer mock PBX, and develop FEM simulations for a HPC. Some of the weak points or issues in Banerjee et al is the lack of fundamental physical properties of PBX in their glass-polymer mock and a detailed description of their manufacturing process.

Yeager and colleagues also conducted a research study on the material selection and manufacturing process for a mock PBX [69]. In Yeager et al, the energetic particles are substituted by acetaminophen that is a crystalline powder typically used in the pharmaceutical industry as a pain reliever to produce different Mock PBXs. The manufacturing process described in Yeager et al closely resembles the typical slurry formulation process used in the explosive industry; however, many details are missing, modified, or not described at all. Overall, Yeager et al provides different compositions of PBXs, a few compositions of Mock PBXs, a brief description of the manufacturing process, measurements of the crystal-binder bond in different PBXs and Mock PBXs, and the different effects of additives like plasticizers and oxidizers to the crystal-binder bond in each composition of PBXs and their mock counterparts. A few important details are missing in Yeager et al such as the materials specifications, the weight or volume percentage of each composition, and a detailed description of the manufacturing process and its justification.

In Xu and colleagues an expensive yet similar effort to the above studies was approached as they used a simulant of the so called octogen explosive or HMX called pentaerythritol or also called pentek, to replace the actual energetic material [64]. No material selection discussion is delivered; however, they mentioned that a molding powder of the mock 900-21 was provided by

a national laboratory. This molding powder is commonly used to simulate the mechanical properties of PBX 9501 [47]. The composition of the molding powder and the different properties of its components is given in the form of a table. It is important to remark that the high modulus contrast between the energetic particles and the binder material is present in the molding powder as well as the particle morphology. The manufacturing process was a simple high pressure press of the molding powder into their desired geometry for testing, typically a cylindrical geometry. This method of manufacturing mock PBX is very specific and easy to follow, but is expensive for repetitive production. Overall, Xu and colleagues provided the properties of a typically used mock PBX and a manufacturing/machining process.

Siviour and colleagues take a different approach. Since the main objective of Siviour et al is to predict the mechanical behavior of the materials solely from their composition, a relative inexpensive approach was taken as caster sugar crystals were used to simulate the energetic particles [44]. They mentioned that such substitution is commonly used to simulate the mechanical properties of polymer bonded explosives. Special emphasis is given to the material selection particularly in the crystal-binder interaction and the particle size effects in the mechanical strength of the material. For instance, in Siviour et al it is mentioned that the mechanical strength of the material is not only dependent in the binder material that absorbs the mechanical energy and prevents crystal-crystal friction, but also in the crystal size and crystal separation or homogeneity in the crystal distribution [44]. Siviour and colleagues used hydroxyl terminated polybutadiene (HTPB) as a binder material because several research studies have previously used this material to successfully recreate the mechanical properties of a PBX. Besides, the HTPB is typically used as binder material in the explosive industry. However, no more information is given about the caster sugar crystals other than a percentage. Siviour et al describes very briefly the manufacturing process used to obtain their polymer bonded sugar (PBS), but most of its results and discussion are based on several research studies making it a reliable source.

In this study the material selection and manufacturing process are based on the above and referenced research studies, with the objective of creating and develop a safe and relative inexpensive method to study energetic particulate composite materials or PBXs. The mock PBX created with the manufacturing process presented in study is expected to closely resemble the mechanical properties of a real PBX. A description of our manufacturing process is included in the manufacturing section of this report.

2.1. Material Justification

Since the specific mechanical behavior of each respective constituent material will develop the mechanical properties of the PBX, it is important to consider the material selection in the development of a “mock” PBX, particularly the binder material. The binder material is responsible of coating and creating strong bonds between the energetic particles which will eventually form the mechanical strength of the PBX, and to ensure the safety during the manufacturing process. For instance, a sensitive explosive will required certain properties of the binder material to avoid accidental stimuli by crystal-crystal friction during the manufacturing process. A list of different binder materials used in industry is available in Table 7. In order to adequately select the binder material to accommodate explosive sensitivity, a parameter must

exist that eases the selection process. The glass-transition temperature, T_g , is a parameter that among the material properties of the binder material, will determine if it will reduce or increase

Table 7. Different Polymer Binder Materials used in the manufacturing process of PBX.

Polymer Binder Material	Melting Temperature (°C)	Adhesive Properties
Polyurethane (PUR/PU)/ Estane	240-280	Excellent
Polystyrene (PS)	100-200	Excellent
Polyethylene (PE)	130-137	Good
Fluoroelastomer / Fluoropolymer (Viton, Fluorel)	177-232	Good
Poly(methyl methacrylate) / (PMMA)	160	Excellent
polyisobutylene (PIB)	106.5	Good
Polyvinylpyrrolidone (PVP)	100	Good
Hydroxy-terminated Polybutadiene	Neglible	Good

the sensitivity of the PBX to impact [71]. T_g is the temperature region where the polymer transitions from a hard glassy material to a soft rubbery material. Therefore, T_g is an imperative parameter for the material selection process and the adequate pairing of the binder and energetic material [44]. Even though, T_g is a parameter that helps in the selection of the binder material, it is not considered in many of the previous research study as a parameter during the selection process. Another parameter that plays an important role in this selection process is repetition or usability. In several of the research cases mentioned above, the selection of the binder material took place due to their common used in the manufacturing process of real PBX. Since this seems to be the case, the polymeric material selected in this study to act as a binder material is a special form of Polystyrene. This selection for a binder material is reseanoble since the first composition of a PBX included polystyrene as a binder agent [70]. The special form of the polystyrene is in fact to reduce the impact or to enhance the properties of the polystyrene to absorb energy, the high impact polystyrene (HIPS).

The energetic crystal or particles possess certain qualities that make them optimal for the polymer binder explosive application. The main qualities that are obvious, yet they have to be mentioned, are the explosive and mechanical properties. However, for the manufacturing of a mock or simulant energetic material the explosive properties are obsolete. Another set of parameters like the particle morphology and the mechanical properties must be taken in consideration for the adequate selection of the simulant. A list of typical energetic crystals and their sizes can be found in Table 8. One of the main parameters that determines the selection of the simulant of the energetic particles or crystals is the high modulus contrast between the

Table 8. Energetic materials and their simulant counterpart.

Energetic Material	Size (µm)	Mock Energetic Material	Size (µm)
TATB (1,3,5-triamino-2,4,6-trinitrobenzene)	50-70	Spherical Soda Lime glass beads	150-250
HMX (Octahydro-1,3,5,7-tetranitro-1,3,5,7-tetrazocine)	3-100	Acetaminphen (ACM)	12-100
RDX (cyclotrimethylenetrinitramine)	1-124	Pentaerythritol (Pentek)	45-500
HNS(Hexanitrostilbene)	9	Caster Sugar Crystals	2000 coarse
PETN Pentaerythritol tetranitrate	44-850	Barium Nitrate (Ba (NO ₃) ₂)	50-200

energetic particles and the binder material. In another words, the energetic mock or simulant must poses similar mechanical properties when compared to a typical energetic crystal. However, the parameter that eases the material selection in this study is the particle size. As is shown in Table 8, the material that has a similar mechanical properties and size is the soda lime glass beads. Even though the acetaminophen (ACM) are also crystal particles, there exist law restrictions that will create problems in other to obtain them. As well as safety and handling procedures are stricter when handling chemicals. This is the same case of the barium nitrate. The Pentek is not an inexpensive material and there is many restrictions to overcome in order to obtain it making this material not suitable for this study immediate needs. While the soda lime glass beads closely resembles energetic crystals, it does not provide the wanted random geometry of the crystals like the caster sugar crystal do. Still the soda lime beads have a higher modulus and are closer in size, overwhelming the random geometry generated by caster sugar crystals. The soda lime glass beads will provide the necessary high modulus contrast and size distribution necessary to simulate the energetic crystal for this study. The particulate composites explored in this study are composed of Soda lime glass beads contained in a high impact polystyrene polymer binder.

2.1.1. *High Impact Polystyrene (HIPS)*



Figure 20. High Impact Polystyrene Pellets

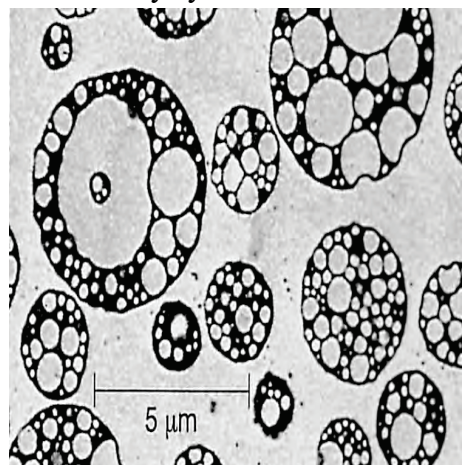


Figure 21. SEM of an ultra-thin section of HIPS

The High Impact Polystyrene (HIPS) pellets used in this study were produced by the polymerization of styrene in the presence of butadiene rubber, which is the typical process used to produce this type of polymer. A picture of the actual HIPS pellets used in this study is shown in Figure 20. If an ultra-thin section of the polymer HIPS is cut, it is possible to detect, in a scanning electron microscope (SEM), that the butadiene rubber particles have a circular structure and are embed in a normal polystyrene matrix as shown in Figure 21. Figure 21 resembles one of the main characteristic of the microstructure of HIPS. The molecular formula of HIPS is present in Figure 22 under this description. The mechanical behavior of HIPS can be considered to be viscoelastic as it is seen in the stress-strain curve in Figure 23. Also, the mechanical behavior of HIPS is characteristic of tough materials such as metals and composite materials like carbon fiber. One explanation for this sort of mechanical behavior in HIPS is the number, size, size distribution and internal structure of these rubber particles which determine the property profile of the HIPS. In another words, the toughness of the high impact polystyrene will increase as the rubber content increases. The commercial grade HIPS used in this study was obtained in pellet form and contained 8.5 wt. % of polybutadiene. It is important to keep in mind that polymers are highly sensitive to the strain rate and temperature. The

high impact polystyrene is temperature and Strain rate dependent as shown in Figure 24 at constant strain rate of 2mm/min. At low temperature it will behave like a glass, but above the glass transition temperature it will behave like rubber. The source of the material asked to remain anonymous due to the nature of the project. The HIPS has a melting temperature of 132° C. The room temperature density of HIPS is 1.04 g/cm³.

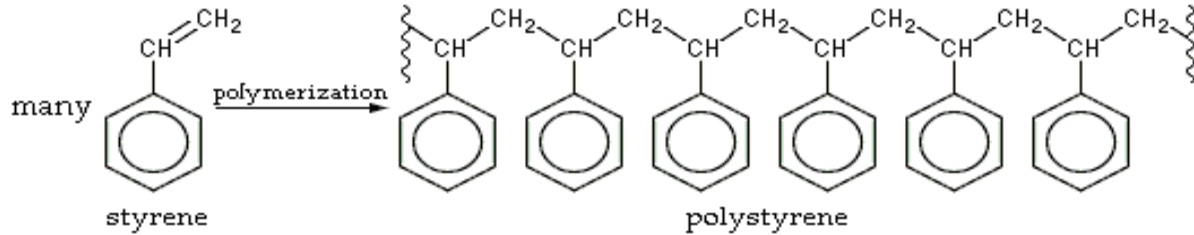


Figure 22. Molecular Structure of HIPS

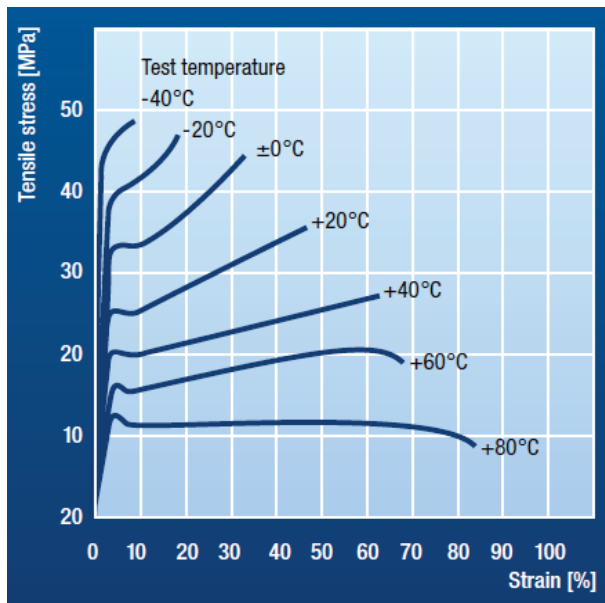


Figure 23. Stress-Strain curve of HIPS at different test temperatures: determined on injection-molded test specimens.

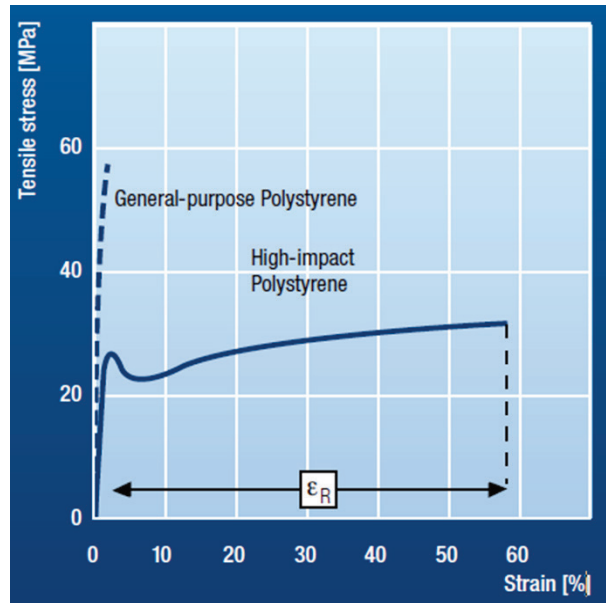


Figure 24. Stress-Strain curve of general purpose polystyrene and HIPS in a tensile test in accordance with ISO 527

2.1.2. Soda Lime Glass Beads



Figure 25. Micron size Soda Lime Glass Beads

The soda lime glass beads used in this study were produced by the typical commercial manufacturing process, but it has a unique washing and polish process free of harmful additives. This gives the soda lime glass beads a pure shiny surface. The glass beads were manufactured by Jaygo Corp as a standard soda lime glass with an average diameter was 200µm ± 50µm. These glass beads are linear elastic in the range of conditions used in the experiments and have a density of 1.02 g/cm³, a Young's modulus of 63 000 MPa, and a Poisson's ratio of 0.20.

2.2. Particulate Composite

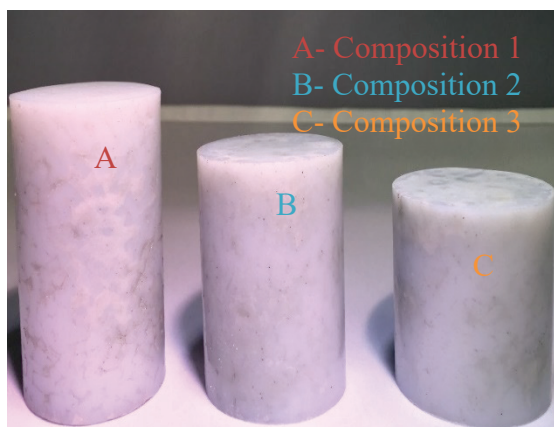


Figure 28. Comparison of the different Compositions

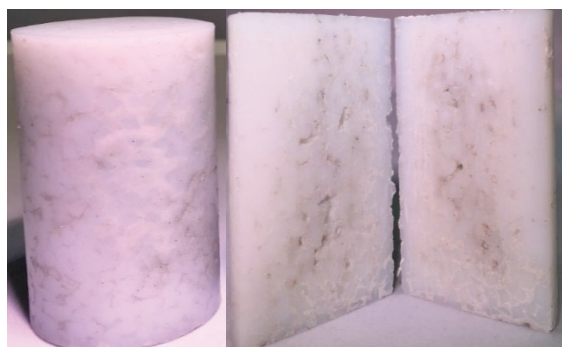


Figure 26. Composition 1 and its internal structure



Figure 27. Composition 3 and its internal structure

A description of the optimized manufacturing process of the glass-HIPS mock PBX is found in the manufacturing section, but the different manufactured compositions are detailed below. Based in literature, several distinct weight compositions where manufactured using the optimized process. A table of the different compositions is shown in Table 9 below. This different compositions are similar to the ones found in literature like Banerjee et al. The glass-HIPS mock PBX specimens started with composition of a high volume fraction of the binder material and concluded with a high volume fraction of the simulant energetic material, however the best composition seem to the composition 2 (50/50). Composition 2 is the selected as the main manufacturing composition for our testing specimens because such composition possess the highest volume of the simulant explosive without affecting the structure of the specimen for machining purposes. Composition 3 seems to be another option for testing specimens as it possess the highest volume of explosive simulant and a relative strong structure for manufacturing purposes. However, as seen in Figure 27, is more probable that during manufacturing big voids will be developed in composition 3 than in composition 2 which could affect machining, polishing, and later on the test. As a results of such voids during manufacturing, composition 3 is not used in this study. Possible solutions to this voids creation will be assess in the near future. Composition 1 was neglected because it did not possessed a high volume of the simulant explosive as seen in Figure 26. No internal structure is found in this study for composition 2 , instead an optical microscopy of the optimal composition is found below.

Table 9. Different manufactured compositions of the glass-HIPS mock PBX.

Composition	Energetic Material Simulant (wt. %)	Polymer Binder Material (wt.%)
Composition 1	25	75
Composition 2	50	50
Composition 3	65	35

2.3. Microstructural Characterization

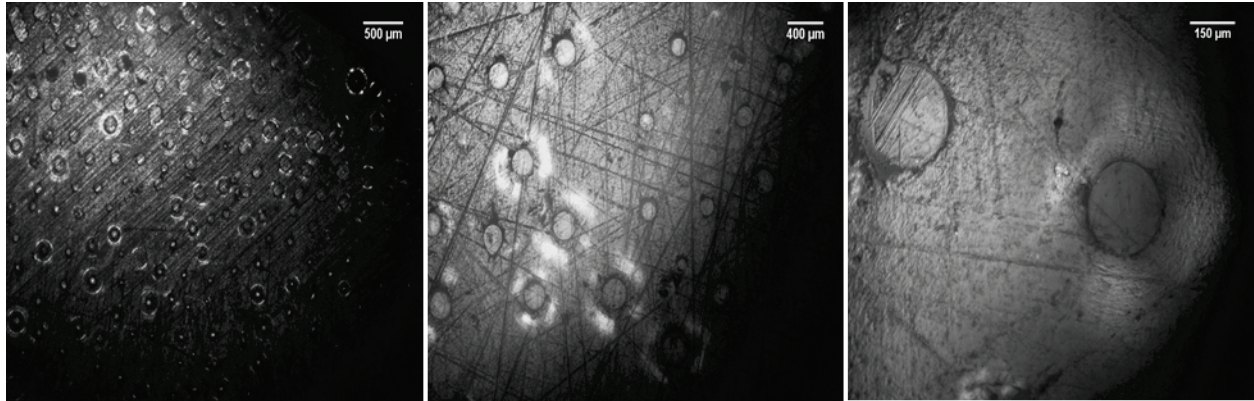


Figure 29. Optical Microscopy of HPC optimal composition (50-50).

The optical microscopy of composition 2 was the key for the selection of composition 2 as the optimal composition. In Figure 29 part A, is possible to see the different sizes of the soda lime glass beads coated and embedded into the HIPS polymer. The distribution shown in part looks like a normal distribution without agglomeration of the soda lime glass beads. It's also possible to see the effects of polishing in the sample. This is more noticeable in part B of Figure 29. In part B is also possible to see that some of the glass beads are deeply incrustated or coated into the polymer. In part C is possible to see that some of the glass beads were cut in half when machining the sample for the microscopy. The fact that a 50-50 composition has such a good distribution was a strong reason to lean towards selecting the optimal composition.

3. SPECIMEN MANUFACTURING PROCESS OF MOCK PBX/HPC

3.1. Overview and Background Information

The Materials at Extremes Research Group (MERG) at the University of Texas at El Paso (UTEP) has developed and optimized an ingenious manufacturing process of a Heterogeneous Particulate Composite (HPC) for a project concerning the characterization and modeling of the multiaxial constitutive and damage response of energetic materials for Sandia National Laboratories. MERG is creating a mock or simulant of energetic materials using two constituent materials. A polymer, that acts as a binder material, and micron size soda lime glass beads (150-250 micrometers in diameter), to emulate the energetic particles or crystals. These materials are mixed with a very small volume of water to create clusters and make the consistency clumpy, i.e. half a gram in weight. The mixing process involves stirring the two constituent materials during three minutes, and pouring this mixture back and forth between glass beakers at least four times to improve the results of the resulting mock polymer-bonded explosive samples. The mixture is

then placed inside a legacy metallographic hot pneumatic press, resulting in a cylindrical coupon 1-1/2” in diameter and up to 2-1/2 inches tall. This coupon is then machined to the desired geometry, using a CNC Lathe to introduce a circular circumferential notch on the specimen, or in a Buehler abrasive cutter to cut the specimen to the required testing geometry of a shorter, circular “coin”, or a semicircular “coin”. After machining, all the specimens are carefully polished in a Buehler Polimet 1000 grinder-polisher to remove any unwanted surface roughness that might affect the results of mechanical tests. It is important to reemphasize that investigators handling these materials are required to wear the appropriate personal protective equipment (PPE), which was selected based on the material safety data sheets (MSDS) of both constituent materials.

The manufacturing process used in this study was based on the idea of completely coating particles in a binder material or matrix to ensure that the final product will closely resemble the mechanical properties of a mock PBX, and to prevent the segregation of the constituent materials. The idea behind this process consist in the replication of a dry granulation process with obvious alterations. This method, typically used in the pharmaceutical industry for tablets manufacturing. It consist in shredding large materials into smaller particle like geometry, then combining the just shredded particles with a micron geometry material to create the final particulate composite that can be manufactured to a desired geometry. The combination process consist in either using a high compressive force to bond the materials or by using a binding agent. For the purposes of this study, the high pressure idea was preferred over the binding agent. The idea of this process helped the MERG research team to develop a similar yet still effective process to develop a heterogeneous particulate composite (HPC). The details and steps of the manufacturing procedure, along with several images of the key steps of the process are described below in the next section.

3.1.1. *Personal Protective Equipment and Safety*

In order to be able to create a safe manufacturing and machining process environment, it is critical to understand all possible risks and complications that could arise from using the equipment and then provide solutions. In accordance to the material safety data sheets (MSDS) of the constituent materials of the self-manufactured heterogonous particulate composite, investigators handling these materials are required to wear the following personal protective equipment (PPE): lab coat, steel toe boots, EN 166 compliant eye protection, welding gloves (for handling of the hot press), 8 ml disposable nitrile gloves, and disposable N95 respirator masks.

3.1.2. *Manufacturing and Equipment*

These equipment and machinery served a specific purpose in the manufacturing process; their uses are listed in the manufacturing protocol that the research team followed to effectively produce the samples needed.

3.1.3. *Manufacturing Procedure of Heterogeneous Particulate Composite (HPC)*

All of the equipment should be gathered as an initial step. Both the PPE (must be worn) and the tools used during the manufacturing process, are listed and described in detail in the Appendices of [75]. The station set up and tools required to manufacture the mock polymer-bonded explosive are presented in Figure 30, with the extra details provided in the respective Appendices of the PPE and the manufacturing equipment in [75].



Figure 30. Station Preparation with Tools for Manufacturing Process.



Figure 31. HIPS (Left) and SLGB (Right).

3.1.3.1. **Stage 1: Preparation and Weigh-In of Constituent Materials**

The dry granulation process begins by plugging in the heating element that is attached to the Leco PR-22 Pneumatic Mounting Press Plug, and turning the switch to 'ON'. The heater requires an approximated time of 30 minutes to reach its maximum temperature of 190°C. Then the scale is turned on and 5 minutes are allowed for the scale to stabilize (indicated on the instructions) and then it is calibrated using the corresponding 100 gram weight. After the calibration, the constituent materials, shown on Figure 31, which will make up the mock PBX sample are collected, and the beakers, flasks, and plastic scoops are checked for complete neatness before the materials

are added. Posteriorly, the desired amount of each component material, i.e. 37.5 grams, is measured separately using the plastic scoop that weighs approximately 11.88 grams. This is significant because the weight shown on the electronic balance should be subtracted from the total amount to determine the correct, true mass of anything that is measured. This is illustrated in Figure 32 to the right. The plastic scoops were used because the glass beakers and flasks exceeded the 100 gram weighing capacity of the balance. Then, the balance and plastic scoop should also be used to weigh the proper amount of water (H_2O), the used amount is half a gram. All of these different materials should be placed in their respective containers, the polymer and glass beads in a beaker, and the H_2O in a flask. The next part of the procedure is to ensure that the metallic cylindrical container (or mold in which the mixture will be placed), the moving platform that comes in contact with the mixture, and the upper die that locks the specimen, are free of residues from previous manufacturing sessions. At this point the air pressure valve connected to the pneumatic press is turned on.



Figure 32. Weighing of Constituent Material.

3.1.3.2. Stage 2: Mixing of Constituent Materials

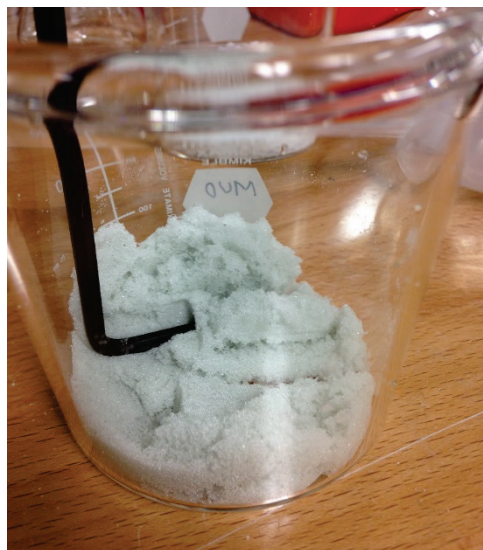


Figure 33. Resulting Desired “Clumpy” Texture of Soda Lime Glass Beads with H₂O.

In the next phase of the manufacturing process, a key step takes place, which is the mixing of the high impact polystyrene pellets and the soda lime glass beads with H₂O. The step-by-step procedure with specific chronological order that yielded the highest-quality results is described next. First, the half-gram of H₂O is added to beaker containing the soda lime glass beads, and mixed for a minute with a mixing stick, such as a hexagonal key to result in a texture similar to that shown in Figure 33. Then, about 10 grams of polymer, should be put away for the first layer of PBX mixture that will be added to the mold in the pneumatic press. After this, the now lumpy soda lime conglomerate can be added to the beaker of the polymer and mixing with the stick should be done for 3 minutes. An extra measure to ensure the correct mixing of the materials is pouring this mixture from one beaker onto another at least four times. The justification and proof of the added amount of water is described below in the section of manufacturing issues, as it improved the

distribution of the glass beads with the binding polymer material in the resulting mock PBX samples.

3.1.3.3. Stage 3: Preparing Mold in Pneumatic Press

At this point in the manufacturing process, the temperature of the inner part of the heating

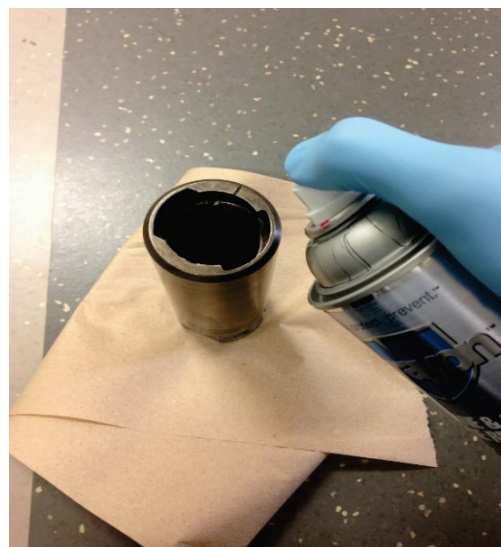


Figure 34. Applying Silicone Release Spray to PBX Mold.

element should be measured using an appropriate Fluke multimeter, to ensure it is close to its maximum temperature. This in turn means that the heat can be put on the mold and the heat transfer rate will be the highest possible, making the process the most time-efficient it can be. Next, it is necessary to ensure the appropriate dust-proof respirator mask is being worn. Then to apply the silicone spray to the cylindrical metallic tube (in a place with enough ventilation), the surface of the upper locking die, and the moving platform to prevent the sticking of the PBX specimen to these surfaces and thus affect its quality once it's been removed from the mold. It is important to consider that both the silicone release spray and the acetone are highly flammable, and should not be placed near a heat source at any point, as indicated on their Material Safety Data Sheets [72-73]. The procedure of applying the silicone release spray as lubricant onto the metallic cylindrical container is

shown in Figure 34. Next, this previously mentioned mold has to be fit correctly into the respective opening, and tightened securely using the screw. Then, the moving die should be moved all the way to the lowest possible point so that it simplifies the process of placing and

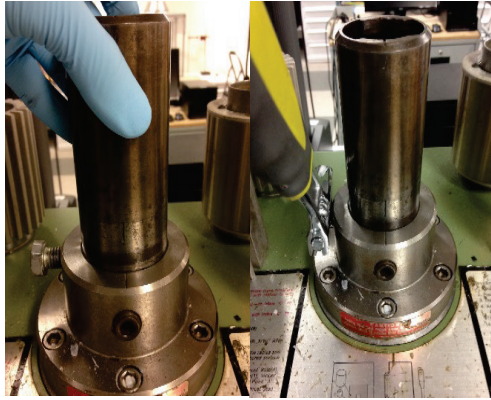


Figure 35. Placing and locking with cylindrical mold in pneumatic press.

fixing the cylindrical tube. The placing and locking of the cylindrical, metallic mold onto the pneumatic press using the adjustable screw and a wrench is also depicted in Figure 35. The next step is to raise the moving die to the highest point using the RAM control lever, as shown on Figure 37. This is done in order to posteriorly apply the electric heater around the moving die to optimize the heating of the polymer and soda lime glass mixture. The resulting PBX specimens, along with the added half gram of water, were consistently the highest quality specimens as opposed to the samples in which these two extra steps were no taken. The electrical heater being applied to the cylindrical mold is depicted as well, in Figure 36 in the next page. The heater should be left fitted onto the cylindrical container with the adjustable



Figure 37. RAM control and die moved fully up.



Figure 36. Electrical Heater applied to the cylindrical mold.

die, until the temperature of this aforementioned die reaches 135 °C. The motivation for this is that at this temperature the polymer pellets that come into the contact with the surface will begin to melt and will stick to the surface more easily, thus enhancing the process of creating a layer of polymer that can encompass the whole cylindrical sample and prevent concentrations of soda lime glass beads, which will inevitably occur, from falling out of the specimen and creating voids on the surface, disabling the PBX specimen for the purpose of testing.

3.1.3.4. Stage 4: Pouring Mixture into the Cylindrical Mold and Locking It In

After the mold has been fitted in place, and the desired temperature of 135°C has been reached (which usually takes an average of 15-20 minutes at a room temperature in the low 20's) the



Figure 38. Moving die adjusted up to eliminate the space with the mold.

mixture can now be poured into the mold where it will be heated and compressed to form the desired mock PBX sample. In order to do this, the adjustable, cylindrical die must be raised, however just enough in order to completely fill the void at the bottom and completely eliminate the space between moving die and the inner wall of the cylindrical mold. This is shown on an image to the left, on Figure 38. Following this, now very carefully the heterogeneous mixture of constituent materials into the cylindrical metallic tube can be poured (See Figure 39-A). This, should be preceded by the pouring of the 10 grams of polymer that were set aside from the mixture with added H₂O to it, in order to create a 'floor' on which the mock PBX specimen can be formed. It was discovered that prior to adding this extra step to it, if a significant amount of soda lime glass fell isolated on the bottom layer it would tend to fall off as it would not have a coating of polymer to bond to and remain solid and compact after the solidification and removal process. After all of the mixture has been poured in the cylindrical tube, the external cylindrical die should be placed into

the cylindrical metallic tube (See Figure 39-B) in such a way that the die should fit inside the tube and leave a small gap for the die holder. Then the die holder is placed on top of the external

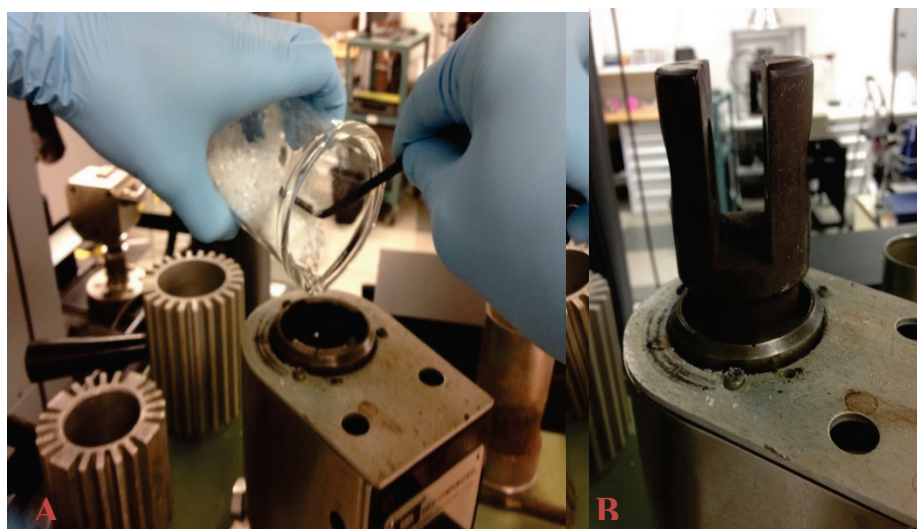


Figure 39. Pouring in of mixture into metallic tube (A). Locking, external die being place on top of cylindrical mixture to compress the mixture (B). Locking die turned to 'locked' position to ensure safe compression of materials (C).

cylindrical die and inside of the metallic tube. The die holder must be switched into its locked position by twisting it 90 degrees, as shown in Figure 39-C. The die holder face reads "Lock" and "Open" for either case, so the user should ensure the former is securely adjusted. Another manner to ensure that the die holder has been placed into its correct position is to gently try to remove the die holder (it should not come out if locked in properly). At this point, the pressure should be raised to its maximum (4,000 psi with the given diameter of the locking die of 1.5

inches), and a crushing sound will be heard representing the densification of the mixed constituent materials with H₂O. After this, the pressure and heating element should be maintained at its current position for approximately 180 minutes to ensure adequate heat transfer through the metallic tube and into the mixture to yield the best resulting mock PBX possible.

3.1.3.5. Stage 5: Solidification and Removal of Mock PBX Sample

The final steps which will be described next involve the solidification or cool down process, and the removal of the cylinder-shaped resulting mock PBX sample that has been manufactured. The first step of the solidification process is to turn off the electric heating element within the pneumatic press. Then the researcher should place the two heat sinks with finned exterior around the metallic cylinder, to increase the surface area and the overall heat transfer rate through natural convection [74]. This can be seen Figure 40. Due to the heat expansion coefficient of the metallic, cylindrical mold in which the mock PBX sample solidifies, the research team used experimental results (i.e., the process of removing the specimen) to conclude that the higher the temperature at

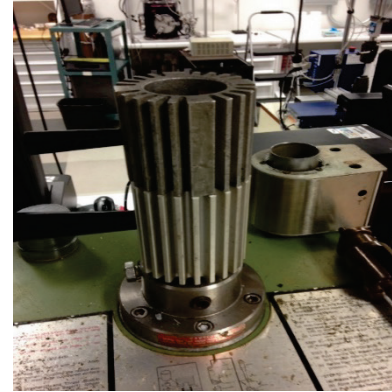


Figure 40. Heat Sinks applied over the metallic mold.



Figure 41. Mock PBX sample within the metallic mold (A). The mock PBX sample after removal from the mold (B), and the locking die as well (C).

which the sample is removed the less mechanical force it is required to remove accomplished, the fastening screw has be loosened in order to remove with the specimen inside using the appropriate wrench. After the mold is removed from the pneumatic press, the final step is to remove the mock PBX specimen from the mold (See Figure 41-A) , and this can be accomplished using a steel rod and a steel hammer to impact the upper, locking die with a downward force repeatedly to push down the mock PBX sample manufactured. The end product should come out of the metallic mold after several impacts (See Figure 41-B), so an absorbing layer of paper or plastic underneath the hammer is recommended to protect the integrity of the

PBX sample. In other words, at higher temperatures, the expansion of the metallic mold allowed for a more straightforward removal of the PBX sample with less force and a reduced number of impacts of the steel rod and hammer that were used to push down the specimen and remove it). As a result, the recommended time to wait after the heater is turned off, is anywhere between 10-15 minutes (with the heat transfer through natural convection occurring between the heat sink and the air a room temperature in the low 20's). This should cool down the temperature of the exterior of the metallic mold to 50°C- 60°C, making it manageable with the use of the heat resistant gloves, which should be worn for the process of removal of the mock PBX sample. After this time range, and the user has ensured that the temperature of the mold is not high, the pressure using the RAM lever should be removed. This is in order to remove the die holder that would otherwise be pressed against and would be extremely difficult to remove. Then the die holder has to be turned to its "Open" position. An important note is that if the die holder is tightened very strongly then a metallic rod or wrench can be used in conjunction with the hammer to turn the die hold loose and then to its "Open" position. After this has been sample once it hits the ground. And finally, the locking die is removed using the exact same approach (See Figure 41-C), to prepare for the next manufacturing batch.

3.1.4. *Manufacturing Issues*

3.1.4.1. Inadequate Mixing of Constituent Materials

The previously described and finalized novel process for manufacturing mock polymer-bonded explosives or its abbreviation PBX, was the end result of an experimental trial-and-error approach and the analysis of resulting specimens. Since the PBX specimen is supposed to be a heterogeneous particulate composite material, from the initial step of mixing the two constituent materials, High Impact Polystyrene and Soda Limes Glass beads, a great deal of attention was required. This is quite simply because the resulting mixture which would be later added to the cylinder lubricated with silicone release spray within the pneumatic press would largely determine the mixing interaction between the polymer pellets and the glass beads. Several mixing methods of the PBX component materials were at experimented with during the first trials. One method consisted of mixing the two materials in a beaker after being weighed individually and then proceeding to add the resulting mixture to the cylinder in the pneumatic press. Another method was adding each constituent material to the cylinder individually and then using the mixing stick to mix the materials into what should turn into a heterogeneous composite material that should, by definition, not be uniform throughout to resemble more closely an actual polymer-bonded explosive. Both of these mixing methods, however, yielded PBX specimens that revealed a fundamental issue with the process: the glass beads were not adhering to the polymer pellets adequately to stick to them once the polymer was melted. Therefore, the resulting solid specimens had clusters of pure soda limes glass that would not only fall off from the specimen easily and leave large voids on the surface, but were not yielding an acceptable heterogeneous composite material. Further analysis by cutting the PBX specimen revealed that these concentrations of soda lime glass beads were occurring on the inside, and overall these described mixing processes were deemed unsuccessful in creating the desired heterogeneous composition of the mock PBX. An image of one of the specimens created using this ineffective method is depicted on Figure 43.

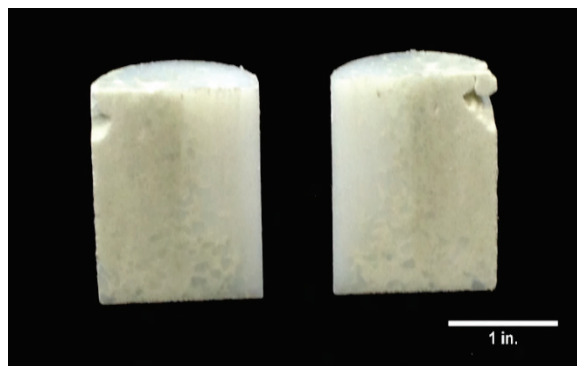


Figure 43. Several Defective PBX Samples Made with no amount of water.

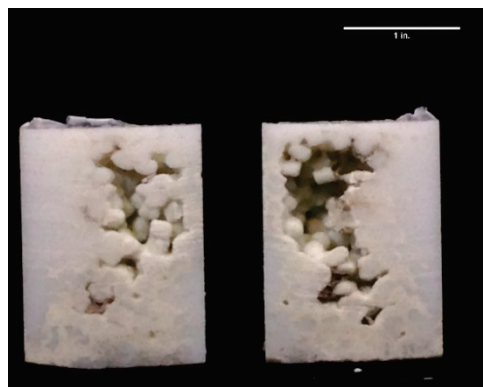


Figure 42. Interior Voids within Defective PBX Samples Made with 2 grams of H_2O .

On this image, it can be appreciated that the glass beads and the polymer are completely apart, and the mock PBX sample is not a good imitation of the actual heterogeneous particulate material, which does not have a definite, repeatable pattern but is instead mixed in a heterogeneous manner. It is also important to note, that the heating time was increased from the original 50 minutes that were calculated (using the arithmetically calculated rate of heat transfer from the metallic mold onto the PBX mixture, assuming a perfectly linear and constant rate of heat transfer for calculation purposes) to 90 minutes because the polymer pellets on the inside of the cut specimens near the center of the specimen were not melted and remained solid.

3.1.4.2. H₂O Excess and Heating Time

The next development resorted to in an attempt to fix this issue was the addition of a small amount of water to the mixture of both materials before pouring it in the cylinder within the pneumatic press. At first, the amount of liquid H₂O was arbitrarily selected to be 2 grams, resulting in a ratio of approximately one gram per 35 grams of the heterogeneous composite materials for every specimen. The ratio is described as approximately because the mass of the resulting specimens varied slightly from specimen to specimen, even while following the same process identically. This is presumably due to losses of the aforementioned materials caused by sticking to the inside of the flasks during the weighing and mixing process, and to the cylinder surface during the heating and pressurization process. After going through the manufacturing process numerous times with the arbitrarily selected amount of H₂O of 2 grams, the resulting specimens showed a great improvement over the previous specimens that had no H₂O added to the mixture, but still had some deformations in the form of air voids on both the outer surface and on the inside of the mock polymer-bonded explosives. At the bottom of the previous page, on Figure 42, the interior of one of these aforementioned samples is shown. As it can be seen, these large voids make the sample impractical for mechanical testing purposes because the large size of the voids would greatly affect the results, since it would fail faster in any given test due to the lack of material. The heating time at this point of the manufacturing process remained at 90 minutes, since it consistently yielded higher-quality samples than before with only 50 minutes. The images of other samples with defects caused presumably by excessive water in the mixture are presented next, and one that shows the outer part, the top part in fact are presented below in Figure 44. The meaningful conclusion from these defective specimens using 2 grams of water, and a heating time of 90 minutes, is that these voids were being caused by the water since the original specimens did not have these defects. The experimental results were analyzed and it was concluded that there were trade-offs between the amount of water and the heterogeneity of the mixture. In other words, the amount of water improved the mixing of the polymer pellets and the glass beads, but resulted in large voids in the exterior and interior that made the specimens useless for the desired purposes. This could be attributed to a number of factors. Such as improper mixing of the component materials, resulting in clusters of glass beads that could fall off the specimen at the moment of impact when the specimen is removed from the cylinder. By inadequate pressure levels throughout the melting process, resulting in air gaps within the PBX

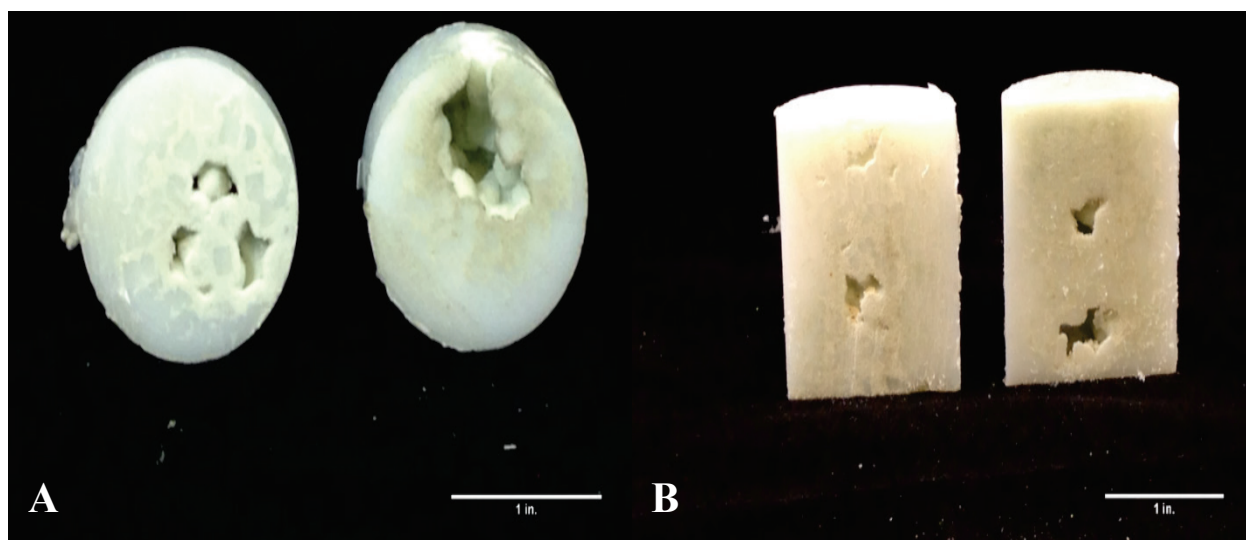


Figure 44. Inner Face (Left) and Top Face (Right) of a PBX Samples Made with 2 grams of H₂O (A) and the Inside of Another PBX Sample Made with 2 grams of H₂O (B).

specimen that remain after the cooling and solidification stage. The first parameter to be modified to further increase the quality of the mock polymer-bonded explosives, was the amount of water used due to indicative evidence. The rationale for this was that the amount of water in the mixture could be a factor in creating the air voids since 2 grams is significant enough that it was presumed that the physical change to its gaseous state could be modifying the PBX specimen as it is heated and when it is cooled down and solidifies. This could be explained in an alternative way that the liquid H₂O turning into water vapor gains thermal energy and moves within inside the cylinder with the mixture and could create voids of air and/or H₂O within the specimen that remain after the specimen solidifies and the water condenses and turns into liquid droplets.

The next measure taken was to experiment with lesser amounts of H₂O to reduce the negative effects it appeared to be having on the quality of the specimens. The practical approach for this was to use the least amount of water possible in order to create the desired ‘lumpy’ texture of the glass beads in multiples of half a gram. The team discovered that half a gram of H₂O was sufficient to create that required texture. Several mock PBX specimens were created with this process, yielding much higher-quality specimens overall. The reduced amount of water and the relationship to the increase of quality of the specimens presumably confirms that the amount of water was the likely responsible for the defects in earlier specimens. An example of this high-quality specimens produced can be seen on Figure 45. On this image, it can be observed how the mixture of the component materials has mixed enough resulting in great quality of heterogeneity of the mock PBX sample. The image also shows the outer face and the interior with a horizontal cut to view its inside. This method of manufacturing with a new fixed amount of water, lead to another parameter to adjust, the heating time. While overall good resulting specimens were

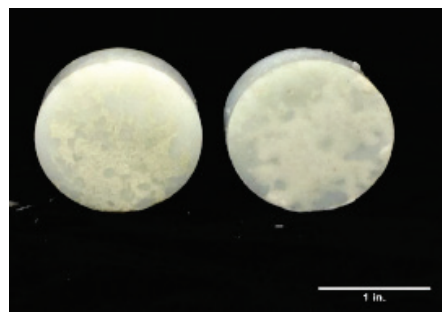


Figure 45. Outer Face (Left) and Inner Face (Right) of PBX Samples Made with .5 grams of H₂O.

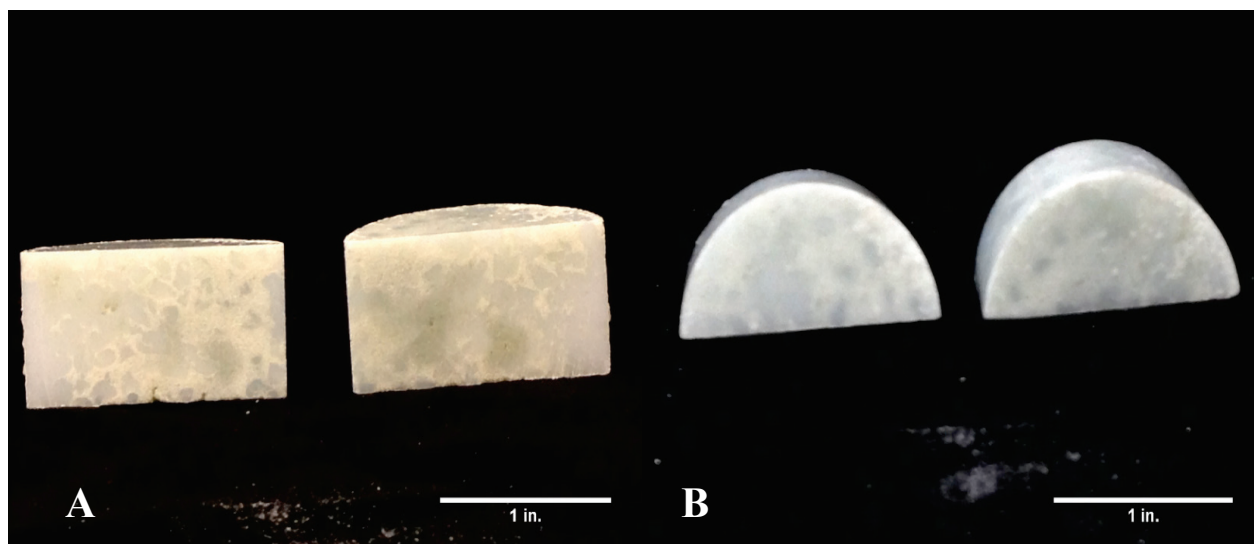


Figure 46. (A) Inner face (left) and top and bottom face (B) of a PBX Specimen manufactured with the finalized manufacturing process.

manufactured with 0.5 grams of water and with a heating time of 90 minutes (such as the previous figure shown), some polymer pellets that had not melted properly near the center of the specimen (meaning that the heat transfer from the metallic mold was not occurring all the way through the center) and taking advantage of the fact that the heating process does not require any active supervision the heating time was doubled to the current ideal time of 180 minutes. Therefore, all of the specimens that were used for mechanical testing were manufactured and had these two parameters adjusted. Some of these high-quality specimens with the finalized parameters used are shown in Figure 46. As it can be appreciated on the images of the same specimen, which were cut for the half-bending mechanical test, these samples are solid throughout and show a high-quality mixture of the constituent materials with one another, giving it a more realistic characterization of the real heterogeneous particulate composite energetic material that the research team is attempting to emulate to determine its mechanical behavior. It is important to disclose, that using this final manufacturing procedure with optimized parameters of H₂O amount and heating time, some specimens manufactured had some internal vacancies even if the exterior looked neat. This ratio, however, was very small to the number of high-quality mock PBX samples that were produced using this method. A visual reference of such imperfect specimens can be seen to the right, on Figure 47. Another plausible explanation for this voids, is that at the time of using the abrasive cutter there was a concentration of soda lime glass beads in the region that was not coated by the polymer and simply fell off during the process. This theory also provides a possible explanation for the polymer pellets that did not melt, in correlation with the significant discrepancy thermal properties of both component materials. The material data sheets on these material types indicate that the thermal conductivity and specific heat of the polymer and the soda lime glass are quite different. The thermal conductivity of the soda lime glass beads is more than four times larger than that of the polymer, and the specific heat is 59% less than the specific heat of the polymer as well [76, 77], creating a less than ideal uniform heat transfer situation. In simpler terms, it means that the soda lime glass beads are better conducting the thermal energy while the mixture is being heated, but takes much longer to increase its temperature due to its higher specific heat. This in turn could resulted in polymer pellets that are isolated in clusters of soda lime glass beads and that do not receive enough heat conducted in their direction to melt as desired, explaining the internal voids in the manufactured specimens.

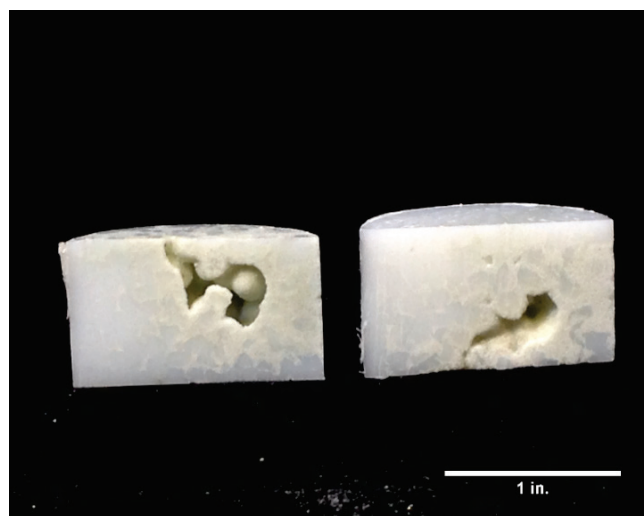


Figure 47. Voids Within Defective PBX Samples Made with Optimized Process.

3.1.4.3. Amount of Component Materials

Another issue that was faced as the development of the novel PBX manufacturing process was the amount of component materials used; first it was opted for a mass-based composition to determine the ratio of each material in the mixture, the total weight had to be calculated based on experimental attempts and observations. For the most part, the problem that would occur would

be when the material would overflow from the mold, and the upper locking die and the die holder could not be properly attached, creating a mechanical hazard. The solution for this that the team figured out was to revise the amount, and after a repetition of attempts, the total mass ideal to yield the desired height (diameter of the specimen was constant) was reached at 70 grams.

3.1.4.4. Removing Specimen from Cylinder

Perhaps the least straightforward step during the manufacturing process was removing the mock energetic material specimen once it had cooled down and solidified. This step was simplified to the greatest extent possible by applying a lubricant, in this case Silicone Release Spray, to make the task of taking out the manufactured specimen less physically demanding. This step, still involved a significant amount of physical effort since a hammer and a solid, steel tube were used to impact the locking piece of the cylinder until the specimen could be taken out. It also presented unforeseen problems since the strenuous impacting of the cylinder would cause some areas with glass beads on the surface to fall off from the manufactured sample. Thus, rendering the specimen useless as it had too many surface defects and voids to be considered to yield reliable results during the mechanical tests. This problem really stems from the procedure in itself and it was not something that could be altered to improve the manufacturing results, other than ensuring that sufficient time was given to allow the PBX sample to cool down and solidify throughout.

3.1.4.5. Other Issues

Other non-systematic problems that were faced at least once during the manufacturing process and that were directly related to the equipment and process in itself involved the air pressure hose connected to the pneumatic press. As mentioned, this was not a problem with the procedure in itself but rather of the nature of the equipment being used. For example, the hose was disconnected due to improper moving of the pneumatic press causing it to be in an awkward position. In other cases, the pneumatic press, presumably due its use, did not maintain the maximum pressure required for the specimen to be compressed and yielded very porous specimens, one of which can be viewed on the right, on Figure 48.

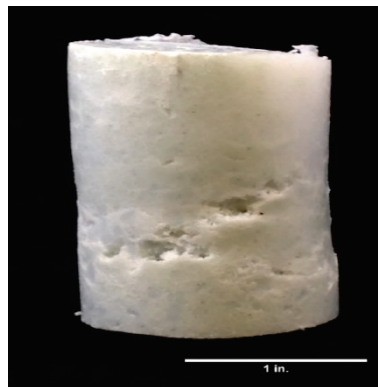


Figure 48. Flawed PBX Due to Pressure Failure.

3.2. SPECIMEN MACHINING

3.2.1. Machining Equipment

The detailed, technical specifications of the equipment utilized for the machining of the manufactured cylindrical-shaped, mock energetic materials into the required geometry required for the mechanical tests is given in Appendix C of [75].

3.2.2. Machining Process

To obtain the desired geometry on the manufactured PBX samples for the mechanical tests several different machining equipment were necessary. A full description of the machining equipment is found in Appendix C of [75]. The compression test did not require any mayor

modification because the manufactured product was of a cylindrical nature, resulting in the desired geometry directly from the manufacturing process. The only necessary machining was to polish the specimen. The dimensions are further specified in the mechanical testing section along with its respective figures. Overall, however, the diameter remained constant for all machined specimens, except for the Bridgman Notch sample, which had a circular notch of .3 inch-diameter cut at the center (See Figure 50-Figure 49). For the bending and semi-bending tests, the abrasive cutter simply had to be used with care to make a clean cut, and result in the desired geometry (See Figure 45 for bending test or indirect tensile test geometry, and Figure 46 for semi-circular bending geometry test) each with its respective required thickness for valid mechanical testing results; and at the end, to remove any unwanted residues that might affect the test results in the form of surface roughness or extra materials that results from the abrasive cutting the polisher was used.

3.2.3. *Bridgman Notch Procedure for Mock Polymer-Bonded Explosive*

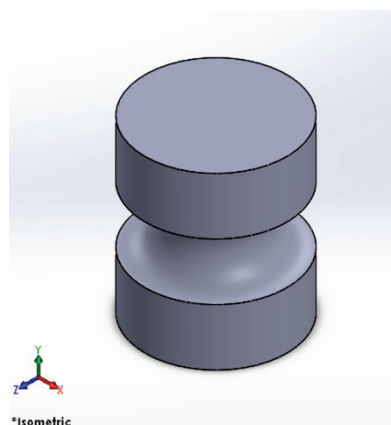


Figure 50. CAD Model of Bridgman Notch Specimen.

The procedure followed to obtain the desired geometry on the polymer-bonded explosive required the use of a CNC lathe, and its software, along with the corresponding CAD drawing done in SolidWorks 2015. The CAD drawing of the model can be seen on Figure 50. Since Computer Numerical-Control (CNC) machines do not require much input during the actual machining process, the only task was to convert the CAD file into 'IGS' format to make it readable for the CNC software to process and perform the desired machining. The resulting and actual mock PBX sample is



Figure 49. Bridgman Notch Specimen.


seen Figure 49, where it can be appreciated the high quality not only of the sample in itself, but of the cut performed by the CNC Lathe. It is important to repeat that the height of this Bridgman Notch Test mock polymer-bonded explosive is the same as the original manufactured cylindrical explosive, and only had a semi-circular notch cut into it with a radius of .30 inches right at the center of the specimen in the vertical direction. More details about the equations utilized for this are given in the mechanical testing section.

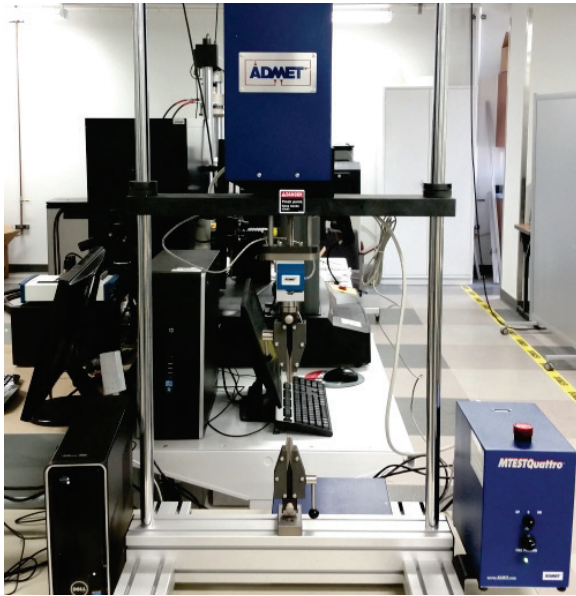
3.3. MECHANICAL TESTS

MERG performs several distinct mechanical tests on a variety of materials. Currently, the group is conducting tests on HPCs, steels, and additively manufactured polymers. Our mechanical testing involves the use of Universal Testing Machines (UTMs). These machines are designed to measure the mechanical response of diverse materials when subject to mechanical loads. The outcomes are the mechanical properties of materials. They can perform several ASTM International standardized tests including but not limited to: tension wedge, tensile threaded,

compression, spherical seat compression, three- and four-point bending, shear, compact tension, punch, etc. The only limited factors are the availability of appropriate grips, load cells, and displacement measurement devices. All tests must be performed according to ASTM International standard in order to be viable for publication. Tests that are not according to ASTM International standard are not performed by MERG, unless they involve materials and processing yet to be standardized by the relevant ASTM international committee. So far, no test of that nature have been performed or are planned by MERG. Students conducting these tests are required to wear several personal protective equipment including: lab coats, closed toe shoes, EN 166 compliant eye protection, and ear protection (for tests that produce audible acoustic emissions, none so far). A detail description of each UTM and examples of the mechanical testing capabilities of MERG are located below in Table 10. All tests were performed using a universal testing machine, Instron 5969 Tabletop Universal Testing System.

Table 10. MERG Testing Equipment

<p>Instron 5969 Tabletop Universal Testing Systems</p> 	<p>5969 Dual Column Tabletop Testing Systems are universal, static testing systems that perform tensile and compression testing; also perform shear, flexure, peel, tear, creep, cyclic, and bend tests.. Typically used for plastics, metals, rubber materials, automotive components, composites, and non-ambient temperature applications.</p> <ul style="list-style-type: none"> • $\pm 50\text{kN}$ Load Cell • 1/2"-20 Threaded Self-Aligning Tension Grips • 6" compression platens • 3+4 point bending test fixtures • Instron T3119-600 environmental chamber (-150°C to +350°C) • Synchronized with Vic-3D DIC System <p>Product Link: http://www.instron.us/wa/product/5960-Dual-Column-Testing-Systems.aspx</p>
<p>ADMET eXpert 5600 Series UTM</p>	<p>Highly configurable 5603 Universal Test System with MTESTQuattro Controller. A dual column frame for extended horizontal test space capable of performing tension, compression, and bending tests. While the 5000 series testers are highly configurable, they maintain their rigidity and precision needed for precise control.</p> <ul style="list-style-type: none"> • $\pm 4.5\text{kN}$ Load Cell • 5kN 10mm Wedge Grips

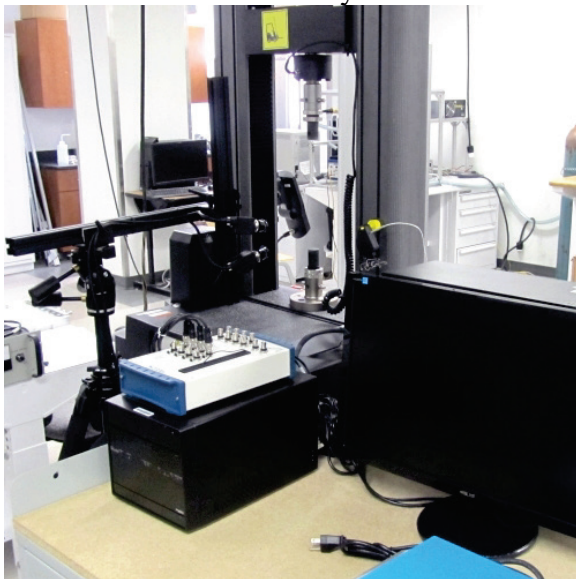


- 5kN 56mm Compression Platens
- Detachable Actuator
- Synchronized with Vic-3D DIC System

Product Link:

<http://admet.com/products/universal-testing-machines/expert-5000/>

Correlated Solutions Vic-3D Digital Image Correlation System



Vic-3D provides full-field, 3-Dimensional measurements of shape, displacement and strain, based on the principle of Digital Image Correlation. Using this method, actual object movement is measured and the Lagrangian strain tensor is available at every point on the specimen's surface. Vic-3D can measure arbitrary displacements and strains from 50 microstrain to 2000% strain and above, for specimen sizes ranging from <1mm to >10m.

- Synchronized with UTMs
- Two 2.0 Megapixel Digital Cameras (1624 x 1224 @ 30 fps)
- Fulcrum Software for vibration or fatigue synchronization

Product Link:

<http://www.correlatedsolutions.com/vic-3d/>

3.3.1. Overview

The mechanical properties of PBX subject to various loading conditions is important to avoid the risk involved in the manufacture, storage and transportation of these energetic materials [77, 50]. Direct tensile test is the most conventional test to measure tensile properties. However, for brittle materials, the direct tensile test is inconvenient due to difficulties in specimen preparation and test operation [78]. Uniaxial compression tests, full-Brazilian tests and semi-circular tests are the common alternatives for measuring tensile properties of brittle materials. Applied load, strain

rate, and deformation are the raw data generally collected from experiments for post-processing to characterize the material properties. Optical techniques of measuring deformation during mechanical testing has become popular instead of strain gauge measurement. Strain gauges attached to the specimen and give a measure of the deformation between two points and may provide local reinforcement due to the contact with the specimen. On the other hand, digital image correlation (DIC) compares images captured before and after the test without contact with the specimen [80]. A micro-scale level of deformation analysis can be recorded using DIC [77]. Rae et al. [79] have applied the DIC technique to determine microscopic displacement and strain fields of PBX during Brazilian disc test. Zhou [81] used DIC to calculate strain fields and analyze micro-scale deformation and fracture behavior of a PBX simulant under tensile stress. Zhou and colleagues have applied DIC to study the quasi-static compression deformation and fracture behavior of PBX [81]. Later, Zhou and colleagues applied DIC to obtain dynamic deformation information of Brazilian disc tests (BDT), flattened Brazilian disc (FBD) tests and semicircular bending (SCB) tests [81].

Multiaxial response of material is another important mechanical property. Test under uniaxial loading on Bridgman notch specimen can emulate multiaxial load phenomena [82, 83]. Under uniaxial loading the radial deformation resistant produces by the notched bar develops the state of triaxial stress thus emulates the study of discontinuous shaped components under triaxial stress conditions [84].

The subject material in this study is a complex composite of glass beads in a polymer matrix. Crystal properties such as size, distribution, and weight compositions; and binder property such as elastic-plastic behavior affects the performance of the composite [85]. Interfacial properties such as surface energy, interfacial strength, and glass beads-polymer intermixing control the small scale mechanical behavior influencing the block properties [85, 86]. In this study uniaxial compression test, indirect tension test, semicircle bending test and Bridgman notch specimen test will be performed.

In this section, a description of each test will be provided with a discussion of test standards, equations used for analysis, test conditions, the raw data to be collected, and any non-conformity criteria.

3.3.2. *Uniaxial Compression Test*

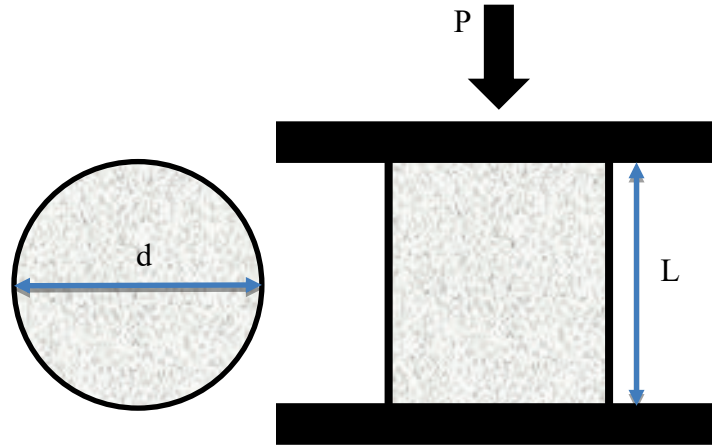


Figure 51. Uniaxial compression test configuration

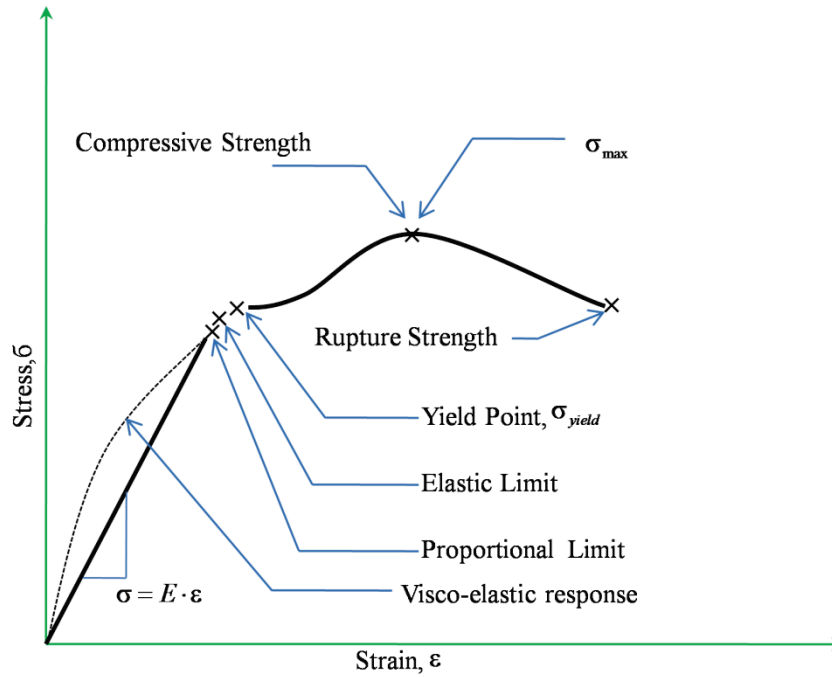


Figure 52. Typical Stress-Strain curve

Glass beads- polymer composite may exhibit viscoelastic behavior. During deformation viscoelastic material undergoes viscous and elastic behavior. Models for viscoelastic materials stress-strain behavior is different than that of elastic material. Maxwell model, Kelvin-Voigt model, and the standard linear solid model are used to predict viscoelastic material response under different loading conditions.

Uniaxial compression is important to study the yield properties of glass beads-polymer matrix. Direct tensile test is not suitable for this type of material. This is due to the comparative high tensile stress of the complex composite such that fracture occurs prior to macroscopic yield [80]. A compressive load is applied along the centerline of the specimen till fracture [Figure 51].

Usually compressive properties are expressed per unit of minimum original cross sectional area [ASTM D695-10]. Most of the compressive properties can be found in typical stress-strain curve [Figure 52]. According to ASTM D695-10, compressive strength is the maximum compressive stress (σ_{\max}) carried by the specimen during the compression test,

$$\sigma_{\max} = \frac{F_{\max}}{A_i} \quad (9)$$

Where A_i is the initial cross-sectional area and F_{\max} is the maximum applied compressive load. The compressive yield strength is the yield load required per unit initial cross sectional area. The first point on the strain-stress diagram where an increase in strain is visible without an increase in stress is defined as compressive yield point. Brittle material may not exhibit a yield point.

$$\sigma_{com,yield} = \frac{F_{yield}}{A_i}, \quad \frac{\partial \sigma}{\partial \varepsilon} = 0 \quad (10)$$

Nominal longitudinal strain is a dimensionless parameter defined as the deformation per unit initial length.

$$\varepsilon_{n,l} = \frac{l - l_0}{l_0} \quad (11)$$

Where, l is the final length and l_0 is the initial length of the specimen.

The relation between true strain and the nominal longitudinal strain is defined as follows

$$\varepsilon_{t,l} = \ln(1 + \varepsilon_{n,l}) \quad (12)$$

The Poisson ratio is obtained by dividing the nominal transverse strain by the nominal longitudinal strain.

$$\nu = - \frac{\varepsilon_{n,t}}{\varepsilon_{n,l}} \quad (13)$$

Modulus of elasticity is obtained by the ratio of stress to the corresponding strain below the proportional limit of the material.

$$E = \frac{\sigma}{\varepsilon} \quad (14)$$

Materials may exhibits viscoelastic deformation upon loading. Maxwell, Kelvin-Voigt, standard linear model can be used to accommodate viscoelastic response of the subject material.

To assess the repeatability and reproducibility of the experiment, multiple test must be performed. Standard deviation can be calculated using the following equation

$$s = \sqrt{\sum (X - \bar{X})^2 / (n - 1)} \quad (15)$$

Where X is the value of single observation, \bar{X} is the arithmetic mean of all observations, and n is the number of observations.

3.3.2.1. Test conditions

Load is applied at a constant deformation rate on the specimen. According to ASTM D695-10 the standard speed of the uniaxial compression test shall be (1.3 ± 0.3) mm/min for rigid plastics

including high modulus composites. The standard preferred specimen size for a right cylinder is 12.7 mm diameter by 24.5 mm height. Colak [88] has conducted uniaxial compression test on PBXW-128 at a strain rate of 0.01/sec. PBXW-128 is a soft, rubbery solid comprised of approximately 60% by volume HMX powder in a polymer binder. Zhou and colleagues [81] conducted uniaxial compression test on plastic bonded explosive (PBX) samples with aspect ratios of 1.8, 2.0 and 2.3, at a speed of 0.1 mm min⁻¹. Jerabek and colleagues [88] have suggested that for a right cylinder the dimensional ratio should range $1.5 < l/d < 2$ to avoid buckling, barreling, and friction effects.

In the current study

- Dimensions, diameter (d) and height (L)
- Specimen Aspect ratio: $1.5 < l/d < 2$
- Test speed: 0.14 mm/min

3.3.2.2. Raw data collection

Instron 5969 Tabletops Universal Testing System can record load, crosshead displacement and time. The specimen dimension have to be measured before testing. From these data sets the compressive properties can be calculated. Beside this data collection, a 3D DIC analysis will provide the Poisson ratio and better understanding of compression properties.

In the current study the report contains

- Compressive Stress-Strain curve.
 - Compressive strength σ_{\max} .
 - Compressive yield strength, $\sigma_{\text{com,yield}}$.
- Poisson ratio, ν_n .
 - Nominal longitudinal strain, ϵ_l .
 - Nominal transverse strain, ϵ_t .

3.3.2.3. Non-conformity criteria



The material may be prepared by compression or injection molding of the material to be tested. Careful machining is required to ensure a smooth surface. The contact between the compression plate and specimen surface is very important. Friction at the contact surface may lead to a multiaxial stress state and specimen barreling. Use of PTFE (poly-tetrafluoro-ethylene) lubricant or tape is common to avoid friction at the contact surface [87, 88]. The specimen center line is aligned with the center line of the compression plate, and the specimen is parallel with the surface of the compression plate. A misaligned specimen surface and compression plate may generate nonlinear force-displacement curves [88].

Figure 53. Quasi Static Uniaxial compression Testing Specimen

3.3.3. Indirect Tensile (Brazilian) Test

In the Brazilian (indirect tensile) test, a disc of material is subjected to two opposing normal strip loads at the disc periphery [Figure 54]. Brazilian test is suggested method for determining the

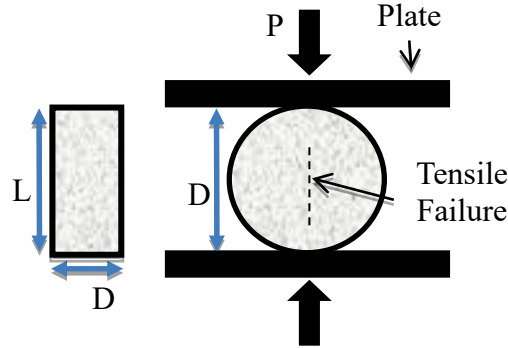


Figure 54. Indirect tension test

tensile strength of brittle material like concrete [89]. However, indirect compression test is also a common practice for studying the deformation and fracture behavior PBX simulant material (highly particle filled composites) [50].

The analytical solutions to the stress field during Brazilian tests founded [90-94] formulated stress on the axis of the circular cross-section as follows

$$\sigma_{xx}(x, 0) = \frac{2 \cdot P}{\pi a L} \left[\frac{(1 - \bar{x}^2) \sin 2\alpha}{1 + 2\bar{x}^2 \cos 2\alpha + \bar{x}^4} - \tan^{-1} \left(\frac{1 - \bar{x}^2}{1 + \bar{x}^2} \cdot \tan \alpha \right) \right] \quad (16)$$

$$\sigma_{yy}(x, 0) = -\frac{2 \cdot P}{\pi a L} \left[\frac{(1 - \bar{x}^2) \sin 2\alpha}{1 + 2\bar{x}^2 \cos 2\alpha + \bar{x}^4} - \tan^{-1} \left(\frac{1 - \bar{x}^2}{1 + \bar{x}^2} \cdot \tan \alpha \right) \right] \quad (17)$$

$$\sigma_{xx}(0, y) = \frac{2 \cdot P}{\pi a L} \left[\frac{(1 - \bar{y}^2) \sin 2\alpha}{1 + 2\bar{y}^2 \cos 2\alpha + \bar{y}^4} - \tan^{-1} \left(\frac{1 + \bar{y}^2}{1 - \bar{y}^2} \cdot \tan \alpha \right) \right] \quad (18)$$

$$\sigma_{yy}(0, y) = -\frac{2 \cdot P}{\pi a L} \left[\frac{(1 - \bar{y}^2) \sin 2\alpha}{1 + 2\bar{y}^2 \cos 2\alpha + \bar{y}^4} - \tan^{-1} \left(\frac{1 + \bar{y}^2}{1 - \bar{y}^2} \cdot \tan \alpha \right) \right] \quad (19)$$

where, P is the applied load, L and R is the length and radius of the cylinder, 2α is the radial angle, $\bar{x} = x / R$ and $\bar{y} = y / R$. Stress at any point along the axis can be determined using these aforementioned equations.

Indirect tensile strength can be calculated using following equation

$$\sigma_{in} = \frac{2P_{\max}}{\pi \cdot (D \cdot L)} \quad (20)$$

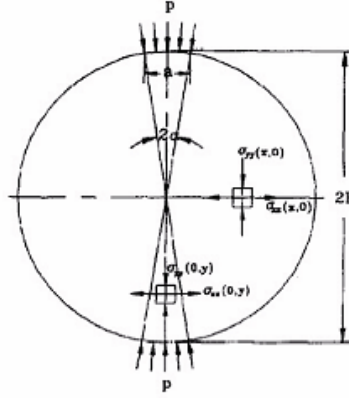


Figure 1. Indirect compression test

3.3.3.1. Testing conditions

According to TEX-226-F and ASTM D6931 the test deformation rate for bituminous mixture is $50 \pm 5 \text{ mm/min}$ at temperature of 25°C . Chen and colleagues [50], have conducted indirect tension test on PBX simulant material at 0.05 mm/min . It is suggested that the surface in contact with the specimen needs to be machined to the curvature of the test specimen. Liu [95, [50] has stated that a flat loading surface can be used for indirect tensile test. It is shown that for a contact angle ranging from $0^\circ \leq 2\alpha \leq 15^\circ$ the displacement profile change is negligible. In this study, a flat loading surface is used.

According to TEX-226, for a specimen of 4 inch diameter the core height should be 1.5 inch and for a specimen of 6 inch diameter the core height of 2 inch is recommended. ASTM D6931 recommended that the minimum height of the specimen should be at least half of the diameter. The length of the loading strip shall exceed the length of the specimen. $D/t \geq 2$. Chen and colleagues [50] has conducted Brazilian test on PBX simulant material of 20 mm diameter and 8 mm thickness of dimension at 0.05 mm/min strain rate.

In this study

- Specimen Aspect ratio: $D/t \geq 2$
- Test speed: 0.05 mm/min

3.3.3.2. Raw data collection

Instron 5969 Tabletop Universal Testing System can register load with corresponding time increase. The specimen dimension have to be measured before testing. From these data sets the required indirect tensile strength can be calculated. Beside this data collection, a 3D Digital Image correlation analysis will provide better understanding of this properties.

- Dimensions, Length, and diameter.
- Indirect tensile stress, σ_{in}
- Poisson ratio, ν_n

- Nominal longitudinal strain, ε_l .
- Nominal transverse strain, ε_t .

3.3.3.3. Non-conformity criteria

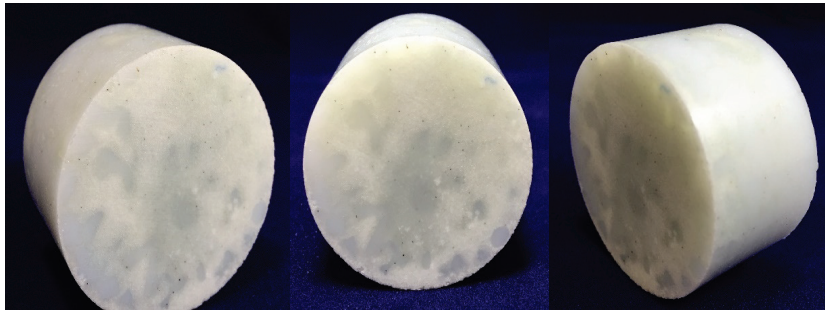


Figure 55. Indirect Tensile (Brazilian) Specimen before Speckle pattern.

It has been observed that tensile strength obtained by Brazilian test may be lower than the direct tensile test. Yu and colleagues [89] has suggested that this is due to the compressive stress opening vertical microcracks thus failure occurs at a slightly lower (around 11% reduced) tensile stress.

3.3.4. Semi-Circular Bending (Half Brazilian) Test

Materials with weak tensile properties can be tested using the semi-circular bending test [Figure 56] to induce tensile fracture [50]. It is suggested that semi-circular bending test (SCB) can be used as alternative to the Indirect tensile test [96]. SCB tests can also be used to calculate fracture energy, G_f . Fracture energy is defined as the energy required to create a unit surface area of a crack [AASHTO]. The fracture energy can be used as an index parameter to identify mixtures with increased fracture resistance.

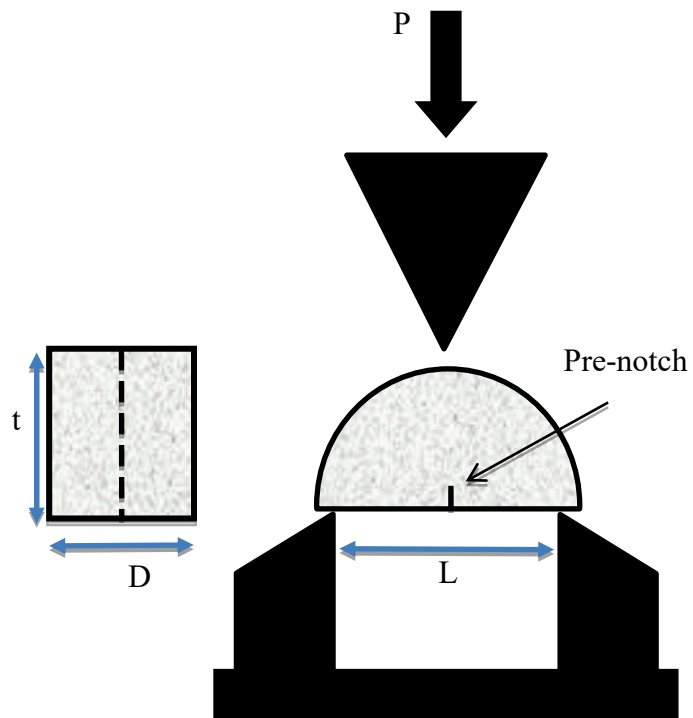


Figure 56. Semi-circular bending test configuration

The tensile stress at the notch of the lower surface can be calculated as follows [91]

$$\sigma = \frac{3PL}{2th^2} \quad (13)$$

Where, P is the load, L is the spacing between the supports, t is the thickness of the specimen, and $h = D/2$ is the height of specimen.

The fractural resistance, J_c can be calculated from the following equation

$$J_c = -\left(\frac{1}{t}\right) \cdot \frac{dU}{da} \quad (14)$$

where a is the notch depth, and U is the strain energy to failure. This strain energy can be determined from load versus deformation curve [96].

The fracture toughness can be determined by using following equations [50]

$$K_{IC} = \frac{P_c \sqrt{\pi \cdot a}}{D \delta} Y_k \quad (15)$$

Where P is the applied force, D is the diameter of the SCB specimen and δ is the thickness. Y_k is the dimensionless stress intensity factor.

The fracture energy can be calculated by dividing the work of fracture by the ligament area:

$$G_f = \frac{W_f}{A_{lig}} \quad (16)$$

Where G_f is the fracture energy (J/m^2), W_f is the work on fracture defined as the area under the

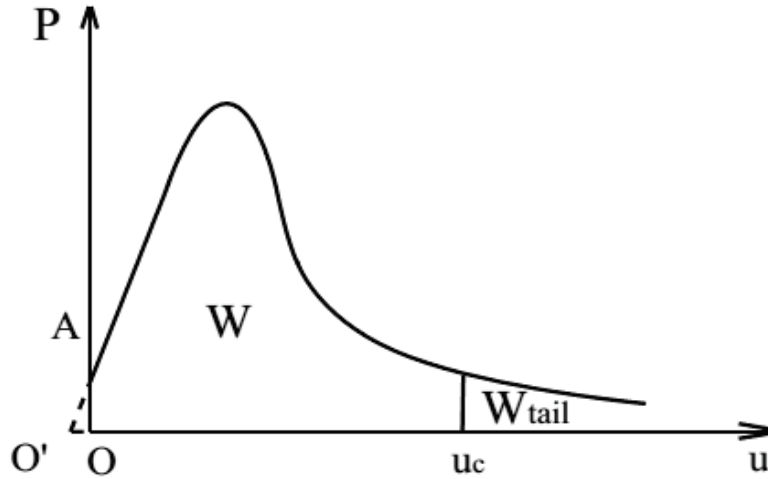


Figure 57. Expected Load versus displacement curve

load versus load line displacement curve defined as $W_f = \int P du$. P is the applied load and u is the load line displacement. A_{lig} is the ligament area defined as $A_{lig} = (r-a) \cdot t \text{ mm}^2$ and r is the specimen radius[AASHTO].

3.3.4.1. Testing conditions

Wu et al [97] has conducted SCB test on asphalt at 25°C at a deformation rate of 0.5 mm/min. AASHTO standard also suggest the same rate of 0.5 mm/min for asphalt mixture. Each semi-circular specimen contains a notch along the symmetrical axis. It is a common practice to use

different notch depth with a fixed notch thickness. According to AASHTO/ASTM 1559 the semi-circular specimen is to be 150 mm diameter and 57 mm of height with the notch width of 3.0 mm. It is suggested that three nominal notch depth of 25.4 mm, 31.8 mm, and 38 mm with tolerance of $\pm 1 \text{ mm}$ can be used. AASHTO have suggested a different deformation rate of 0.0005 mm/s to calculate fracture energy. And the suggested dimension is 150 mm diameter with $25 \pm 2 \text{ mm}$ thickness. According to AASHTO for an asphalt specimen with diameter of 150 mm the span between the lower supports is 120 mm. In this study the diameter of the specimen is 38 mm and the space between the supports is 30 mm.

In this study

- Specimen is of 38 mm diameter and 19 mm of height.
- Test speed: 0.047 mm/min
- Space between the supports 30 mm.

3.3.4.2. Raw data collection

Before the test is carried out, is necessary to first measure the room temperature and the dimensions of the specimen. During the test time increase, the corresponding load and the deformation data is collected. Instron 5969 Tabletop Universal Testing System can register this data points automatically given the time step. According to AASHTO the test report should include mainly the fractural resistance J_c , with mean value and standard deviation.

- Dimensions of the specimen, h and t
- Ligament area, $A_{lig} = (r - a) \cdot t \text{ mm}^2$
- Spacing between the supports, L
- Maximum applied load, P

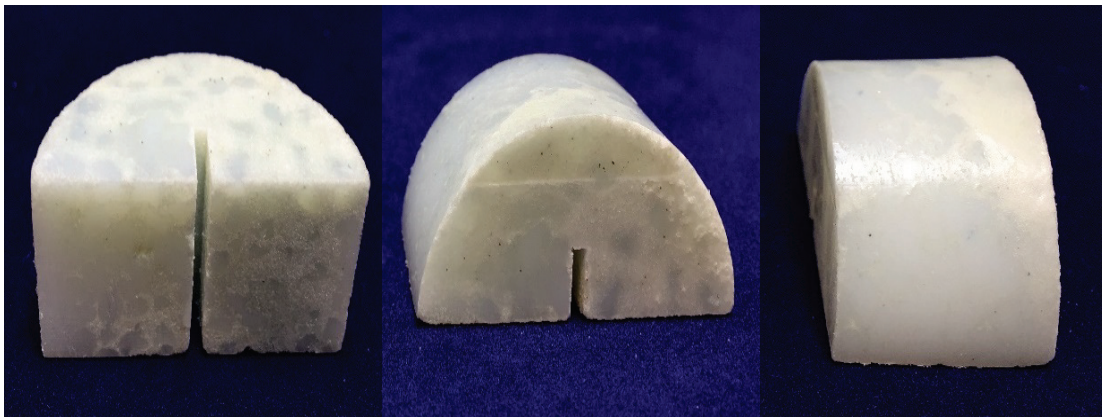


Figure 58. Semi-circular (Half-Brazilian) testing Specimen

- Notch depth, a

3.3.5. Bridgman Notch Test

Bridgeman notched specimen [Figure 59] is used to study triaxial stress condition and damage progression in subject material. Stress triaxiality is a key parameter controlling the fracture strain [97]. The stress and strain distribution of the specimen around the minimum cross-section area is

analytically derived by Bridgman [98-100]. This distribution is given as a function of the tensile load acting on the bar, the neck diameter, and the radius of curvature of the neck profile at its root. Upon uniaxial loading at the remote end, a triaxial state of stress is developed at the notched area. The triaxiality is maximum at the axis of the bar [98]. It is assumed that controlled triaxiality state of stress can be generated by means of artificial neck, and Bridgman notched specimen became popular in fracture mechanism study, determining influence of triaxiality stress on strain and fracture toughness. For the triaxial or 3D conditions the stress state is defined as shown in Figure 60.

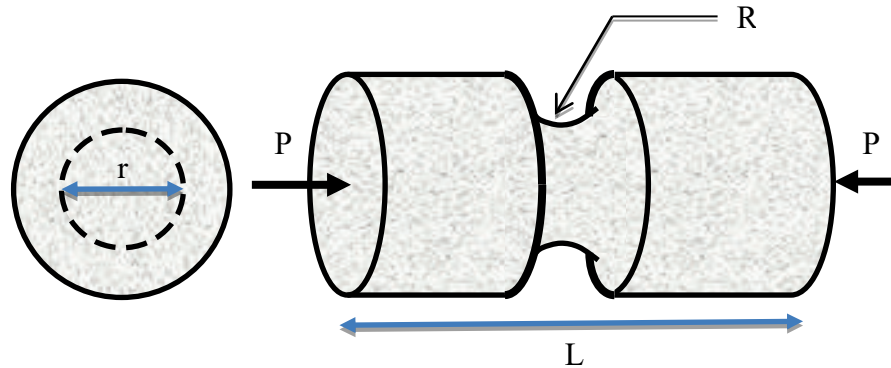


Figure 59. Bridgman notched testing configuration

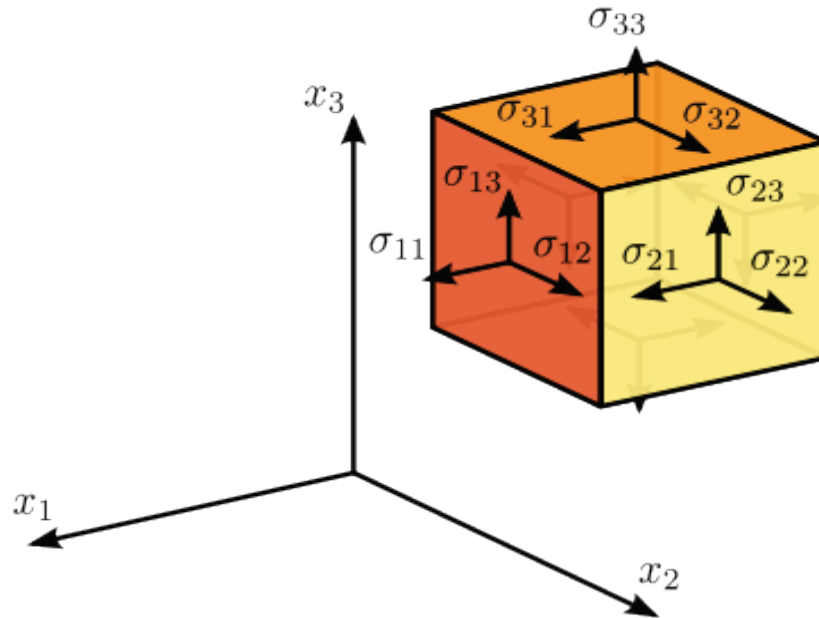


Figure 60. Characterizations of 3D stress state

A stress field in 3D space is defined as [Figure 60]

$$\bar{\sigma} = \begin{bmatrix} \sigma_{11} & \sigma_{12} & \sigma_{13} \\ \sigma_{21} & \sigma_{22} & \sigma_{23} \\ \sigma_{31} & \sigma_{32} & \sigma_{33} \end{bmatrix} \quad (17)$$

Assuming material model is isotropic, material model can be formulated in terms of three invariant of stress tensors [97-101]

Hydrostatic stress p , and von misses stress q

$$p = -\sigma_m = -(\sigma_1 + \sigma_2 + \sigma_3)/3 \quad (18)$$

$$q = \sqrt{\frac{1}{2}[(\sigma_1 - \sigma_2)^2 + (\sigma_2 - \sigma_3)^2 + (\sigma_3 - \sigma_1)^2]} \quad (19)$$

σ_1 , σ_2 and σ_3 are the principal stress assuming $\sigma_1 \geq \sigma_2 \geq \sigma_3$. A dimensionless hydrostatic pressure/ stress triaxiality parameter (η) has been used in literature [101-103].

$$\eta = \frac{-p}{q} \quad (20)$$

Bai [101] used a third invariant of stress tensor in Bridgman notch specimen as follows

$$r = \left[\frac{27}{2}(\sigma_1 - \sigma_m)(\sigma_2 - \sigma_m)(\sigma_3 - \sigma_m) \right]^{1/3} \quad (21)$$

Using this invariant Bai used another important parameter is Load angle θ which is related to the third deviatoric stress invariant ξ .

$$\xi = \left(\frac{r}{q} \right)^3 = \cos(3\theta) \quad (22)$$

The range of Load angle is $0 \leq \theta \leq \pi/3$, and the range of ξ is $-1 \leq \xi \leq 1$. These parameters can be related through following relation assuming plane stress condition (σ_3) [101,104]

$$\xi = \cos \left[\frac{\pi}{2}(1 - \bar{\theta}) \right] = \frac{27}{2} \cdot \eta \cdot \left(\eta^2 - \frac{1}{3} \right) \quad (23)$$

It is suggested that for Bridgman notched specimen the expression for stress triaxiality and Load angle as follows [101, 100]

$$\eta = \frac{1}{3} + \ln\left(1 + \frac{r}{2R}\right), \quad \theta = 1 \quad (24)$$

R is the radius of the notch and r is the radius of a round bar at the notch. And the equivalent strain to fracture can be calculated as

$$\bar{\varepsilon} = 2 \ln \left(\frac{r_0}{r} \right) \quad (25)$$

r_0 is the radius of initial minimum cross-section of r .

3.3.5.1. Testing condition

In this study

- Specimen is of 38 mm diameter and 45.72 mm of height.

- Test speed: 0.11430 mm/min

3.3.5.2. Raw data collection

Before the test the room temperature and the dimensions of the specimen is to be measured. During the test time increase, the corresponding load and the deformation data is to be collected. Instron 5969 Tabletop Universal Testing System can register this data points automatically given the time step.

- Force, F
- Stress, σ
- Displacement

Often Bridgman specimen test results are used in finite element calculation to analyze the triaxiality state of stress.

3.3.5.3. Nonconformity criteria

It is assumed during analytical derivation that the axial strain rate is uniform at the minimum cross-sectional area [98]. A uniform deformation rate during the test will conform to the assumption and derived formulation can be used.

Effect of triaxiality: Due to triaxiality of stress material may go plastic strain before ductile failure occurs.

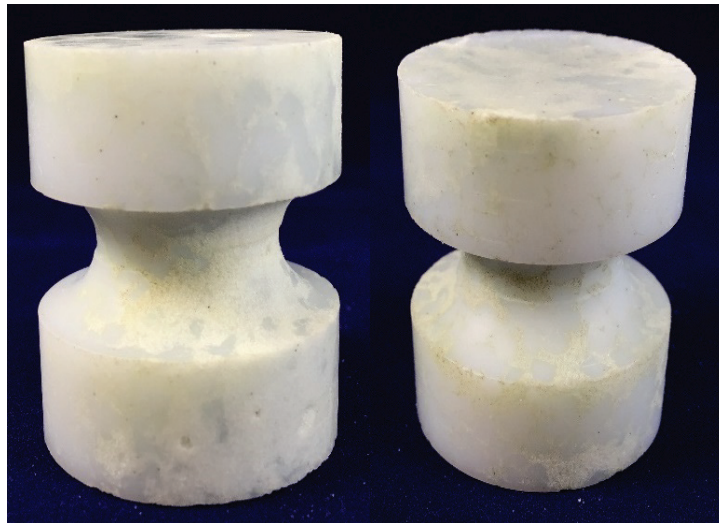


Figure 61. Bridgman Notch Testing Specimen

4. DIGITAL IMAGE CORRELATION (DIC)

4.1. Digital Image Correlation Overview

Digital Image Correlation (DIC) refers to the application of non-contacting two-dimensional and three-dimensional image correlation methods that acquire images of an object or specimen, store images in digital form and perform analysis to extract full-field shape, deformation and/or motion measurements [106]. A digital image correlation technique will be applied to each of the

mechanical tests presented in the present work, to measure the out of plane effects, surface displacements, and strain fields on each specimen geometry. The used equipment is a Correlated Solutions VIC-3D DIC system which performs in-site measurement of the surface displacement and strain fields on specimen during mechanical testing using the three-dimensional digital image correlation technique. Three-dimensional digital image correlation is a modern optical measurement technique that allows for full-field and non-contact shape, displacement, and strain measurement of the surface of objects. Two carefully aligned and calibrated cameras allow for in-plane and out-of-plane displacement to be recorded at the micron level. In the DIC technique, displacements are measured by correlating “physical distance” to “pixel distance.” A black speckle pattern on a white background is required, this is because the black speckles represent nodes in a mesh used to calculate displacement and strain. The outcome are displacement fields that can be converted into contours of surface strain using the image correlated software VIC 2D (Correlated Solutions). Such contours include: normal and shear terms, principal strains, equivalent strains, and Poisson’s ratio. Measurements of the surface crack length will be recorded using 3D-DIC (post processing software). As this is a passive system that requires only cameras and appropriate lighting, the Test Procedure and Approval document focuses on speckle pattern disposition, trip hazards, and proper operation to prevent damaging hardware. Examples of the images of DIC results in different materials and geometries are presented in Figure 62.

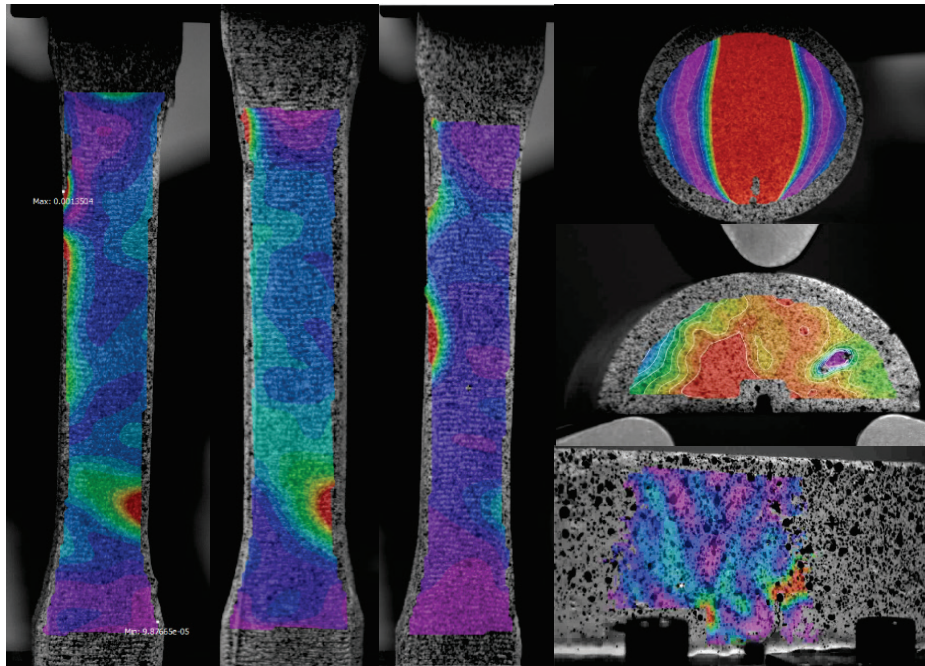


Figure 62. Digital Image Correlation Contour Examples

4.1.1. Introduction

Digital Image Correlation referred to as DIC in this report from this point on, is used among other non-contact methods to measure the mechanical response of a material [107-108]. The DIC method has seen a rise in popularity due to its advantages, which include simple setup and specimen preparation, low requirements in measurement environment, and its ability to measure the strain field over a large area [108-109]. It has particularly gained recognition in the field of experimental mechanics, in which it is used to obtain strain and displacement measurements [109-115], operating under the crucial supposition that no cracks appear in the area analyzed during the deformation process [114]. Studies have further solidified the validity and accuracy of the results produced by DIC methods when used properly [114-116]. The DIC technique has also previously been applied effectively to particulate composites and used to predict fracture behavior [111]. The DIC operates on basic, theoretical pinhole image equations, and can be used for a two-dimensional analysis with a one-camera setup, considering only in-plane deformation, or a three-dimensional examination using two cameras (stereovision) that also accounts for out-of-plane deformation [50]. Therefore, the 3D DIC method (also called digital image stereo-correlation technique (DISC) [117]) holds an important advantage over its 2D counterpart in that it detects and measures planar translation, out-of-plane translation, and out-of-plane rotation [115]. In practice, the investigator is obligated to use the 3D DIC if the test is on a curved surface or if significant 3D deformation occurs [109]. In reality, however, out-of-plane motions are practically unavoidable due to factors such as Poisson's Effect, bending of the specimen, local necking during the loading process, and deviances from the perfect grip conditions [116]. The classic two-camera stereovision system setup that supports three-dimensional digital image correlation is shown in Figure 63. This technique utilizes a software algorithm that identifies and processes surface and out-of-plane deformations by comparing the set of points in the subset of a given 'Reference Image' to the 'Deformed Image' [117].

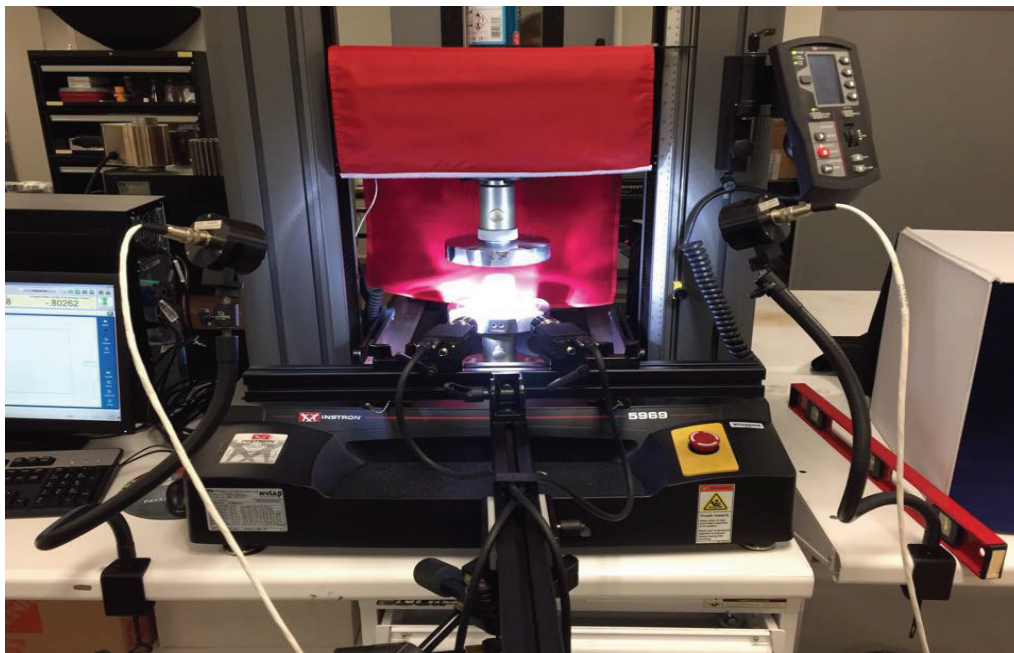


Figure 63. Actual VIC-3D Setup Used During Mechanical Tests. Uniaxial compression test shown.

Since it is comparatively new, however, the DIC technique has a significant amount of uncertainty as far as the optimum parameters that should be used for each case, generating an unknown error margin in the results analyzed by the investigator. This has led investigators to study and research the parameters that factor into the results generated by the DIC method, most notably the speckle pattern, subset size, and the correlation algorithm in an attempt to determine the optimal testing conditions [117-121]. Extensive research work has also been done on the errors that affect the quality of results [123-127], which can be systematic errors such as deficient calibration and restricted camera resolution or the inherent uncertainty that derives from the correlation algorithm used by the software. An emerging topic of interest is doing Digital Image Correlation of materials at high temperature, which presents its unique challenges such as the lack of focus by the cameras caused by the flow of hot air around the object being examined and undergoing any type of stress [106]. This is a topic that is soon to be investigated by the research team, as equipment and techniques are being gathered and studied at this present

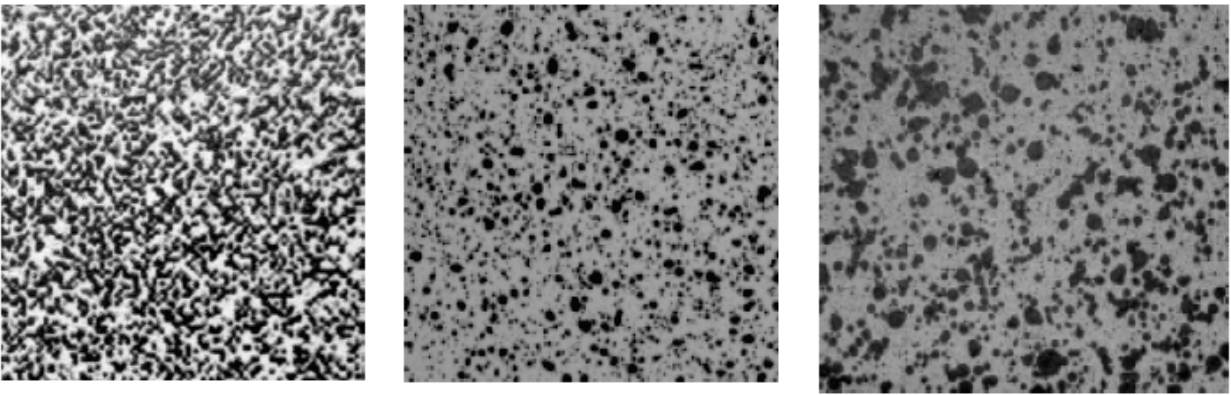


Figure 64. Examples of High-Quality Speckle Patterns.

moment. Since the DIC technique relies greatly on the contrasting pattern on the surface of the test specimen, the development of a speckle pattern will be discussed thoroughly. The speckle pattern can be painted, naturally occurring or even projected to the surface. Several techniques to recreate such pattern are available, but in order to provide or achieve an effective correlation several distinct requirements must be fulfilled by such techniques. A good speckle pattern should consist of a layer of speckles sprayed onto a different color surface that results in high contrast between, not necessarily a black on white pattern although it is the popular choice. The speckle pattern should be non-repetitive, isotropic, and high contrast. The pattern also must be of the adequate size for the subset, or vice versa, since a too large or too small pattern will yield inaccurate results. If a pattern is too large for the subset, it could completely encompass a subset and the matching algorithm done in digital image correlation would not be correct due to the fact that it could match that subset across everywhere on the field. An alternative solution suggested when this occurs is to utilize a larger subset, but it does sacrifice spatial resolution. On the other hand, if the pattern is too fine, the DIC system cameras will not be able to represent the specimen correctly. This image-information issue is called 'aliasing', and a clear sign that this is an issue is a characteristic moiré pattern in the visual data that is generated by the software. In general, speckles should be the size of at least 3-4 speckles in size to avoid image aliasing [128]. In Figure 64 there are examples of speckle patterns that effectively produce a good correlation, as

given in [128]. Overall, any colors that create a high contrast will complete the requirement. There is future possibility of work in the area of speckle patterns application, however, for the relevant DIC tests carried out in this investigation and all of the images shown, the widely accepted technique of spray paint was utilized. One very popular parameter that has been the subject of numerous research studies done by researchers is the speckle pattern, which has been deemed important enough to have studies focus solely on developing quality assessment methods and their effect on the DIC results [119-121]. The VIC 3D apparatus has in its technical specifications for out-of-plane measurements that it offers a resolution of up to $\frac{1}{50,000} FOV$

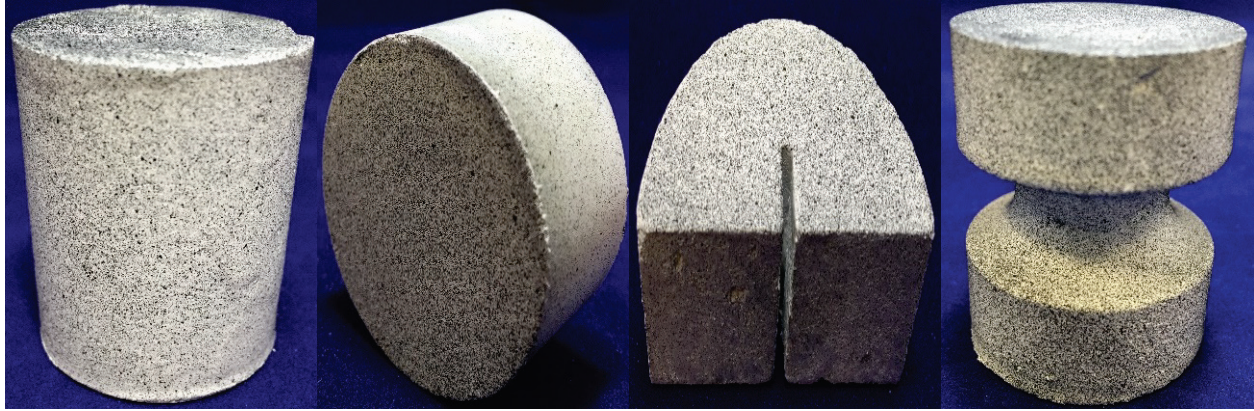


Figure 65. Speckle pattern on Testing Specimens

(Field of View), which is the area (m^2) on which the stereovision system is focused. Nevertheless, only one paper presenting work done on actual numerical error estimation using 3D DIC was found in literature [119]. The speckle pattern applied to the testing specimens of this study is shown in Figure 65.

4.1.2. 3-D Digital Image Correlation

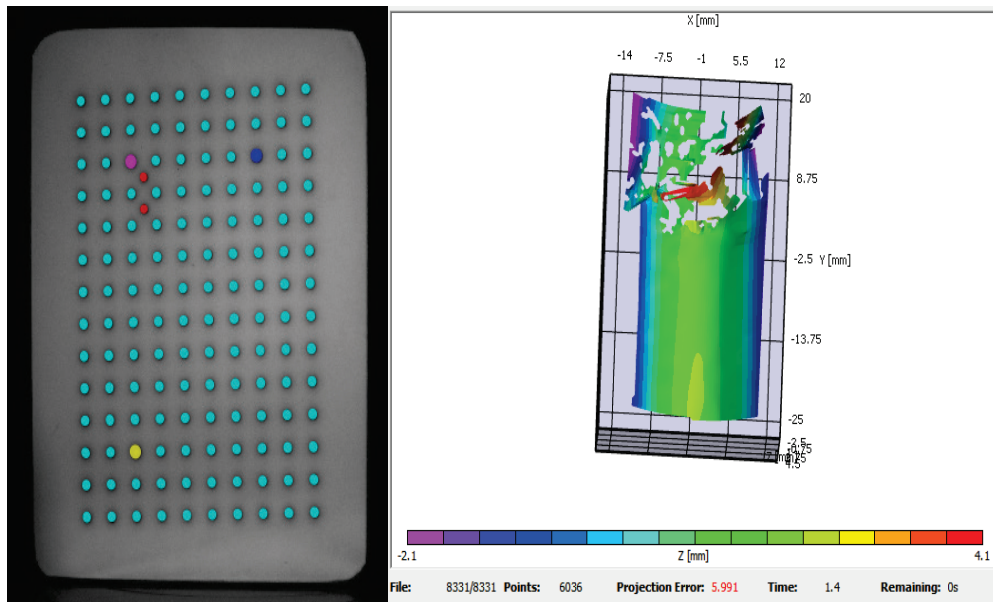
Errors in three-dimensional DIC can be classified into two major groups: correlation errors and calibration errors. Correlation errors, as the name suggests, refers to the errors that inevitably result from the nature of the correlation of the subset images can be further divided into two subtypes, systematical and statistical errors. Systematical errors are naturally resulting from subpixel effects, while statistical errors result from the limited correlation of pixels from subset to subset, i.e. the correlation will always introduce some minimal error in the measurements. Calibration errors, on the other hand, impact the 3D reconstruction coordinates directly and can be modified and optimized [115].

4.1.3. DIC Parameters

Several factors affect the results of DIC methods used, and one very important parameter is the stereo angle (also referred to as pan angle), which is the angle between the imaginary lines formed by the position of the cameras relative to the specimen analyzed. Literature recommendations were followed of maintaining the angle between 10° and 30° for 3D DIC for optimal results [106]. The user manual that is included with the DIC System VIC-3D is more specific and suggest 25° as the ideal stereo angle. For all tests, therefore the angle was maintained constant at 25° . It is worth noting, however, that literature also states that a stereo

angle of up to 60° can be used for 3D image correlation if needed, with the sacrifice in the loss of accuracy in in-plane measurements.

As mentioned previously on this investigation, the speckle pattern has been the subject of several studies with the aim of more precisely defining a “good” speckle pattern. Some notable studies that covered this matter are mentioned next, along with their important conclusions. One study found that the size of both the subset and the speckles applied have a considerable influence on the accuracy with which heterogeneous and homogenous deformations are calculated in image correlation [119]. Another study found that a high-quality speckle pattern should have a speckle size from two to four pixels and large density, referring to the quantity of speckles applied to the area of interest [120]. And lastly, another study worth mentioning established a parameter called mean intensity gradient as a quality assessment check to evaluate the quality of the complete speckle pattern applied to the area of interest. The mean intensity gradient parameter is calculated using the modulus of local intensity gradient vector and the dimensions of the image in pixels. The investigation concluded that the mean intensity gradient should be large, and coupled with the appropriate subset size, to improve the accuracy of the displacement fields calculated. This practical parameter can be generally used as a guide for surface sample preparation [121]. While no one specific method was followed for the application of the speckle pattern, all of these results and findings were considered and this author judges them noteworthy and relevant to this presented paper. The speckle pattern used however, as mentioned earlier, was applied through the spray painting technique in a random pattern of dark paint over a layer of white paint, since it is considered by literature to be speckle pattern application method that historically yields the most accurate results [106]. One factor that also affects the accuracy of the DIC is the calibration Pad. The knowledge to choose the required calibration pad is a must when doing an accurate DIC. Also, is very important to put attention to the error score given when calibrating. An example of these parameter is shown in Figure 66.



5. RESULTS & DISCUSSION

5.1. Uniaxial Compression

Quasi-static uniaxial compression loads were applied on the glass-HIPS specimens with the objective of characterizing the particulate composite material in order to develop a valid computational model in the near future. DIC technique was applied during the test in order to determine the full displacement and strain fields. A full description of the DIC method can be found at the DIC section of this report. The dimensions for the cylindrical uniaxial specimen is 1.5 in. diameter, 2.275 in. of height. Base in the specimen's geometry and Table 11, the

Table 11. Expected Failure modes table for HPC

Length/Diameter ratio (l/d)	Expected Failure Mode	Frictional Effects
≤ 1.5	Barreling	Strong
1.5 - 2	Barreling	Strong
2-2.5	Doble Barreling	Above minimal
2.5-5	Shear	Minimal
$5 \leq$	Buckling	Minimal

specimen is expected to fail by barreling and it will be affected severely by frictional effects. However, as explain in the testing section of this report some steps are taken in order to reduce or minimize the frictional effects that are seen during the compression test in between the surface of the compression platen and the specimen. Also, is necessary to take in consideration that such failure modes belong to pure polymer testing. Yet, they serve as a reference point since it's a possibility that the glass-HIPS specimen might also be affected by those frictional effects.

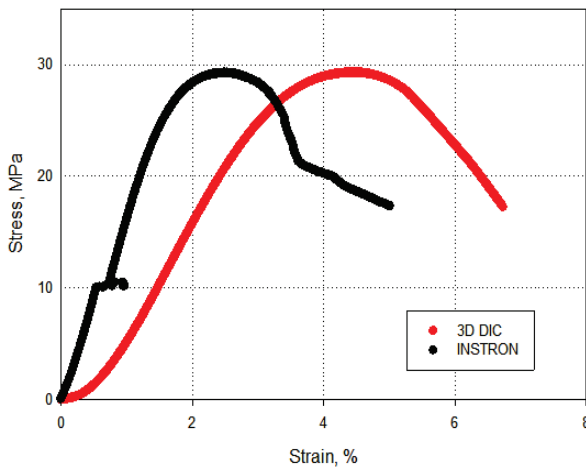


Figure 68. Stress vs Strain curve of glass-HIPS specimen

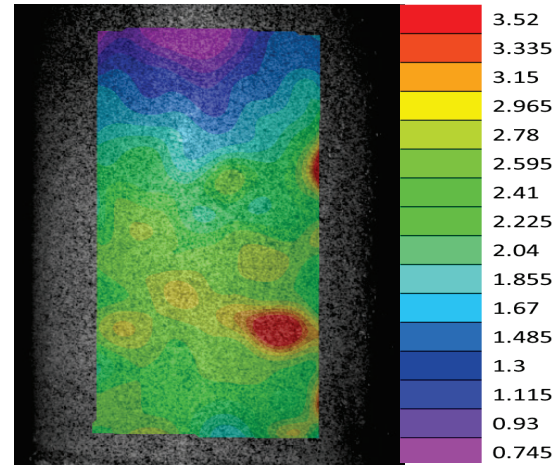


Figure 67. Initial Effective Poisson's Ratio

Experimental results from the quasi-static uniaxial compression test are depicted in Figure 67 , which plots the stress with respect to the strain for the glass-HIPS specimen. Since it is known that particulate composites such as the glass-HIPS specimen exhibit a strong dependence on the loading rate, temperature, and pressure, careful consideration was taken in order to take in consideration the strain dependent behavior of the mock PBX. It is difficult to distinguish the yield point. However, the yield point of the

specimen is located at 33390 N of load and at 2.7% of strain. The elastic region of the PBX simulant was determine to end at 0.8% of strain. The plastic region seems to be quite extensive

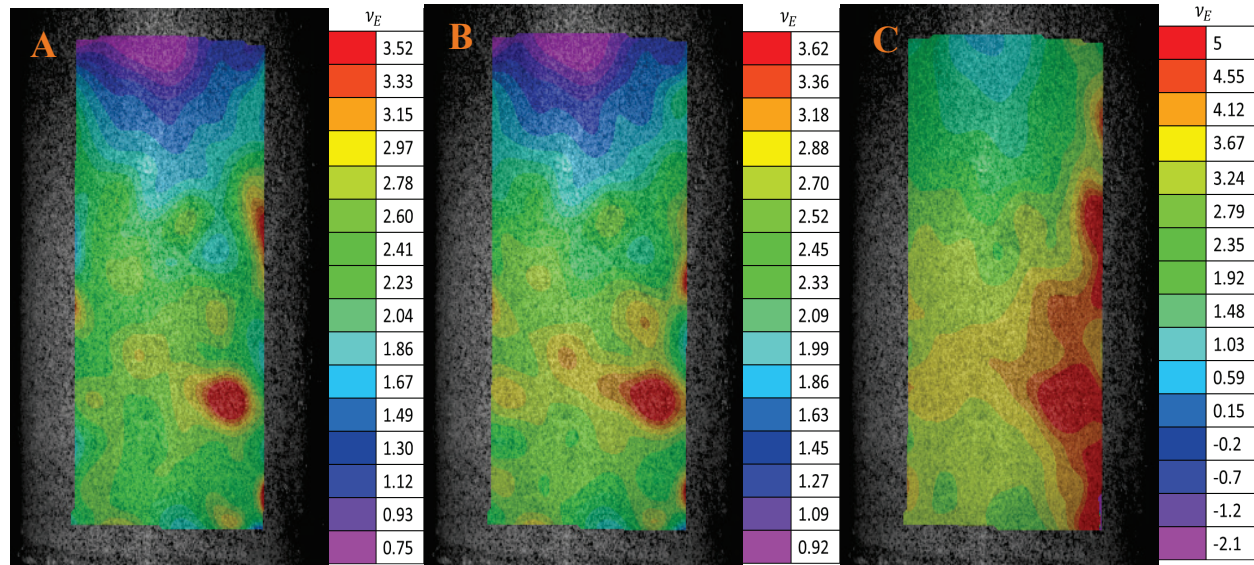


Figure 69. Effective Poisson's Ratio at different applied strain as it starts evolving from 0.8% of strain to 2.7% of strain to the rupture point. The maximum stress is determined to 29 MPa. This indicates that the binder material and the micron size soda lime glass beads developed a strong bond during the manufacturing process. In Figure 67 is possible to see the data acquired by the DIC system through the analog system and the data saved by the Instron 5969. The analog signal seems to be a little off, but the data from the DIC is more precise and accurate than the one provide by the load frame displacement.

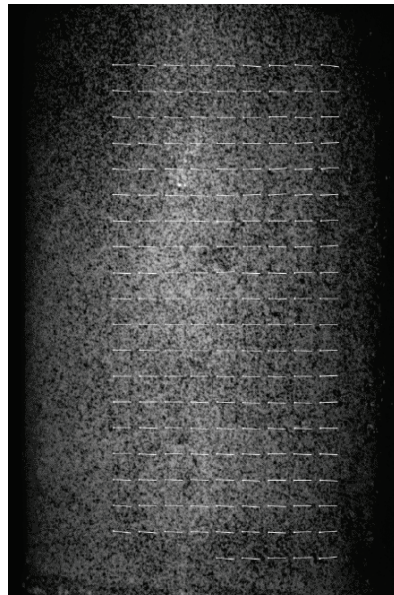


Figure 70. Displacement Vector Prior to total fracture

Since the Poisson's ratio is the ratio of different measurements (the transverse strain and axial strain), attempts to measure these by the use of extensometers have proven to be too erratic. Also, is necessary to take in consideration that the glass-HIPS specimen is a composite ergo not a continuous material. The nature of the specimen introduces an error or a variation in behavior utilizing the extensometer method to measure. DIC method has the advantage of averaging strains over large surface areas and of providing the wanted strain data from the same measurement. As shown in Figure 68 , the initial Poisson ratio is of 2.41. However as the test evolve, so does the Poisson ratio increasing. The Poisson ratio increases with increasing strain.

This sort of behavior makes sense in a particulate composite such as the glass-HIPS specimen. The reason for this sort of behavior lies in the nature of the particulate composite. Voids that could have been introduced during the manufacturing process or develop within the specimen while the material is deforming start to increase in size as the strain increases. These voids, which are caused mainly by the separation of the binder material and the energetic crystal surfaces, have a bulking effect in glass-HIPS specimen. Figure 69

shows the evolution of the Poisson ratio during testing. It's important to take in consideration that larger strains will cause a large variation or evolution.

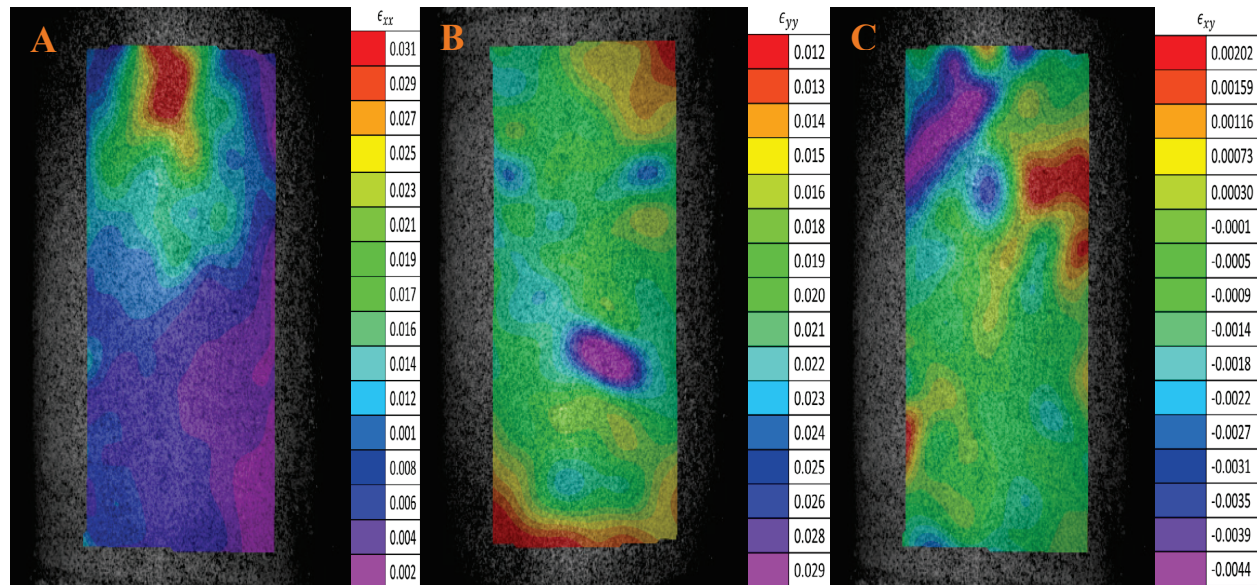


Figure 71. Strain components contour distribution of (a) extensive strain (b) compressive strain and (c) shear strain prior to total failure

At point A there is just a slight variation when compared to the initial effective Poisson's ratio because there is not a significant change in time. At B the application of the strain rate to some extent change the initial value of the Poisson's ratio when compared to point A has expected. At B the Poisson's ratio increases from the original initial value, but not an unexpected value. However, at C, the Poisson's ratio increases to a value of 5. After C, the Poisson's ratio continues to increase reaching a significant change to the original value. This is caused by the creation and/or development of the voids. In order to discuss the deformation and fracture behavior of the glass-HIPS specimen under compressive load, different images were captured while performing DIC. Figure 71 shows different contours prior to total failure. In Figure 71 picture A can be easily distinguish that a strain concentration is located in an area that runs along the load axis close to the top center of the specimen. Meanwhile, a localized shear strain band concentrated in the area near the diagonal line, as shown in Figure 71 part C. From these strain maps, it can be seen that the extension strain is larger than the compression and shear strain in the top right, demonstrating that the macroscopic fracture mode of the specimen is dominant caused by extension and shear action when under external force. The whole vector field of displacement distribution gives an initial impression of the failure mode of the specimen, as shown in Figure 70 . First is clearly that the specimen is going to fail by the barreling effect that was previously mentioned. Also, the direction of the vector field gives the impression that the specimen is going to fail by a shear fracture. As shown in Figure 72 , the specimen fails by

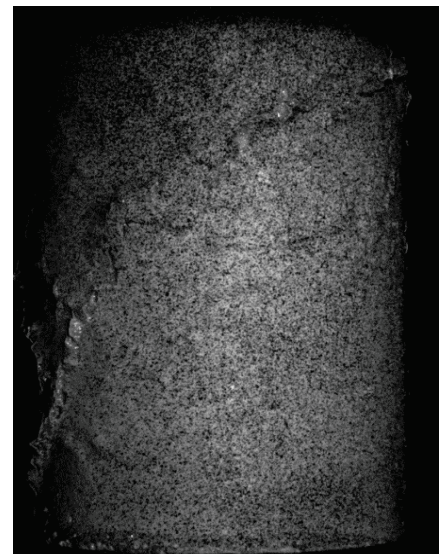


Figure 72. Fractured Specimen

shear. This is consistent with the failure mode and the heterogeneous nature of the HPC or mock PBX.

5.2. Indirect Tensile (Brazilian) Test

Indirect Tensile compression loads were applied on the glass-HIPS specimen with the objective of characterizing the particulate composite material in order to develop a valid computational model in the near future. DIC technique was applied during the test in order to determine the full displacement and strain fields. The dimensions for the disc specimen are 38 mm diameter and 22 mm thickness. The Brazilian specimen was diametrically compressive loaded in the Instron 5969

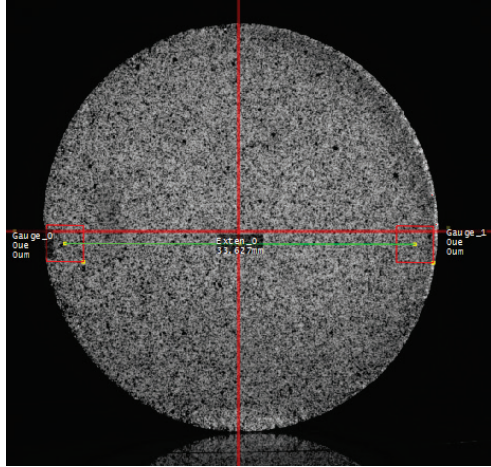


Figure 74. Virtual gauges and extensometer applied to Brazilian Specimen

with compression platens. The applied strain rate was 0.05 mm/min. Images of the evolving movement were recorded at rate of 5 frames per second. Two virtual gauges and a virtual extensometer were applied during the test as shown in Figure 73. Similar virtual gauges were applied to all the tested specimens. It is obvious that the applied force will at behave linearly at the earliest moments of the test and that due to the HIPS the specimen will plastically deformed before fracture. In another words the glass-HIPS specimen was never going to fail by a brittle fracture due to the nature of the HIPS. This is because even though the soda lime crystal are brittle, they are completely coated by the polymer. It is possible that the crack developed around the soda lime glass beads that were not completely or partially coated.

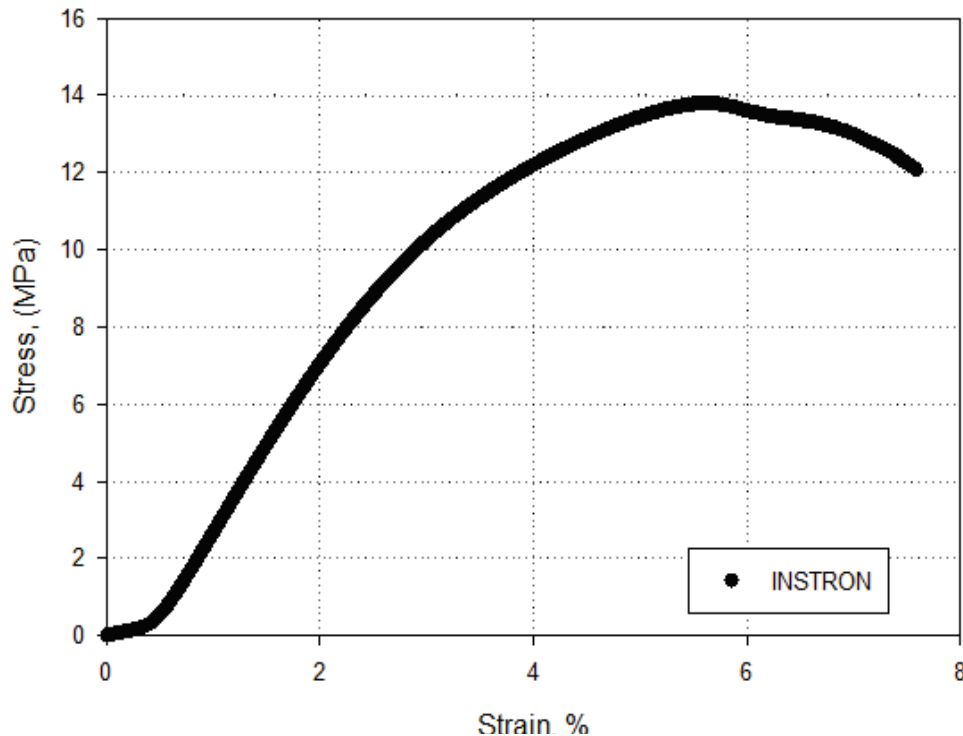


Figure 73. Stress vs Strain Curve of Brazilian Test

This can be seen in Figure 74.

The maximum load that was reach was 5838 N. Therefore the indirect tensile stress is equal to 4.45 MPa. This seems to contradict Figure 74, however the plot only takes into consideration the compressive strength, ergo these two quantities cannot be compare rationally. Figure 75 shows the Poisson's ratio corresponding to the Brazilian specimen. It is worth to mention that the Poisson's ratio increases as the strain evolves.

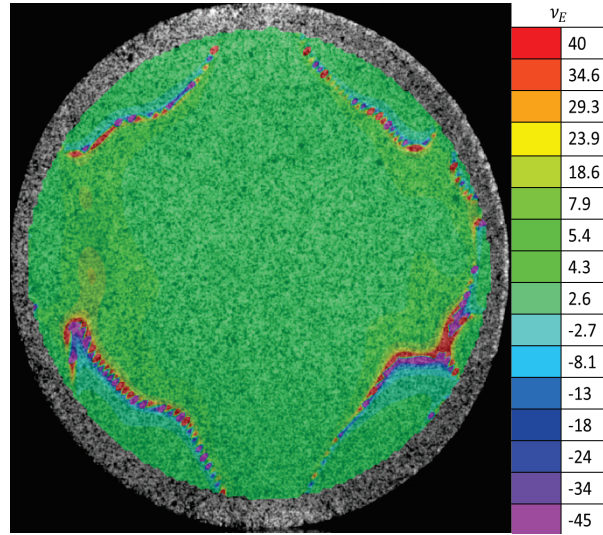


Figure 75. Effective Poisson's ratio of Brazilian Specimen

The strain field distribution equivalent to the state where the fracture occurs is shown in Figure 76. The images shows how the strain localizes along the load axis. The high strain spots might indicate the possible crack route and the possible sites for stress concentration. Another contour that proves that the strain field is predicting the crack route is the equivalent strain shown in Figure 77. It's possible that the equivalent strain contour shows the strain field is developed by

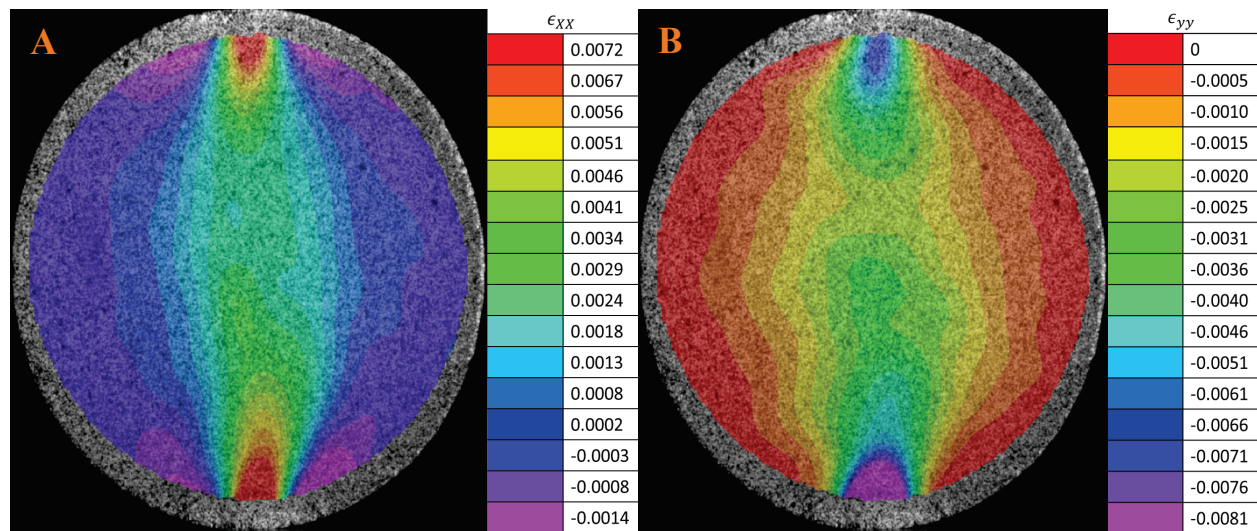


Figure 76. Strain components contour distribution of (a) extensive strain (b) compressive strain

the load.

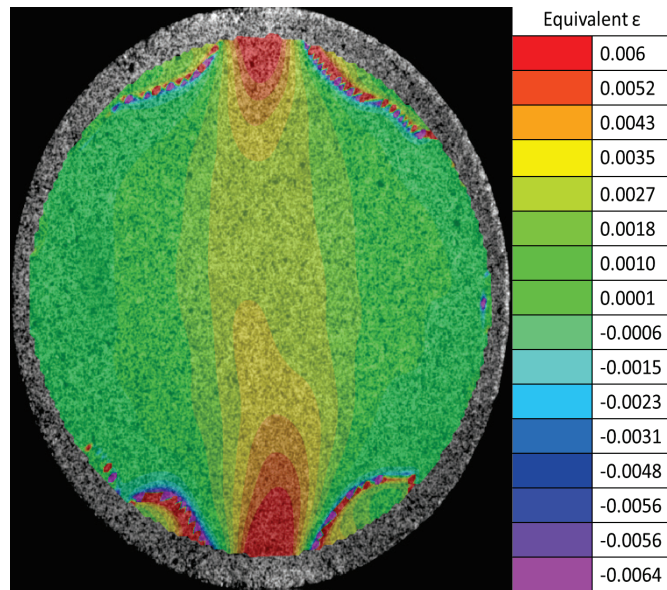


Figure 77. Equivalent Strain Contour

Failure occurs as a crack propagated along the previously designated crack route. Fracture morphology of the specimen is shown in Figure 78.

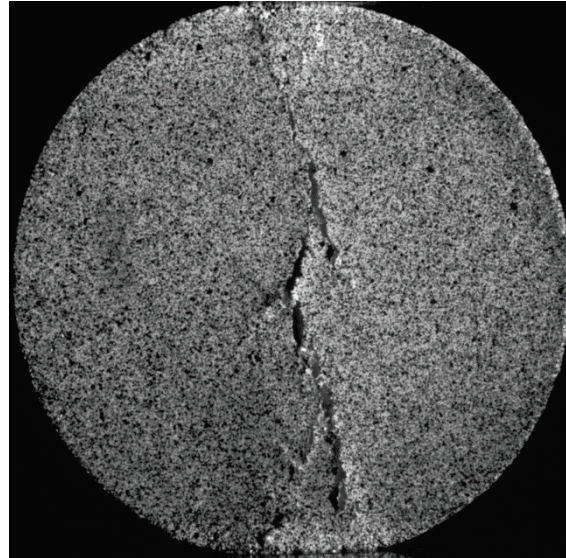


Figure 78. Fracture morphology

Based in the results of the test, the strain field calculated from the DIC system can validate the material damage underneath the surface of the specimen. Even though more test are necessary to prove the above validation. The principal crack initiated from the contact surface, but quickly propagated through the center of the specimen. This means that the crack was developed in the center prior to the crack from the contact surface. One of the cracks located at the bottom surface

was developed due to shear stress in the specimen, but quickly fuse with the primary crack and followed the crack route.

5.3. Semi-Circular Bending (Half Brazilian) Test

Semi-circular three point bending compression loads were applied on the glass-HIPS specimen with the objective of characterizing the particulate composite material in order to develop a valid computational model in the near future. DIC technique was applied during the test in order to determine the full displacement and strain fields. The dimensions for the semi-circular specimen are 38 mm diameter and 19 mm of height. The notch was machined with a blade of 1.65 mm of thickness. The notch of 6 mm length was along the line of symmetry at the edge of the specimen. The orientation was along the direction of compression. The half Brazilian specimen was uniaxial compressive loaded in the Instron 5969 with a 3 point bending set up. The applied strain rate was 0.047 mm/min which was calculated based on literature just like mentioned in the mechanical test section. Detailed description in the mechanical testing section. Images of the evolving movement were recorded at rate of 5 frames per second. The ligament area for the mentioned geometry is 265.18 squared millimeters. Figure 81 shows the vector distribution of displacement under a tensile stress calculated by the DIC system. As

is shown in the figure several directions are given by the vector field. This is because of the nature of the mock PBX. It is possible that the location with the most diverse direction is the location of an agglomeration of soda lime glass beads partially coated by the HIPS polymer. The vector field direction and magnitude indicates that the SCB specimen is suffering from a large

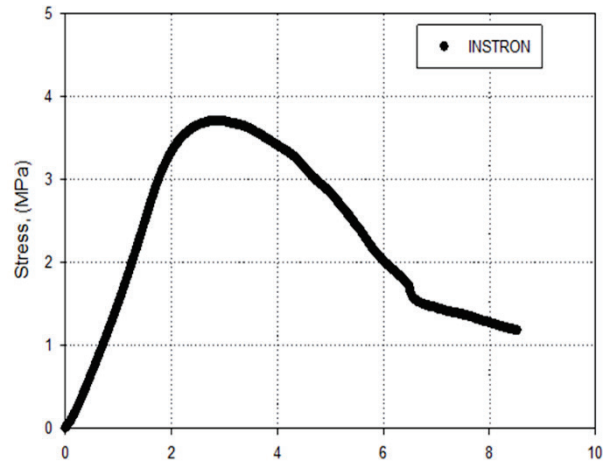


Figure 79. Stress vs Strain curve of SCB specimen

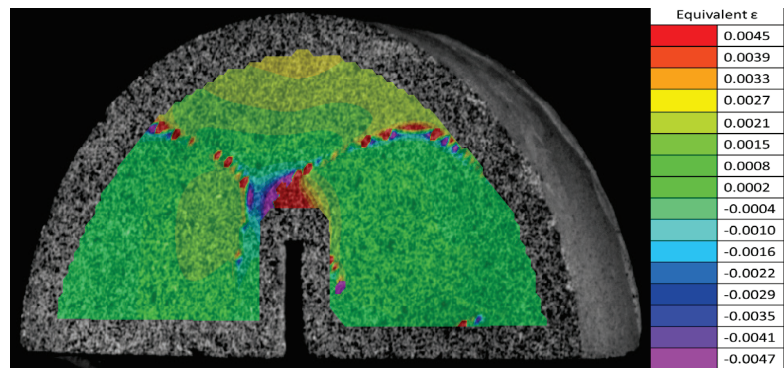


Figure 80. Equivalent Strain of SCB specimen

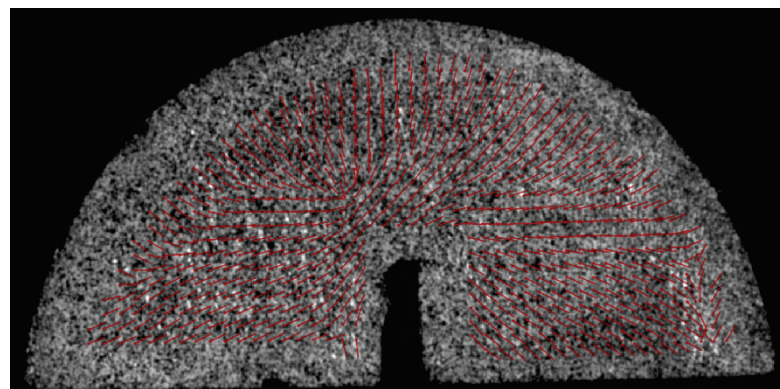


Figure 81. Vector Field of displacement for a post-failure

extension stress under the compressive loading. Even though it is not visible because it occurred on the other side of the specimen, the arrows are pointing towards the crack and predicting its path. The stress vs strain curve shows the viscoelastic behavior of the mock PBX SCB specimen. The curve can be seen in Figure 79. In Figure 80 it is possible to see the maximum strain located right at the point where the main crack initiated its route. The DIC calculations provide an excellent starting point for fracture analysis. Fracture analysis can be carried out in order to see the relationship between load and the crack propagation. Due to the lack of literature a model will be developed that will reproduce and validate the above relationship.

5.4. Bridgman Notch Test

Uniaxial compression loads were applied on the Bridgman notch glass-HIPS specimen with the objective of characterizing the particulate composite material in order to develop a valid computational model in the near future. DIC technique was applied during the test in order to determine the full displacement and strain fields. Images of the evolving movement were recorded at a rate of 5 frames per second. The dimensions for the cylindrical Bridgman notch specimen are 38 mm diameter and 46 mm height. The circumferential notch has a diameter of 15 mm. The Bridgman notch specimen was diametrically compressively loaded in the Instron 5969 with compression platens. The applied strain rate was 0.1143 mm/min. Due to the triaxial state of stress induced by the Bridgman notch, Table 11 is not applicable to predict the failure mode. However, the test was run like a typical uniaxial compression. In other words, the Teflon tape and grease were utilized during testing.

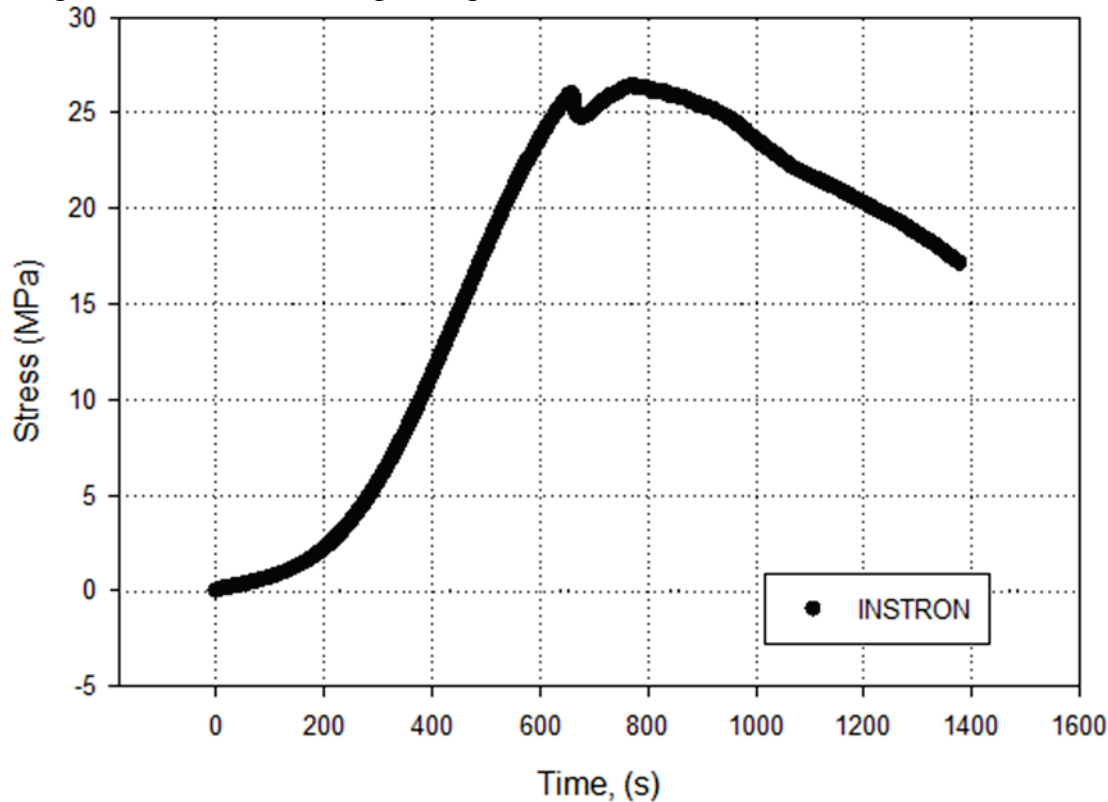


Figure 82. Stress vs Time plot of Bridgman notch specimen

REFERENCES

- [43] Cooper, P. W., and Kurowski, S. R., 1996, "Introduction to the Technology of Explosives". New York: Wiley-VCH.
- [44] Siviour, C. R., Laity, P. R., Proud, W. G., Field, J. E., Porter, D., Church, P. D., Gould, P., and Huntingdon-Thresher, W., 2008, "High strain rate properties of a polymer-bonded sugar: their dependence on applied and internal constraints," *Proc. R. Soc. A Math. Phys. Eng. Sci.*, **464**(2093), pp. 1229–1255.
- [45] Dienes, J. K., Zuo, Q. H., and Kerschner, J. D., 2006, "Impact initiation of explosives and propellants via statistical crack mechanics," *J. Mech. Phys. Solids*, **54**(6), pp. 1237–1275.
- [46] Yeom, K. S., Jeong, S., Huh, H., and Park, J., 2013, "New Pseudo-Elastic Model for Polymer-Bonded Explosive Simulants Considering the Mullins Effect," *J. Compos. Mater.*, **47**(27), pp. 3401-3411.
- [47] Cady, C. M., Liu, C., Rae, P.J., and Lovato, M. L., 2009, "Thermal and Loading Dynamics of Energetic Materials," *Proc. of the SEM Annual Conference*, Albuquerque, NM.
- [48] Cunningham, B. J., Gagliardi, F. J., and Ferranti, L., 2013, "Low Strain Rate Measurements on Explosives Using DIC," *Proc. of the SEM Annual Conference*, Springer, Indianapolis, IN, pp. 25-31.
- [49] Liu, C., 2010, "Elastic Constants Determination and Deformation Observation Using Brazilian Disk Geometry," *Exp. Mech.*, **50**(7), pp. 1025-1039.
- [50] Chen, P., Zhou, Z. and Huang, F., 2011, "Macro-Micro Mechanical Behavior of a Highly-Particle-Filled Composite Using Digital Image Correlation Method," *InTech*, pp. 437-460, Chap. 18.
- [51] Bridgman, P. W., 1952, *Studies in Large Plastic Flow and Fracture*. McGraw Hill, New York.
- [52] Kachanov, L. M., 1986, "On Creep Stresses in a Bridgman Notched Bar," *Mech. Mater.*, **5**(3), pp. 229-234.
- [53] Stewart, C. M., 2013, *A Hybrid Constitutive Model for Creep, Fatigue, and Creep-Fatigue Damage*, Dissertation, University of Central Florida, Orlando, FL, Dec 2013.
- [54] Hyde, T. H., Xia, L., and Becker, A. A., 1996, "Prediction of Creep Failure in Aeroengine Materials under Multi-axial Stress States," *Int. J. Mech. Sci.*, **38**(4), pp. 385-403.
- [55] Kraus, H., 1980, *Creep Analysis*, John Wiley, New York

- [56] Hayhurst, D. R., 1972, “Creep Rupture Under Multi-Axial States Of Stress,” *J. Mech. Phys. Solids*, **20**(6), pp. 381-390.
- [57] Zhang, J., Zhang, J., Chen, X., Sun, C., and Xu, J., 2014, “A Thermovisco-Hyperelastic Constitutive Model of NEPE Propellant Over a Large Range of Strain Rates,” *J. Eng. Mater. Tech.*, **136**(3), pp. 1-8.
- [58] Schapery, R.A., 1990, “Theory of mechanical behavior of elastic media with growing damage and other changes in structure,” *J. Mech. Phys. Solids*, **38**(2), pp. 215–253.
- [59] Schapery, R.A., 1991, “Analysis of damage growth in particulate composites using a work potential,” *Compos. Eng.*, **1**(3), pp. 167–182.
- [60] Ha, K., Schapery, and R. A., 1998, “Three-dimensional viscoelastic constitutive model for particulate composites with growing damage and its experimental validation,” *Int. J. Solids Struct.*, **35**(26-27), pp. 3497–3517.
- [61] Hinterhoelzl, R.M., and Schapery, R.A., 2004, “FEM implementation of a three-dimensional viscoelastic constitutive model for particulate composites with damage growth,” *Mech. Time-Dependent Mater.*, **8**, pp. 65–94.
- [62] Jung, G-D., and Youn, S-K., 1999, “A nonlinear viscoelastic constitutive model of solid propellant,” *Int. J. Solids Struct.*, **36**, pp. 3755–3777.
- [63] Kachanov, L. M., 1986, *Introduction to Continuum Damage Mechanics*, Springer Science & Business Media.
- [64] Xu, F., Aravas, N., Sofronis, P., 2008, “Constitutive Modeling of Solid Propellant Materials with Evolving Microstructural Damage,” *J. Mech. Phys. Solids*, **56**, pp. 2050-2073.
- [65] Doherty, R. M., and Watt, D. S., 2008, “Relationship Between RDX Properties and Sensitivity,” *Propellants, Explosives, Pyrotechnics*, **33**(1), pp. 4–13.
- [66] Compton, D., Hunt, E. and, Jackson, M., 2011, “Coating and Characterization of Energetic Materials,” *FLIR Syst. Inc.*, pp. 1–4.
- [67] Anderson, E. K., Aslam, T. D., and Jackson, S. I., 2014, “Transverse initiation of an insensitive explosive in a layered slab geometry: Front shapes and post-shock flow measurements,” *Combustion and Flame*, **161**(7), pp. 1944–1954.
- [68] Banerjee, B., Cady, C. M., and Adams, D. O., 2003, “Micromechanics simulations of glass-estane mock polymer bonded explosives,” *Modelling and Simulation in Materials Science and Engineering*, **11**(4), pp. 457–475.
- [69] Yeager, J. D., Ramos, K. J., Hooks, D. E., Majewski, J., and Singh, S., 2014, “Formulation-Derived Interface Characteristics Contributing to Failure in Plastic-Bonded Explosive

Materials,” LA-UR-14-24860, *Proc. 15th International Detonation Symposium*, San Francisco, CA.

[70] Xiao, J. J., Wang, W. R., Chen, J., Ji, G. F., Zhu, W., and Xiao, H. M., 2012,” Study on structure, sensitivity and mechanical properties of HMX and HMX-based PBXs with molecular dynamics simulation,” *Computational and Theoretical Chemistry*, **999**, pp. 21–27.

[71] Campbell, M. S., Garcia, D., and Idar, D., 2000, “Effects of temperature and pressure on the glass transitions of plastic bonded explosives,” *Thermochimica Acta*, **357–358**(836), pp. 89–95.

[72] Sunnyside Corporation, 2009, “Acetone 840 Product Data Sheet”.

[73] Sprayon Products, 2014, “Urethane and Styrene Silicone Release Agent Aerosol Material Safety Data Sheet”.

[74] Çengel, Yunus, 2007, “Heat and Mass Transfer: A Practical Approach”, McGraw-Hill, Boston, MA.

[75] Catzin, Carlos Alberto, “Manufacturing and Characterization of Energetic Materials”, Master’s of Science Thesis, The University of Texas at El Paso, 2016.

[76] Jaygo Incorporated, 2013, “SiLibeads Glass Beads Type S, Microglassbeads EU Safety Data Sheet According to Attachment II EC Reg. 1907/2006”.

[77] Total Petrochemicals & Refining USA, Inc., 2012, “Impact Polystyrene Material Safety Data Sheet”.

[78] Zhou, Z., et al., 2012, "Study on Fracture Behaviour of a Polymer-Bonded Explosive Simulant Subjected to Uniaxial Compression Using Digital Image Correlation Method," *Strain*, **48**(4), pp. 326-332.

[79] Zhou, Z., et al. "Dynamic tensile deformation and fracture of a highly particle-filled composite using SHPB and high-speed DIC method." EPJ Web of Conferences. Vol. 26. EDP Sciences, 2012.

[80] Rae, P. J., et al. "Quasi-static studies of the deformation and failure of β -HMX based polymer bonded explosives." Proceedings of the Royal Society of London A: Mathematical, Physical and Engineering Sciences. Vol. 458. No. 2019. The Royal Society, 2002.

[81] Heinz, Stephen R., and Jeffrey S. Wiggins. "Uniaxial compression analysis of glassy polymer networks using digital image correlation." *Polymer Testing* **29.8** (2010): 925-932.

[82] Zhou, Zhongbin, et al. "Experimental study on the micromechanical behavior of a PBX simulant using SEM and digital image correlation method." *Optics and Lasers in Engineering* **49.3** (2011): 366-370.

- [83] Goodall, I. W., & Skelton, R. P. The importance of multiaxial stress in creep deformation and rupture. *Fatigue & Fracture of Engineering Materials & Structures*, 2004, 27(4), 267-272.
- [84] Ha, J., Tabuchi, M., Hongo, H., Yokobori, A. T., & Fuji, A. Creep crack growth properties for 12CrWCoB rotor steel using circular notched specimens. *International journal of pressure vessels and piping*, 2004, 81(5), 401-407.
- [85] Lukáš, P., Preclík, P., & Čadek, J. Notch effects on creep behaviour of CMSX-4 superalloy single crystals. *Materials Science and Engineering*, 2001: A,298(1), 84-89.
- [86] Yeager, J. D., et al. "Microstructural effects of processing in the plastic-bonded explosive Composition A-3." *Materials Chemistry and Physics* 139.1 (2013): 305-313.
- [87] Martin, E. C., and Rena Y. Yee. Effects of Surface Interactions and Mechanical Properties of PBXs (Plastic Bonded Explosives) on Explosive Sensitivity. No. NWC-TP-6560. NAVAL WEAPONS CENTER CHINA LAKE CA, 1984.
- [88] Çolak, Özgen Ü., 2004, "Mechanical Behavior of PBXW-128 and PBXN-110 under Uniaxial and Multiaxial Compression at Different Strain Rates and Temperatures," *Turkish J. Eng. Env. Sci*, **28**, pp. 55-65.
- [89] Jerabek, M., Z. Major, and R. W. Lang. "Uniaxial compression testing of polymeric materials." *Polymer testing* 29.3 (2010): 302-309.
- [90] Yu, Yong, Jianxun Zhang, and Jichun Zhang, 2009, "A modified Brazilian disk tension test." *International Journal of Rock Mechanics and Mining Sciences* **46**(2) .pp. 421-425.
- [91] Hondros, G. "The evaluation of Poisson's ratio and the modulus of materials of a low tensile resistance by the Brazilian (indirect tensile) test with particular reference to concrete." *Australian Journal of Applied Science* 10.3 (1959): 243-268.
- [92] Huang, Baoshan, Xiang Shu, and Yongjing Tang. "Comparison of semi-circular bending and indirect tensile strength tests for HMA mixtures." *Advances in Pavement Engineering* 16 (2005): 225-227.
- [93] Mellor, Malcolm, and Ivor Hawkes. "Measurement of tensile strength by diametral compression of discs and annuli." *Engineering Geology* 5.3 (1971): 173-225.
- [94] Kim, Y., et al. "Dynamic modulus testing of asphalt concrete in indirect tension mode." *Transportation Research Record: Journal of the Transportation Research Board* 1891 (2004): 163-173.
- [95] Fairhurst, C. "On the validity of the 'Brazilian' test for brittle materials," *International Journal of Rock Mechanics and Mining Sciences & Geomechanics Abstracts*. Vol. 1. No. 4. Pergamon, 1964.

- [96] Liu, C. "Elastic constants determination and deformation observation using Brazilian disk geometry." *Experimental mechanics* 50.7 (2010): 1025-1039.
- [97] Wu, Zhong, et al. "Fracture resistance characterization of superpave mixtures using the semi-circular bending test." *Journal of ASTM International* 2.3 (2005): 1-15.
- [98] Bai, Yuanli, Xiaoqing Teng, and Tomasz Wierzbicki. "On the application of stress triaxiality formula for plane strain fracture testing." *Journal of Engineering Materials and technology* 131.2 (2009): 021002.
- [99] Valiente, A. "On Bridgman's stress solution for a tensile neck applied to axisymmetrical blunt notched tension bars." *Journal of applied mechanics* 68.3 (2001): pp. 412-419.
- [100] Bridgman, P. W., 1944, "The stress distribution at the neck of a tension specimen," *Trans. ASM* 32, pp. 553-574.
- [101] Bridgman, P. W., 1964, *Studies in Large Plastic Flow and Fracture*, Harvard University Press, Cambridge, MA.
- [102] Bai, Yuanli, and Tomasz Wierzbicki. "A new model of metal plasticity and fracture with pressure and Lode dependence." *International Journal of Plasticity* 24.6 (2008): 1071-1096.
- [103] Bao, Yingbin, and Tomasz Wierzbicki. "On fracture locus in the equivalent strain and stress triaxiality space." *International Journal of Mechanical Sciences* 46.1 (2004): 81-98.
- [104] Deng, Y. C., et al. "Strain limit dependence on stress triaxiality for pressure vessel steel." *Journal of Physics: Conference Series*. Vol. 181. No. 1. IOP Publishing, 2009.
- [105] Wierzbicki, Tomasz, and Liang Xue. "On the effect of the third invariant of the stress deviator on ductile fracture." *Impact and Crashworthiness Laboratory, Technical Report 136* (2005).
- [106] Sutton, M. A., Orteu, J., and Schreier, H. W., 2009, "Image Correlation for Shape, Motion and Deformation Measurements," Springer, New York, NY.
- [107] Peters WH and Ranson WF, 1982, "Digital Imaging Techniques in Experimental Stress Analysis," *Optical Engineering*, **21**(3), pp. 427-431.
- [108] Haddadi, H., and Belhabib, S., 2008 "Use of Rigid-body Motion for the Investigation and Estimation of the Measurement Errors Related to Digital Image Correlation Technique," *Optics and Lasers in Engineering*, **46**(2), pp. 185-196.
- [109] Pan, B., Qian, K., Xie, H., & Asundi, A., 2009, "Two-dimensional Digital Image Correlation for In-plane Displacement and Strain Measurement: A Review," *Measurement Science and Technology*, **20**(6).

- [110] Wang, Z. Y., Li, H. Q., Tong, J. W., & Ruan, J. T. ,2007. “Statistical Analysis of the Effect of Intensity Pattern Noise on the Displacement Measurement Precision of Digital Image Correlation Using Self-correlated Images,” *Experimental Mechanics*, **47**(5), pp. 701-707.
- [111] Li M, Zhang J, Xiong CY, Fang J, Li JM, Hao Y, 2005, “Damage and Fracture Predication of Plastic-bonded Explosive by Digital Image Correlation Processing,” *Optical Lasers Engineering*, **43**(8), pp. 856–68.
- [112] Sun Z, Lyons JS, McNeil SR, 1997, “Measuring Microscopic Deformations with Digital Image Correlation,” *Optical Laser Engineering*, **27**(1), pp. 409–28.
- [113] Vogel D, Kuhnert R, Dost M, Michel B., 2002, “Determination of Packaging Material Properties Utilizing Image Correlation Techniques,” *J Elect Pack*, **124**, pp. 345–51.
- [114] Lava, P., Cooreman, S., Coppieters, S., De Strycker, M., & Debruyne, D., 2009 “Assessment of Measuring Errors in DIC Using Deformation Fields Generated by Plastic FEA,” *Optics and Lasers in Engineering*, **47**(7), pp. 747-753.
- [115] Becker, T., Splitthof, K., Siebert, T., & Kletting, P., 2006, “Error Estimations of 3D Digital Image Correlation Measurements,” *International Society for Optics and Photonics, Speckle* **6**, pp. 63410F-63410F.
- [116] Sutton, M. A., Yan, J. H., Tiwari, V., Schreier, H. W., & Orteu, J. J., 2008, “The Effect of Out-of-plane Motion on 2D and 3D Digital Image Correlation Measurements,” *Optics and Lasers in Engineering*, **46**(10), pp. 746-757.
- [117] Orteu, J. J., 2009, “3-D Computer Vision in Experimental Mechanics,” *Optics and Lasers in Engineering*, **47**(3), pp. 282-291.
- [118] Yaofeng, S., & Pang, J. H., 2007, “Study of Optimal Subset Size in Digital Image Correlation of Speckle Pattern Images,” *Optics and Lasers in Engineering*, **45**(9), pp. 967-974.
- [119] Lecompte D, Smits A, Bossuyt S, et al., 2006, “Quality Assessment of Speckle Patterns for Digital Image Correlation,” *Optical Lasers Engineering*, **44**(11), pp. 1132–45.
- [120] Hua, T., Xie, H., Wang, S., Hu, Z., Chen, P., & Zhang, Q. 2011, “Evaluation of the Quality of a Speckle Pattern in the Digital Image Correlation Method by Mean Subset Fluctuation,” *Optics & Laser Technology*, **43**(1), pp. 9-13.
- [121] Pan, B., Lu, Z., & Xie, H., 2010, “Mean Intensity Gradient: An Effective Global Parameter for Quality Assessment of the Speckle Patterns Used in Digital Image Correlation,” *Optics and Lasers in Engineering*, **48**(4), pp. 469-477.
- [122] Triconnet, K., Derrien, K., Hild, F., & Baptiste, D., 2009, “Parameter Choice for Optimized Digital Image Correlation,” *Optics and Lasers in Engineering*, **47**(6), pp. 728-737.

- [123] Haddadi H, Belhabib S., 2008, “Use of Rigid-body Motion for the Investigation and Estimation of the Measurement Errors Related to Digital Image Correlation Technique,” *Optics and Lasers Engineering*, **46**, pp.185–196.
- [124] Schreier, H. W., Sutton, M. A., 2002, “Systematic Errors in Digital Image Correlation Due to Undermatched Subset Shape Functions,” *Experimental Mechanics*, **42**(3), pp. 303–10.
- [125] Schreier HW, Braasch JR, Sutton MA., 2000 “Systematic Errors in Digital Image Correlation Caused by Intensity Interpolation,” *Optics and Lasers Engineering*, **9**(11), pp. 2915–21.
- [126] Wang ZY, Li HQ, Tong JW, Ruan JT., 2007, “Statistical Analysis of the Effect of Intensity Pattern Noise on the Displacement Measurement Precision of Digital Image Correlation Using Self-correlated Images,” *Experimental Mechanics*, **47**, pp. 701–707.
- [127] Lava, P., Cooreman, S., Coppieters, S., De Strycker, M., & Debruyne, D., 2009, “Assessment of Measuring Errors in DIC Using Deformation Fields Generated by Plastic FEA,” *Optics and Lasers in Engineering*, **47**(7), pp. 747-753.
- [128] Correlated Solutions, *Vic-3D V7 Testing Guide*, pp. 1-22.

DISTRIBUTION

5 The University of Texas El Paso
 Attn: Prof. Calvin Stewart
 Department of Mechanical Engineering
 Suite A126
 500 W. University Ave.
 El Paso, TX 79968-0521

1	MS0840	Stephen Attaway	01500
1	MS1454	Marcia Cooper	02554
1	MS0836	William Erikson	01516
1	MS0840	Spencer Grange	01554
1	MS0840	Christopher Hammetter	01554
1	MS0836	Michael Hobbs	01516
1	MS0557	Matthew Hudspeth	01528
1	MS1454	Michael Kaneshige	02500
1	MS0840	Chi Lo	01554
1	MS1454	Leanna Minier	02554
1	MS0725	Jaime Moya	00600
1	MS0557	Brett Sanborn	01528
1	MS0557	Bo Song	01528
1	MS0899	Technical Library	9536 (electronic copy)
1	MS0359	D. Chavez, LDRD Office	1911

